AWARD NUMBER: W81XWH-13-1-0361

TITLE: A Novel Tumor Antigen and Foxp3 Dual-Targeting Tumor Cell Vaccine Enhances the Immunotherapy in a Murine Model of Renal Cell Carcinoma

PRINCIPAL INVESTIGATOR: Li Shen Ph.D.

CONTRACTING ORGANIZATION:
Health Research, Inc.

Buffalo, NY   14263

REPORT DATE: December 2015

TYPE OF REPORT: Final Report

PREPARED FOR: U.S. Army Medical Research and Materiel Command
                Fort Detrick, Maryland 21702-5012

DISTRIBUTION STATEMENT: Approved for Public Release;
                        Distribution Unlimited

REPORT DOCUMENTATION PAGE

Form Approved
OMB No. 0704-0188

Public reporting burden for this collection of information is estimated to average 1 hour per response, including the time for reviewing instructions, searching existing data sources, gathering and maintaining the data needed, and completing and reviewing this collection of information. Send comments regarding this burden estimate or any other aspect of this collection of information, including suggestions for reducing this burden to Department of Defense, Washington Headquarters Services, Directorate for Information Operations and Reports (0704-0188), 1215 Jefferson Davis Highway, Suite 1204, Arlington, VA 22202-4302. Respondents should be aware that notwithstanding any other provision of law, no person shall be subject to any penalty for failing to comply with a collection of information if it does not display a currently valid OMB control number. **PLEASE DO NOT RETURN YOUR FORM TO THE ABOVE ADDRESS.**

1. REPORT DATE	2. REPORT TYPE	3. DATES COVERED
December 2015	Final	15 Sep 2013 - 14 Sep 2015

4. TITLE AND SUBTITLE

A Novel Tumor Antigen and Foxp3 Dual-Targeting Tumor Cell Vaccine Enhances the Immunotherapy in a Murine Model of Renal Cell Carcinoma

5a. CONTRACT NUMBER

5b. GRANT NUMBER
W81XWH-13-1-0361

5c. PROGRAM ELEMENT NUMBER

6. AUTHOR(S)

Li Shen

E-Mail: Li.Shen@roswellpark.org

5d. PROJECT NUMBER

5e. TASK NUMBER

5f. WORK UNIT NUMBER

7. PERFORMING ORGANIZATION NAME(S) AND ADDRESS(ES)

Health Research Incorporated,
Roswell Park Cancer Institute
Buffalo, New York 14263-0001

8. PERFORMING ORGANIZATION REPORT NUMBER

9. SPONSORING / MONITORING AGENCY NAME(S) AND ADDRESS(ES)

U.S. Army Medical Research and Materiel Command
Fort Detrick, Maryland 21702-5012

10. SPONSOR/MONITOR'S ACRONYM(S)

11. SPONSOR/MONITOR'S REPORT NUMBER(S)

12. DISTRIBUTION / AVAILABILITY STATEMENT

Approved for Public Release; Distribution Unlimited

13. SUPPLEMENTARY NOTES

14. ABSTRACT

A major barrier in vaccine therapy is represented by the presence of immunosuppressive factors predominant in cancer patients, such as regulatory T cells (Tregs) and suppressive myeloid cells, including myeloid derived suppressor cells (MDSCs) and tumor associated macrophages (TAMs). Here we report a tumor cell vaccine designed to target both tumor cells and Tregs by using Foxp3, a Treg-functional protein as an antigen in tumor cell vaccine.

During first year of the project, we have demonstrated that the dual target vaccine had anti-tumor activity against established tumor. During last year, we tested a combination strategy to target suppressive myeloid cells (MDSCs and TAMs) with a pharmacological approach, tasquinimod, combined with dual targeting vaccine. The combination strategy prolonged survival, compared to vaccine single treatment. Overall, our results suggest that targeting immunosuppressive cells with vaccine or pharmacological strategies, results in greater anti-tumor activity and therapeutic efficacy, and provides foundation to test the strategy in clinical setting for patients with advanced, metastatic kidney cancer.

15. SUBJECT TERMS

Renal Cell carcinoma (RCC), Tumor Cell Vaccine, Regulatory T cells (Tregs),Myeloid Derived Suppressor Cells (MDSCs), Tumor Associated Macrophage (TAMs),Tumor Microenviroment

16. SECURITY CLASSIFICATION OF:

a. REPORT	b. ABSTRACT	c. THIS PAGE	17. LIMITATION OF ABSTRACT	18. NUMBER OF PAGES	19a. NAME OF RESPONSIBLE PERSON USAMRMC
U	U	U	UU	56	19b. TELEPHONE NUMBER *(include area code)*

Standard Form 298 (Rev. 8-98)
Prescribed by ANSI Std. Z39.18

Table of Contents

Introduction:

Renal cell carcinoma (RCC) is the most common type of kidney cancer and a relatively more immunogenic cancer, as compared to other types of cancer. Therefore, immunotherapy such as cytokine and vaccine therapy represents an interest for treatment of RCC. A major barrier in vaccine therapy is represented by the presence of immunosuppressive factors predominant in cancer patients, such as regulatory T cells (Tregs) and suppressive myeloid cells, including myeloid derived suppressor cells (MDSCs) and tumor associated macrophages (TAMs). Here we report a tumor cell vaccine designed to target both tumor cells and Tregs by using Foxp3, a Treg-functional protein as an antigen in tumor cell vaccine. The vaccine is tested in a mouse orthotopic, syngeneic kidney cancer model, and in different treatment schedules. During first year of the project, we have demonstrated that the dual target vaccine had anti-tumor activity against established tumor. During last year, we tested a combination strategy to target suppressive myeloid cells (MDSCs and TAMs) with a pharmacological approach, tasquinimod, combined with dual targeting vaccine. The combination strategy prolonged survival, compared to vaccine single treatment. Overall, our results suggest that targeting immunosuppressive cells with vaccine or pharmacological strategies, results in greater anti-tumor activity and therapeutic efficacy, and provides foundation to test the strategy in clinical setting for patients with advanced, metastatic kidney cancer.

.

Keywords:

Renal Cell carcinoma (RCC)

Tumor Cell Vaccine

Regulatory T cells (Tregs)

Myeloid Derived Suppressor Cells (MDSCs)

Tumor Associated Macrophage (TAMs)

Tumor Microenviroment

RNA sequencing

Overall project Summary:

During the first year period of the project, we've determined the anti-tumor activity of the dual-targeting tumor cell vaccine in a murine RCC model, RENCA, and to evaluate the immuno-modulatory activity of the vaccine in the model (see Appendix 1, fist annual report). We discovered that in a prevention treatment schedule, both RENCA cell lysate vaccine and Foxp3 RENCA cell vaccine (the dual targeting vaccine) can inhibit the tumor growth. However, in an intervention treatment schedule, only Foxp3 RENCA vaccine had anti-tumor activity against established tumor orthotopic.growth. In addition, Foxp3 RENCA vaccine reduced tumor infiltrating Tres without affect peripheral Treg accumulation. Our analysis of tumor microenvironment indicate RENCA tumor accumulate myeloid suppressive cells, which are much more abundant than Tregs in tumor. Foxp3 RENCA vaccine therapy didn't affect these immunosuppressive myeloid populations. This supports our rationale to target these populations to enhance anti-tumor activity of vaccine, which is the plan for second year award period. These experiments of the second year are listed as part of the specific Aim1, Aim 2, and part of specific Aim3. Here I summarize our activities and accomplishment as listed under the Specific Aims and Tasks.

Specific Aim 1: To determine the anti-tumor activity of the dual-targeting tumor cell vaccine in a murine orthotopic RCC model, RENCA. (Month 1-14)

Task 1: Generate a RENCA Foxp3 cell line. (Month 1-4) (accomplished during first year period)

Task 2: Vaccine generation. (Month 5-10) (accomplished during first year period)

Task 3: Conduct therapy experiment to test the RENCA Foxp3 cell derived vaccines in the orthotopic RENCA models. (Month 5-10)

Task 4: Correlated studies. (Month 5-12)

Task 5: Data collection and statistical analysis. (Month 10-12)

During first award period, all the tasks in specific Aim 1 were accomplished except for test vaccine in dendritic cell (DC) form. There was a delay on DC vaccine during first year, as we hoped to further improve RENCA model to a metastatic model, with nephrectomy procedure. However, the development of lung metastasis is still not consistent. So we performed vaccine therapy in the second year period.

Again, majority of task 4 was in parallel with Task 5. The end part of Task 4 and the Task 5 will be data analysis of experiments in Task3. Therefore, the accomplishment from these tasks is summarized together here.

First, we compared the anti-tumor activity of RENCA Foxp3 vaccine in form of DCs with that of vaccine in lysate form. In this experiement, tumor lysate vaccine was prepared as before. RENCA Foxp3 cells were sonicated in PBS without carrier protein, and then the lysates were mixed with Montanide® and injected with GM-CSF. To produce RENCA Foxp3 vaccine, mouse bone marrow cells were isolated from femurs, and put in culture supplemented with 20ng/ml GM-CSF. Lymphocytes and granulocytes floated and were discard from the culture after 2 or 4 days, respectively. On day 6, the DCs were collected and pulsed with RENCA Foxp3 cell lysate for 1.5 hours, and re-plated in 10cm plates with 20ng/ml GM-CSF and 40ng/ml CD40L overnight to promote maturation. Each mouse received 1×10^6 pulsed, mature DCs. Immuno-fluorescent staining and flow cytometry have been performed to phenotype resulted DCs (Figure 1). Result showed that 89.3% of live cells derived from bone marrow are $CD11c^+$ dendritic cells (Fig. 1A). In DC cells, 43% were expressing antigen presenting molecule MHC and 45% were expressing co-stimulation molecule CD86 (Fig. 1B). This indicates that we've successfully derived DCs from marrow, and substantial portion of DCs are activated, mature,

functional DCs. DCs were administered through *i.p.* injection, and expected to undergo further maturation *in vivo*.
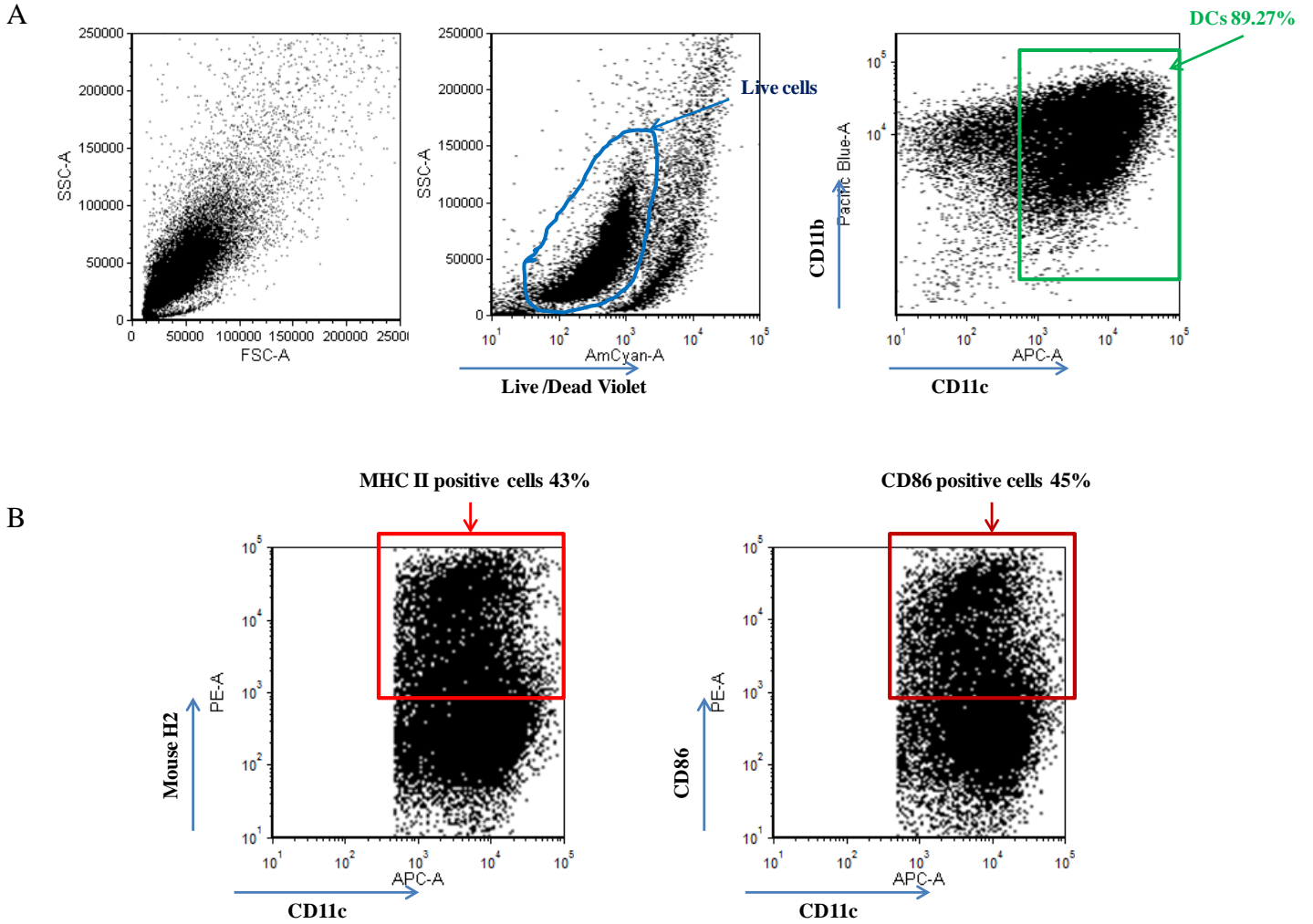
A

B

Figure 1: A. Bone marrow derived cell culture were harvested and subject to immunofluorescence staining and flow cytometry. Live cells were gated and percentage of CD11c positive DCs was determined. B. DCs were gated, and mouse H2 (MHC) or CD86 (co-stimulation molecule) positive cells were quantified.

When we had DC form vaccine ready, we performed an animal study to compare RENCA Foxp3 vaccine in lysate form to DC form. We did comparison in prevention and intervention schedules. We inoculated 30 mice with RENCA Luc cells, monitor tumor growth based on luminescence signals (luciferase activity) from Xenogen imaging 7 days after inoculation. All mice had established tumor growth 7 days after inoculation. Mice used in intervention schedule were randomized based on tumor luciferase signals, and divided into 3 groups: vehicle, RENCA Foxp3 lysate vaccine, RENCA Foxp3 DC vaccine treatments. The other batch of mice were first treated with lysate or DC vaccine, and inoculated with RENCA Luc after 3 doses of vaccine treatment. Lysates were injected subcutaneously and DC vaccine were administered through intra-peritoneal injection in 100ul volume.

As shown in Figure 2, we carried the prevention and intervention experiments in the same animal study. We gave the prevention groups 3 doses of vaccines, then inoculated all the mice. 7 days after inoculation, mice planned for intervention schedule were randomized into 3 groups (as described above) based on xenogeny imaging, and treatment start for the intervention groups.The tumor growth was monitored with Xenogen bioluminescence imaging every week and samples were collected when the study was ended around five weeks after inoculation.

As expected, in prevention schedule, both lysate form and DC form of RENCA Foxp3 vaccines efficiently inhibited tumor growth, as compared to vehicle group (Fig. 2), displayed as both dramatically reduced luminescence signals in imaging (Fig. 2A), as well as tumor weight in vaccine treated group (Fig. 2B). It is noticeable that some mouse from vaccine treated groups had tumors with size comparable to those in vehicle group. The effect of vaccine is not uniform in the same group. This indicates that tumor in some mice may have escaped vaccine therapy.
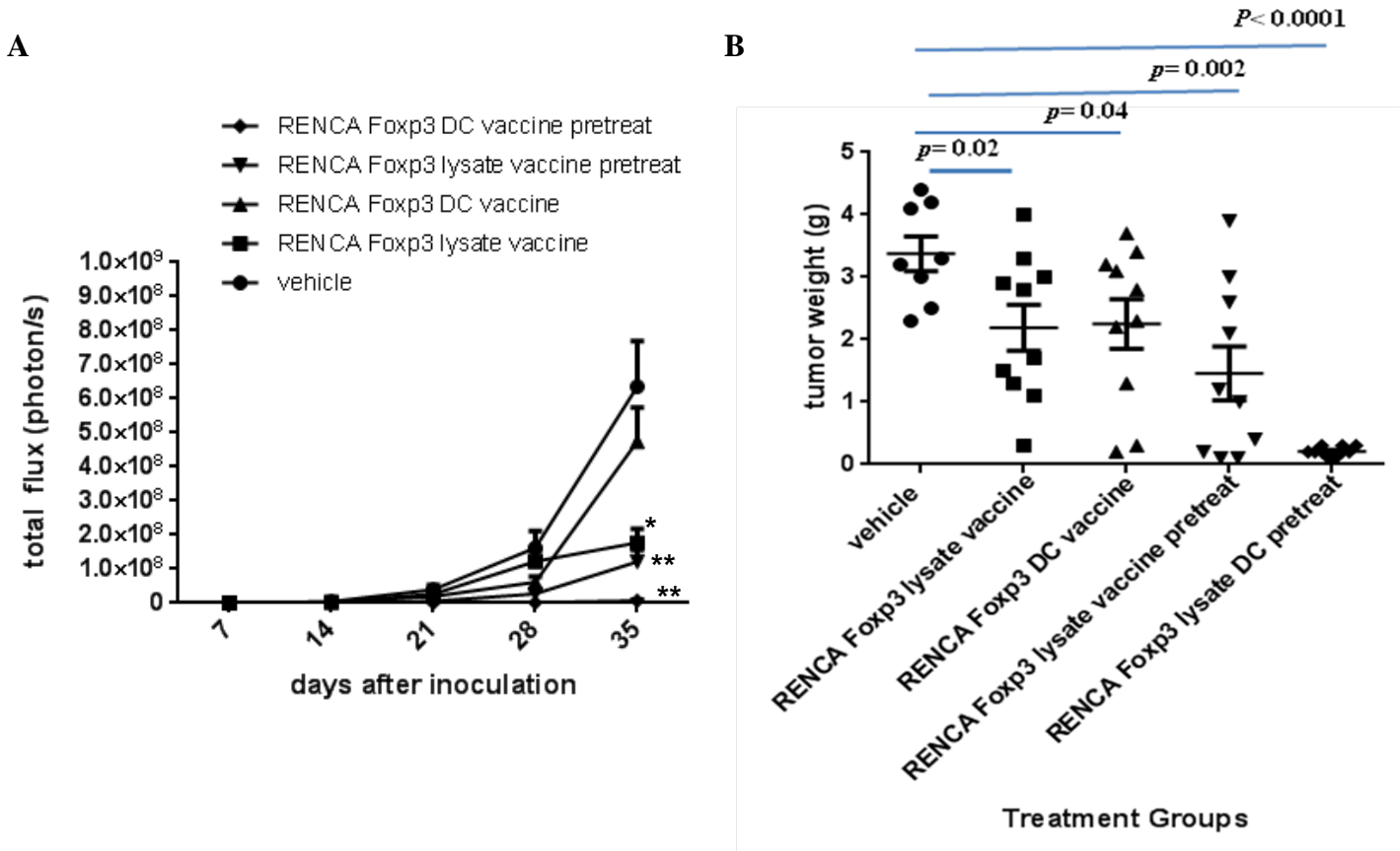

Figure 2: Comparison of RENCA Foxp3 vaccine in lysate form and DC form. Female Balb/C mice planned for prevention schedule received 3 doses of vaccines, then were inoculated with RENCA Luc cells, together with the rest of mice planned for intervention. 7 days after inoculation, the mice were imaged , the mice randomized for intervention groups, vehicle, RENCA Foxp3 lysate vaccine, and RENCA Foxp3 DC vaccine groups. **A.** plot shows tumor growth accessed by luminescence imaging. Tumor growth is represented by luciferase activity. **B**. the end of experiment tumor weights. *$p<0.05$; ** $p< 0.01$.

In intervention schedule groups (vaccine started 7 day after inoculation), as we've observed during first year period, RENCA Foxp3 tumor cell vaccine treated group had significantly lower tumor weight, as compared to vehicle group (Fig. 2B). The bioluminescence imaging assay showed modest difference of tumor growth between vehicle and RENCA Fopx3 lysate vaccine group. During the Xenogen imaging process, we always can notice that some big tumors with little signal, due to poor perfusion in a big tumor, which might have caused a drop of the increase rate of the signal during last two weeks of monitoring (Figure 1A). Therefore, tumor weight results are more reliable to access the effect of treatment. We noticed that anti-tumor activity of RENCA Foxp3 vaccine in DC form was comparable to that of vaccine in lysate form, led to significantly lower tumor weights at end point of the therapeutic study (Fig. 2B). Based on this result, we mainly focused on lysate form of the vaccine when perform experiments in Specific Aim 2 and Specific Aim 3, during the second year award period. This is because lysate form and DC form of vaccines had similar anti-tumor activity, and lysate form is easier to make and keep consistent quality.

Currently, tumor cell vaccine is tested for RCC patients with diagnosed, established disease, and we have a goal to translate our pre-clinical study to treatment for advanced or metastatic disease. Therefore, we focus on

the intervention treatment schedule instead of prevention schedule in the following studies, because the intervention schedule resembles the clinical setting.

Task 6: Conduct survival studies with RENCA Foxp3 cell derived vaccines and the control vaccines. (Month 10-14).

We combined experiment for this task in the Specific Aim 2 part of survival study, which include all the treatment conditions. It turned out the strategy is more work and cost efficient. The survival study in Specific Aim 2 completely included all the treatment conditions, including the groups originally planned for this task 6, in Specific Aim 1.

For the correlative study, we have done extensive analysis to evaluate the components in peripheral immune environment and tumor immune microenvironment, with analysis focus on later. We performed immunofluorescence staining and flow cytometry to access the composition in the tumor infiltrates (tumor microenvironment). Test of CD4 cells, CD8 cells, Tregs, myeloid cell populations including MDSCs macrophages. All these immune-phenotyping and immune-modulation analysis, in addition to immune response analysis, are summarized in the following accomplishment under Specific Aim 3.

Specific Aim #2: To determine the anti-tumor activity of tasquinimod in combination with the dual-targeting vaccines in the RENCA model. (Month 10-19)

Task 1: Conduct therapy experiment to test the combination of the RENCA Foxp3 cell derived vaccines and tasquinimod. (Month 10-15)

To accomplish this task, we performed the combination study of RENCA Foxp3 lysate vaccine with tasquinimod in an intervention schedule. We gave the prevention groups 3 doses of vaccines, then inoculated all the mice. 7 days after inoculation, mice planned for intervention schedule were randomized into 4 groups based on xenogeny imaging, and treatment start for the intervention groups. The tumor growth was monitored with Xenogen bioluminescence imaging every week and samples were collected when the study was ended around five weeks after inoculation.

Similarly, in prevention schedule, RENCA Foxp3 vaccines dramatically inhibited tumor growth, as compared to vehicle group (Fig. 3). Since we consistently observed that sometimes big tumor had low imaging signal due to perfusion problem, we rely more on the end point tumor weight result to access anti-tumor effect of treatment.

In intervention schedule groups (vaccine started 7 day after inoculation), we consistently observed that RENCA Foxp3 lysate vaccine treated group had significantly lower tumor weight, as compared to vehicle group (Fig. 3B). The bioluminescence imaging assay showed no significant difference of tumor growth between vehicle and RENCA Foxp3 lysate vaccine group. Tasquinimod single treatment resulted in modest reduction of tumor weights, but not by a significant level. In the combination group, there were significantly lower tumor weights, as compared to vehicle group (Fig. 3B). However, combination treatment group didn't show additional anti-tumor effect, compared to vaccine single treatment.

In order to further investigate of effect of combination therapy, we expanded the experiment to included RENCA cell vaccine in the combination therapy. We only performed in intervention schedule in the expanded study. 7 days after inoculation, mice with orthotopic RENCA Luc tumors were imaged and randomized into six treatment groups: vehicle, tasquinimod, RENCA lysate vaccine, RENCA lysate vaccine +tasquinimod, RENCA Foxp3 lysate vaccine, RENCA Foxp3 lysate vaccine +tasquinimod (Fig. 4).
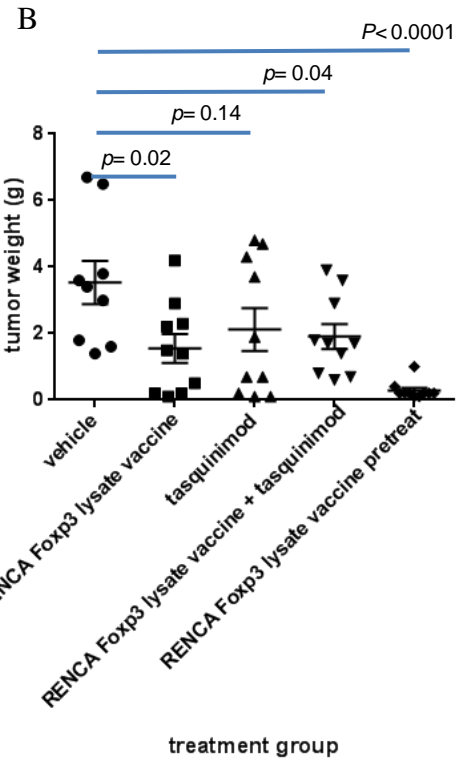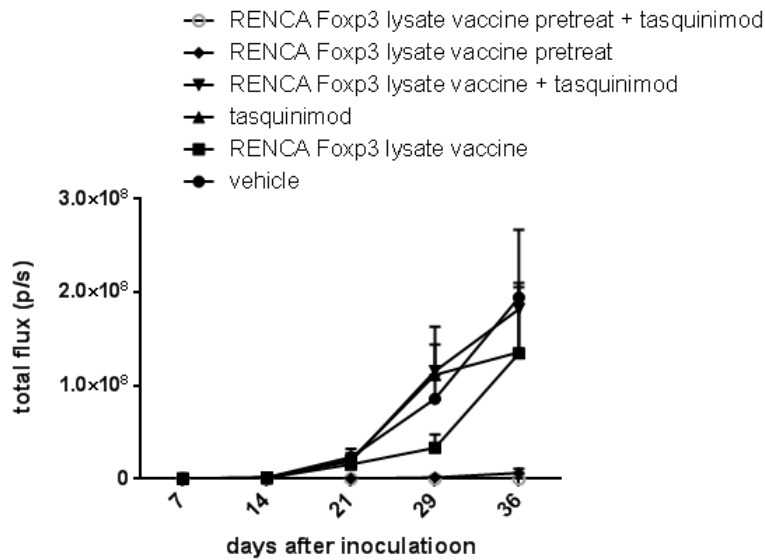
A

B

Figure 3. Comparison of single RENCA Foxp3 lysate vaccine treatment to its combination with tasquinimod. Female Balb/C mice planned for prevention schedule received 3 doses of vaccines, then were inoculated with RENCA Luc cells, together with the rest of mice planned for intervention. 7 days after inoculation, the mice were imaged. Mice randomized for intervention groups, vehicle, RENCA Foxp3 lysate vaccine, tasquinimod, and combination. **A.** plot shows tumor growth accessed by luminescence imaging. Tumor growth is represented by luciferase activity. **B**. the end of experiment tumor weights.
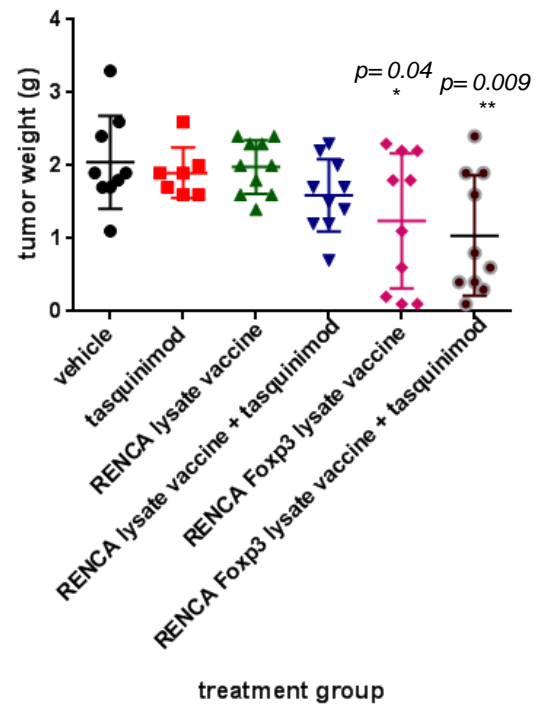
A
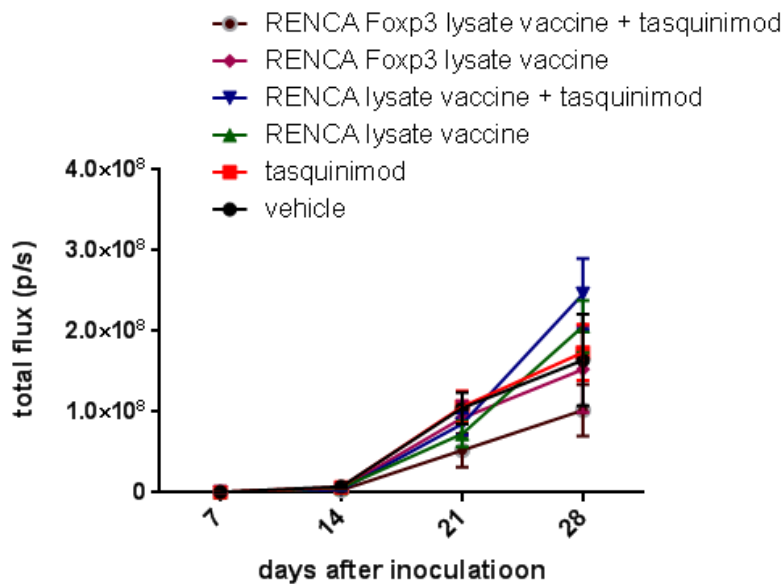
B

Figure 4. combination therapy with tasquinimod and vaccines (RENCA or RENCA Foxp3) in lysate form . Female Balb/C mice were inoculated with RENCA Luc cells. 7 days after inoculation, the mice were imaged and randomized into six treatment groups. **A.** plot shows tumor growth accessed by luminescence imaging. Tumor growth is represented by luciferase activity. **B**. end of experiment tumor weights. *$p<0.05$ **$p<0.01$

As shown in Figure 4, neither RENCA lysate vaccine nor its combination with tasquinimod had significant antitumor activity (Figure 4). On the contrary, both RENCA Foxp3 lysate vaccine and its combination with tasquinimod had significant anti-tumor activity as shown as lower end of experiment tumor weights (Fig. 4B).

It is possible that the model is very aggressive tumor model and there was not enough time window for combination strategy to show additional anti-tumor response, compared to vaccine single treatment. We went ahead to perform survival study to find out effects of vaccines and their combination with tasquinimod in a prolonged experiment setting (see task 4).

Task 2: Correlated studies. (Month 10-17)
Task 3: Data collection and statistical analysis. (Month 15-17)

Correlative studies and data analysis were completed in parallel with animal study, and statistical analysis of anti-tumor activities of therapies have been shown in above Figures. During and at the end of these therapeutic studies, we have done extensive analysis to evaluate the components in peripheral immune environment and tumor immune microenvironment, such as CD4 cells, CD8 cells, Tregs, myeloid cell populations including MDSCs, TAM macrophages, via immunofluorescence staining and flow cytometry analysis and other approached. The tissue and cells harvested from Aim 2 studies has been used to test anti-tumor immune responses, and also to test function of effectors cells. All these immune response and immunomodulation test results are summarized in the following accomplishment under Specific Aim 3.

Task 4: Conduct survival studies to test the combination of the RENCA Foxp3 cell derived vaccines and tasquinimod. (Month 15-19)

We designed survival study include six experiment arms at the same time: Vehicle, tasquinimod, RENCA lysate vaccine, RENCA lysate vaccine and tasquinimod, RENCA Foxp3 lysate vaccine, RENCA Foxp3 lysate vaccine and tasquinimod. Therefore, in this survival study, we can compare RENCA to RENCA Foxp3 vaccine, as well as compare vaccine only to vaccine and tasquinimod combination. This design included Task 6 in Specific Aim 1.

In survival study, tumor inoculation and animal randomization were performed as described in therapeutic study. Mice were count as end of survival from following situation: 1. Mouse found dead. 2. Mouse was euthanized when consider lethargic or moribund, according to institutional IACUC. 3. Mouse that was experiencing pain and/or stress and not showing any sign of improvement. The conduct of survival study is also based on the approved ACURO animal protocol.

As shown in Figure 5, treatments including tasquinimod, RENCA lysate vaccine, and RENCA lysate vaccine and tasquinimod combination didn't lead to any improvement of animal survival. Mice treated with RENCA Foxp3 lysate vaccine showed prolonged survival, as compared to vehicle group. Excitingly, mice treated with RENCA Foxp3 lysate vaccine and tasquinimod combination had additional improvement of survival, as compared to RENCA Foxp3 lysate vaccine only group. By day 58 on treatment, 3 mice were still alive and active in the RENCA Foxp3 lysate vaccine and tasquinimod combination. These mice were euthanized (on the day of end of award period). and it was observed all 3 mice have small, less than 0.4 gram tumor.

In summary, tasquinimod didn't have additional anti-tumor growth activity in end point therapeutic study, but further improved survival when added to RENCA Foxp3 vaccine therapy. It is possible that a longer treatment duration in survival study have given more time for the combination to take into effect. In addition,we have reported that tasquinimod reduced numbers an inhibited function of immunosuppressive MDSCs and TAMs in tumor microenvironment (Shen et al. Cancer Immunology Research, 2015, attached in Appendics), and may have anti-metastasis activity (unpublished result). Interestingly, 2-3 mice (out of 10) were found with lung and/or diaphragm metastasis from other groups, but not in RENCA Foxp3 and tasquinimod combination group.

The anti-metastatic activity of anti-inflammatory agent, tasquinimod is worth future investigation and tests in linical settings.
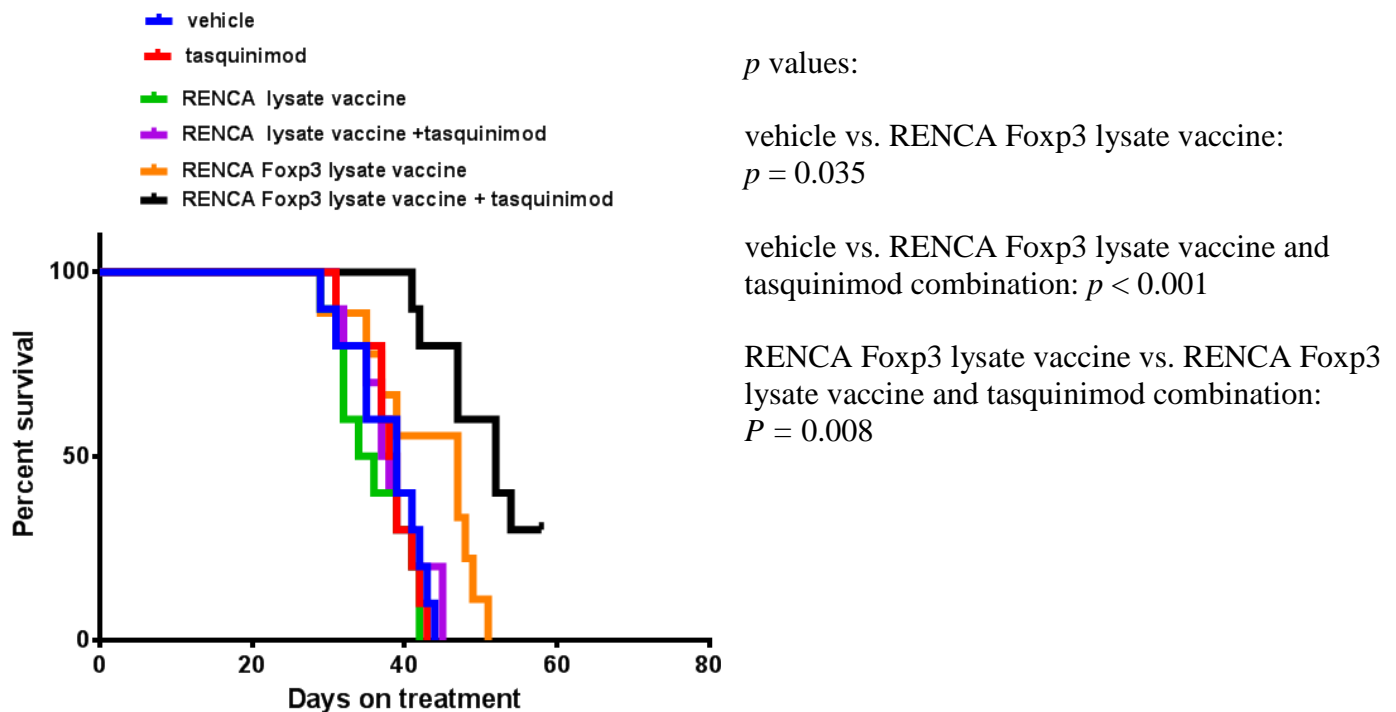

p values:

vehicle vs. RENCA Foxp3 lysate vaccine: $p = 0.035$

vehicle vs. RENCA Foxp3 lysate vaccine and tasquinimod combination: $p < 0.001$

RENCA Foxp3 lysate vaccine vs. RENCA Foxp3 lysate vaccine and tasquinimod combination: $P = 0.008$

Figure 5. Test RENCA, RENCA Foxp3 lysate vaccines and their combination with tasquinimod in survival study. Tumor inoculation and group set up were done as described above. Kaplan-Meier curves is derived to compare survival in different treatment groups and a log-rank test is used to measure the statistical significance.

Specific Aim #3: To assess tumor-specific immune response after the delivery of the dual-targeting vaccine alone or in combination with tasquinimod. (Month 6-24)

Task 1: Assess tumor-specific responses in therapy experiments. (Test after dual targeting vaccine single therapy: Month 10-14; test after combination studies: Month 15-19)

In order to access anti-tumor responses and effector cell function induced by vaccine or combination treatment, we performed three tests: 1). Cytotoxicity of lymphocytes against RENCA luc tumor cells. 2). Interferon gamma expression in effector CD8 cells; 3) Granzyme B expression in effector CD8 cells.

Splenocytes were isolated from tumor-bearing mice of different treatment groups. Some splenocytes were stimulated in CD3 (1ug/ml) and CD28 (0.5ug/ml)—coated plates, and put in culture with fluorescence (Dio)-labeled target RENCA Luc tumor cells. Propidium iodide was used to detected cell death after 5 hours of co-culture. Tumor cell killing then was measured and quantified with flow cytometry analysis.

We found that splenocytes from mice with vaccine therapy (RENCA or RENCA Foxp3) had similar tumor cell killing capacity as those from mice of vehicle group. Tasquinimod single treatment didn't change the cytotoxicity of splenocytes, either. However, tasquinimod in combination with vaccine can improve tumor cytotoxicity of splenocytes from treated mice, when compare RENCA vaccine + tasquinimod with RENCA vaccine, or compare RENCA Foxp3 vaccine +tasquinimod with RENCA Foxp3. Interestingly, when compared together, splenocytes from RENCA Foxp3 vaccine and tasquinimod combination group had significant higher

tumor cell killing capacity, as compared to all other groups. This coincided with the best effect to prolong survival of tumor-bearing animals.
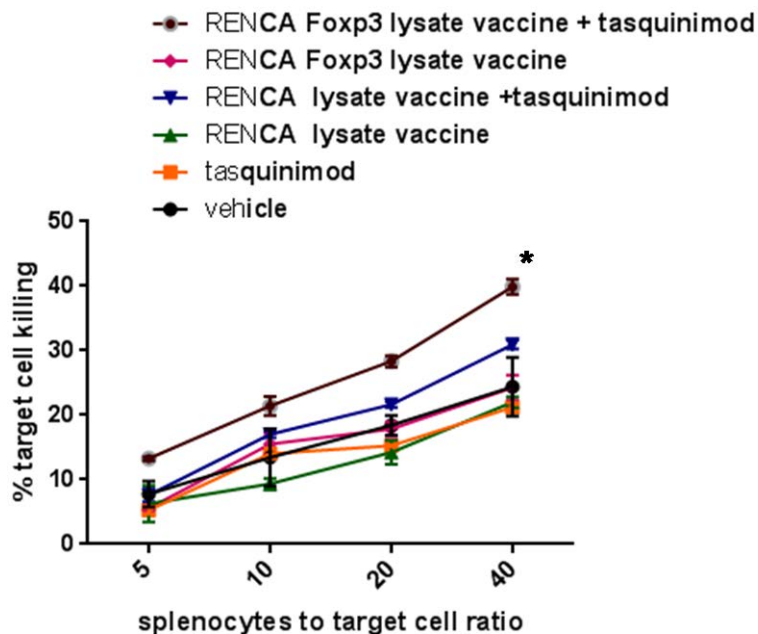

Figure 6. Tasquinimod and vaccine combination improved anti-tumor cytotoxicity of lymphocytes. Splenocytes were isolated from differentially treated mice, and co-cultured with Dio-labeled RENCA Luc tumor cells for 5 hours in different ratios. Propidium Iodide was used to detect dead cells in the culture. Values in plots represent percentage of dead target cells in total labeled tumor cells. * $p < 0.05$

IFN gamma and Granzyme B are proteins critical to effector cell cytotoxic function against tumor cells. Splenocytes were also stimulated in CD3 and CD28 coated plate for 72 hours, with last 12 hour of Brefeldin A to block the protein secretion. These splenocytes were tested for Granzyme B expression. Similarly, Splenocytes were stimulate with PMA and Ionomycin for 5 hours and with Brefeldin A, then tested for IFN gamma expression. Immunofluorescence staining and flow cytometry assay were performed to detect and quantify the expression of the two proteins (Fig. 7).
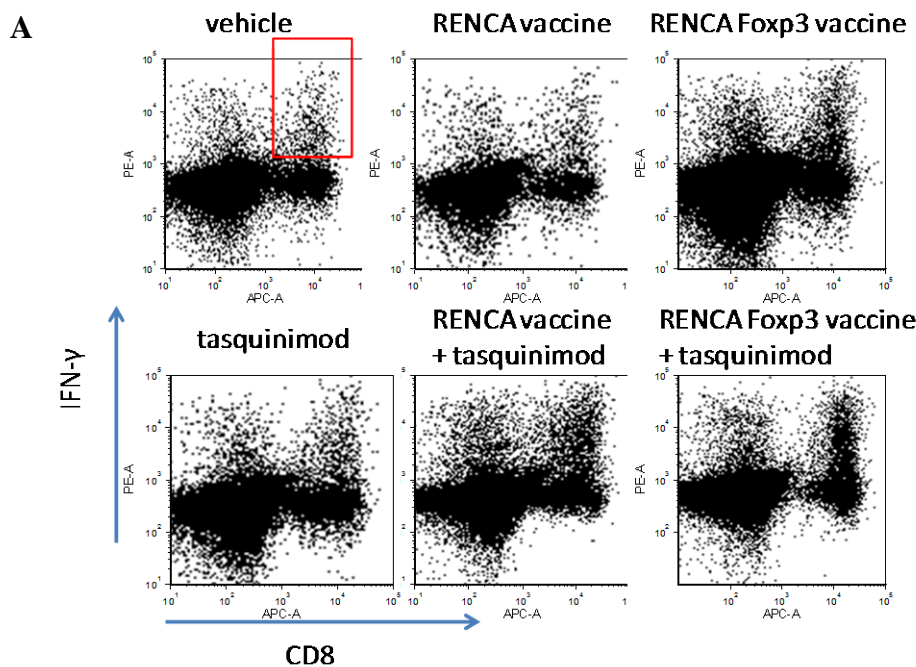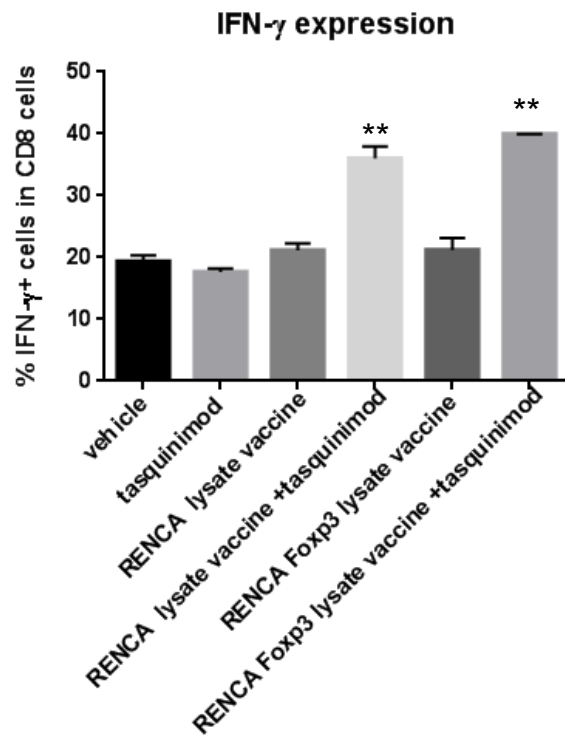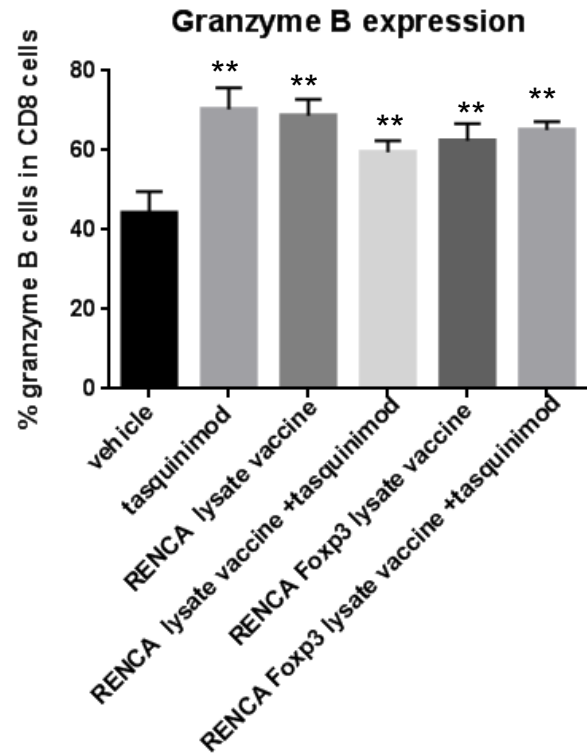
B

C

Figure 7. Effect of tumor cell vaccine and tasquinimod on IFN-γ and granzyme B expression in splenocytes. A. plots of IFN-γ staining. IFN-γ positive CD8 cells are in red rectangle on the first plot. B. Values show percentage of IFN-γ expressing cells in CD8 population. C. percentage of grazyme B expressing cells in Cd8 population. **$p<0.01$

Our results indicate either vaccine or tasquinimod single treatment can't induce IFN-γ expression in CD8 effector cells, but combination treatments dramatically enhanced IFN-γ expression in CD8 cells (Fig. 7A and B). All treatment, single or combination were able to induce granzyme B expression, as compared to vehicle group Fig. C). These result suggest enhanced IFN-γ in combination treatment may be associated with higher cytotoxicity against tumor cells.

Task 2: Evaluate the effect of treatments on immunosuppressive cell populations and other immune cell populations. (Evaluation of dual targeting vaccine single therapy: Month 6-10; evaluation of combination studies: Month 11-15)

During first year of award period, we have accomplished part of **Task 2** and included results in the first annual report. During the recent year, we completed further experiments to investigate the RENCA tumor microenvironment and modulation by vaccine and tasquinimod treatment.

In the first annual report, we demonstrated that RENCA Foxp3 vaccine, but not RENCA cell vaccine, reduced tumor infiltrating Tregs. Here we report the regulation of tumor Tregs by combination strategy. We prepared cell suspension from tumor piece and focus analyzing the different infiltrating immune cell populations. Here in the combination study we observed similar that only RENCA Foxp3 vaccine induced reduction of number of Tregs in tumors. However, tasquinimod treatment seems slightly increased Tregs infiltration. Although in tasquinimod single, or RENCA vaccine and tasquinimod combination Treg increases were not statistically significant, tasquinimod in the RENCA Foxp3 and tasquinimod combination restored the Tregs from a lower level to numbers comparable to that in vehicle group (Fig. 8).
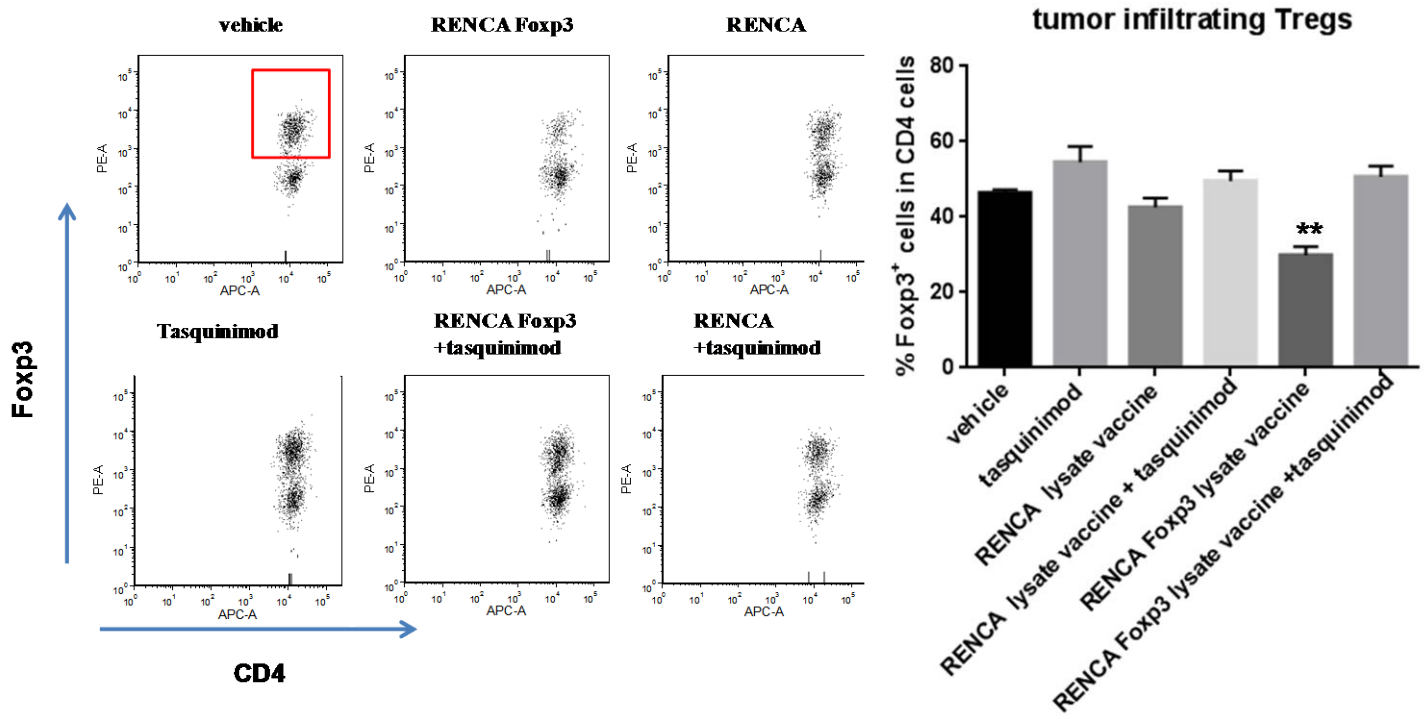
A

B

Figure 8 Effect of vaccine and tasquinimod on tumor infiltrating Tregs. Tumors were harvested from differentially treated mice. Single cell suspensions then were prepared from tumor pieces and subject to immunofuorescence staining and flow analysis. A. flow plots show gating of the infiltrating Tregs. Example: the population in red rectangle in the first plot. B. Quantification of infiltrating Tregs with different treatment. ** $p < 0.01$.

This "side effect" of tasquinimod was probably responsible to the result that tasqunimod didn't further enhance the anti-tumor effect of RENCA Foxp3 vaccine, although tasquinimod has potential to inhibite or modulate multiple myeloid immunosuppressive population in tumors. Tasquinimod did added further benefit in survival study. The slightly "Tregs-promoting" effect compromised its benefit in therapeutic study, probably due to shorter treatment time span.

We also measured the Tregs cells in peripheral blood sample. Tasquinimod slightly increased Tregs in blood, shown in Figure 9B as increased numbers (changes were not significant between RENCA only and RENCA, tasquinimod combination). Interestingly, tasquinimod moderately, but significantly reduced Foxp3 expression level (as Foxp3 MFI) in combination, as compared to vaccine single treatments (Fig. 9C). We have reported that tasquinimode had Tregs promoting effect in other model (Appendices).

A
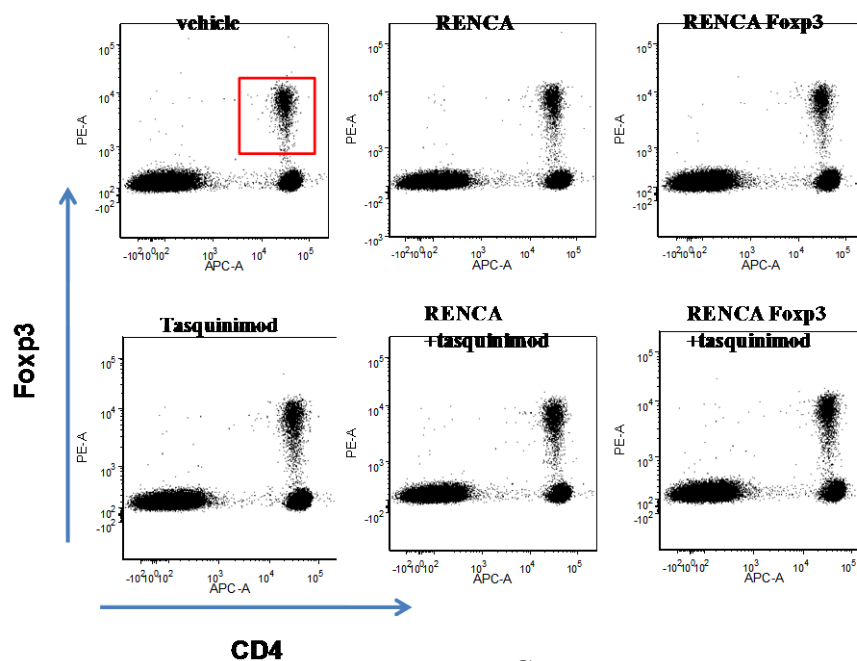
B
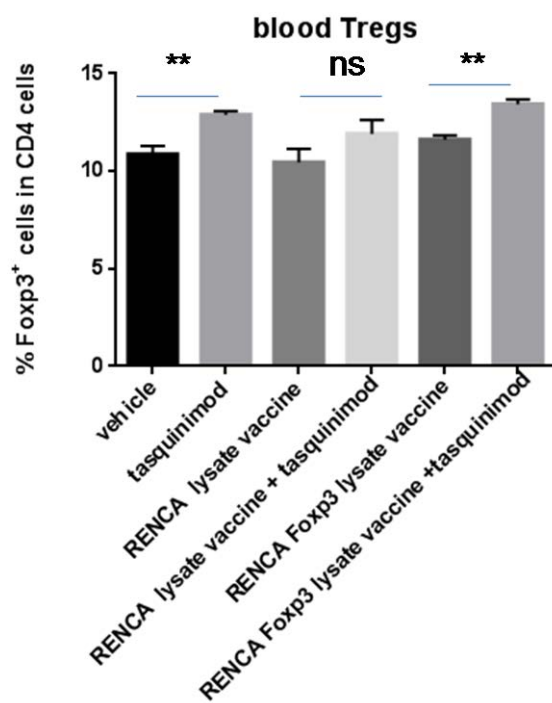
C
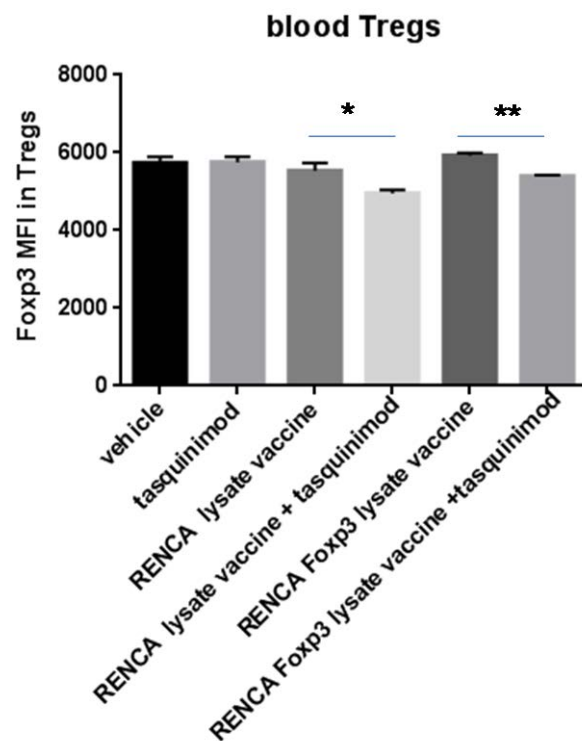
Figure 9 Effect of vaccine and tasquinimod on peripheral blood Tregs. Blood samples were harvested from differentially treated mice and subject to immunofluorescence staining and flow analysis. A. flow plots show gating of the infiltrating Tregs. Example: the population in red rectangle in the first plot. B. Quantification of numberinfiltrating Tregs with different treatment. C. quantification of Foxp3 level in Tregs. (as mean fluorescence intensity). $* p < 0.05$, $** p < 0.01$.

Next, we characterized the phenotype of tumor infiltrating myeloid populations, and access modulation of these populations by different treatments. Again we first focused on myeloid population in the tumor microenvironment (Fig. 10).
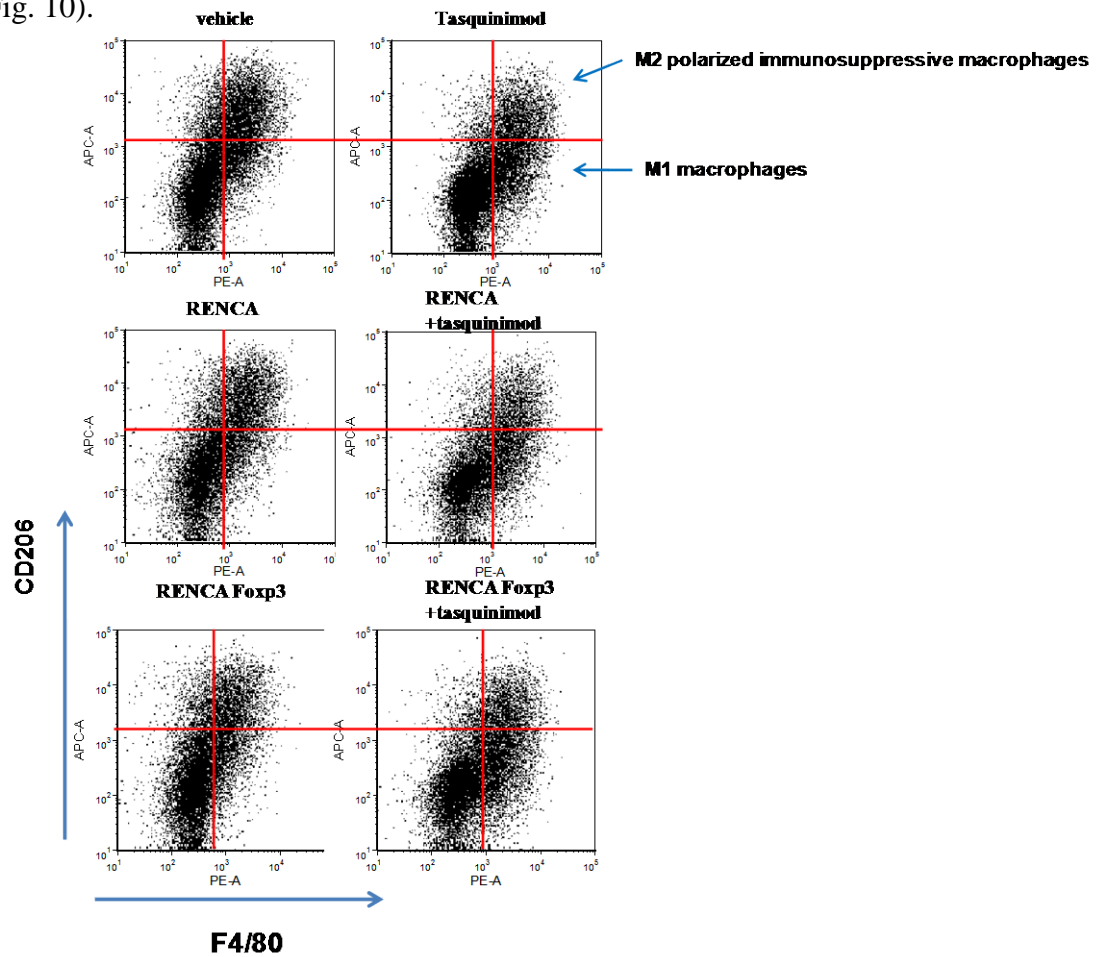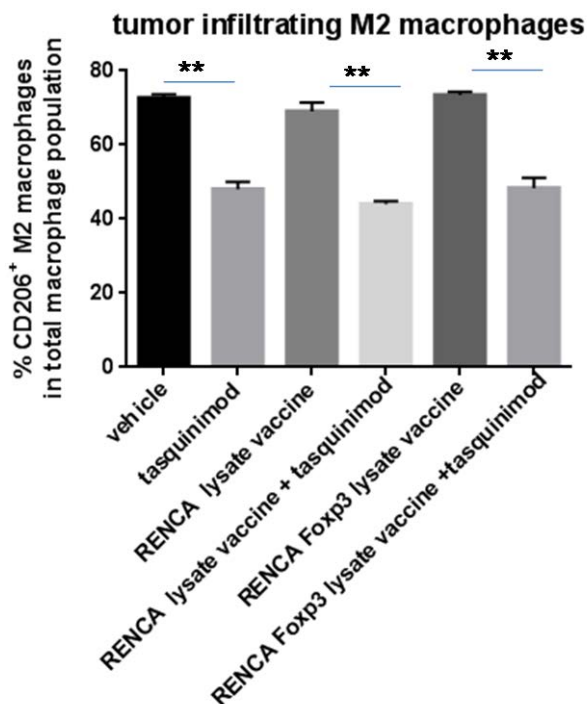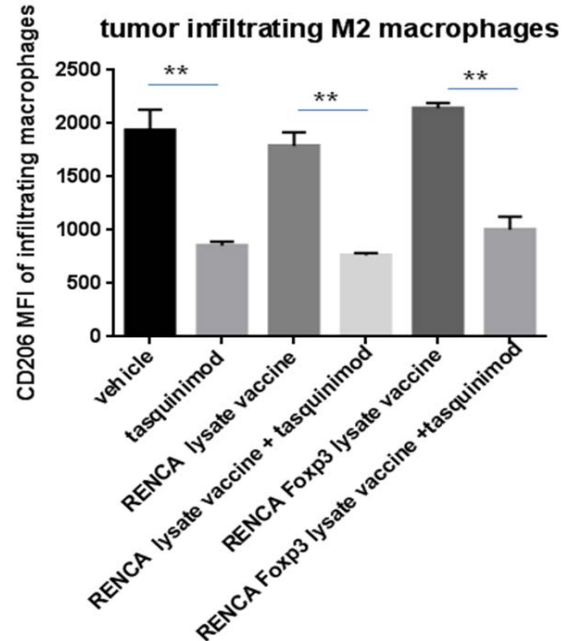

Figure 10 Effect of vaccine and tasquinimod on tumor infiltrating macrophages. Tumors were harvested from differentially treated mice. Single cell suspensions then were prepared from tumor pieces and subject to immunofuorescence staining with macrophage surface markers (F/80 and CD206, etc.) and flow analysis. A.

flow plots show gating of the infiltrating macrophage (F4/80), as well as M2 polarized macrophage (CD206 positive macrophages (upper right). B. Quantification of numbers of infiltrating M2 polarized macrophages with different treatment. C. quantification of CD206 expression level (as MFI) in total macrophage populations ** $p < 0.01$.

As shown in Figure 10, tasquinimod treatment, as single or in combinations) significantly reduced immunosuppressive, M2 polarized macrophages, as reduced numbers or as overall lower CD206 level in total macrophages (CD206 is a surface marker for M2 polarized macrophages). This strong M2 macrophage targeting effect of tasquinimod may counteract with its modest Treg promoting "side effect" to show benefit in survival study.

We also access MDSC populations in the tumor microenvironment. Tasquinimod also reduced tumor infiltrating $Gr1^+CD11b^+$ MDSCs, as single treatment, even more dramatically when in combination with vaccine treatment (Fig. 11).
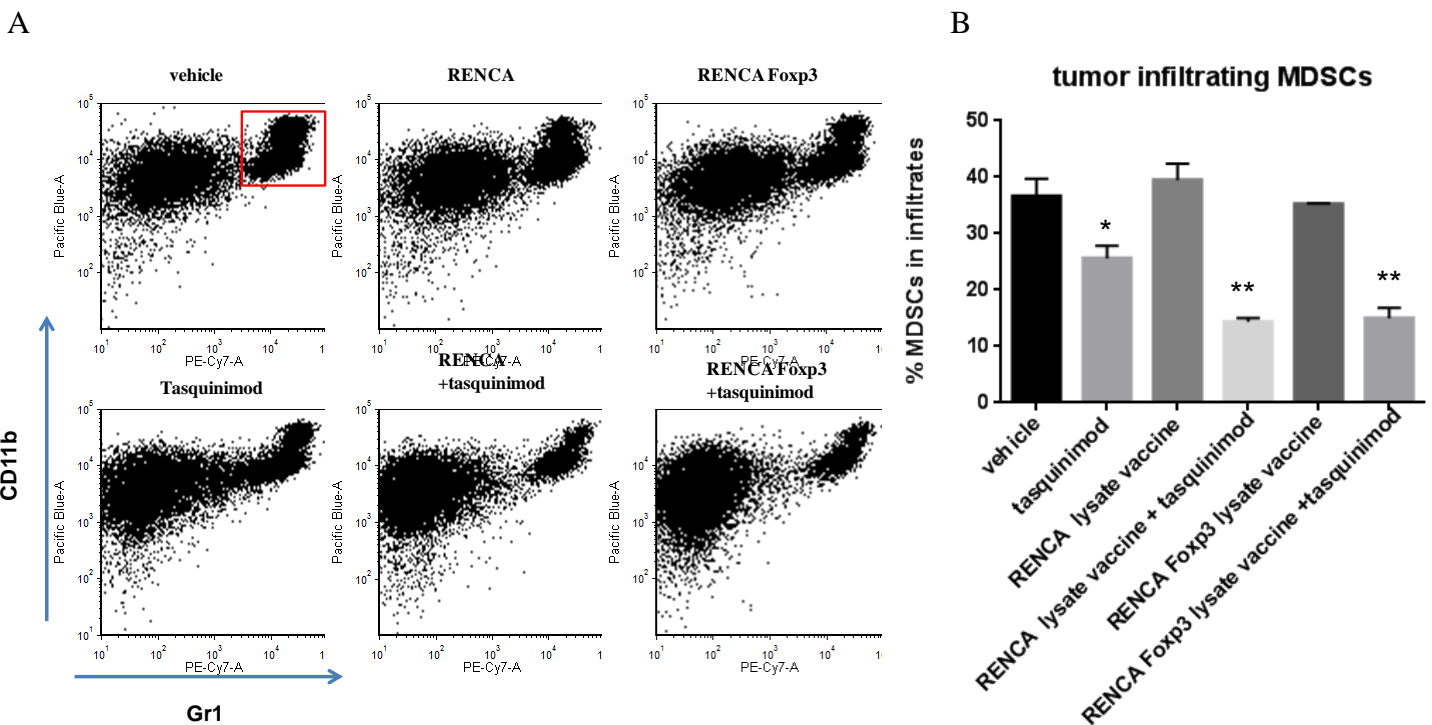
Figure 11. Effect of vaccine and tasquinimod on tumor infiltrating MDSCs. Tumors were harvested from differentially treated mice. Single cell suspensions then were prepared from tumor pieces and subject to immunofuorescence staining and flow analysis. A. flow plots show gating of the infiltrating MDSCs: the population in red rectangle in the first plot. B. Quantification of infiltrating MDSCs with different treatments. *$p < 0.05$, ** $p < 0.01$.

In addition to FACS analysis of tumor suspension, we also tried as planned to access tumor microenvironment in situ with Immunohistochemistry (IHC). Some antigen staining worked, such as CD206 M2 macrophage staining. The IHC results demonstrated significant reduction of CD206 cells in the tumor sections (Fig. 12). This result supported our result from flow cytometry experiment (Fig. 10).
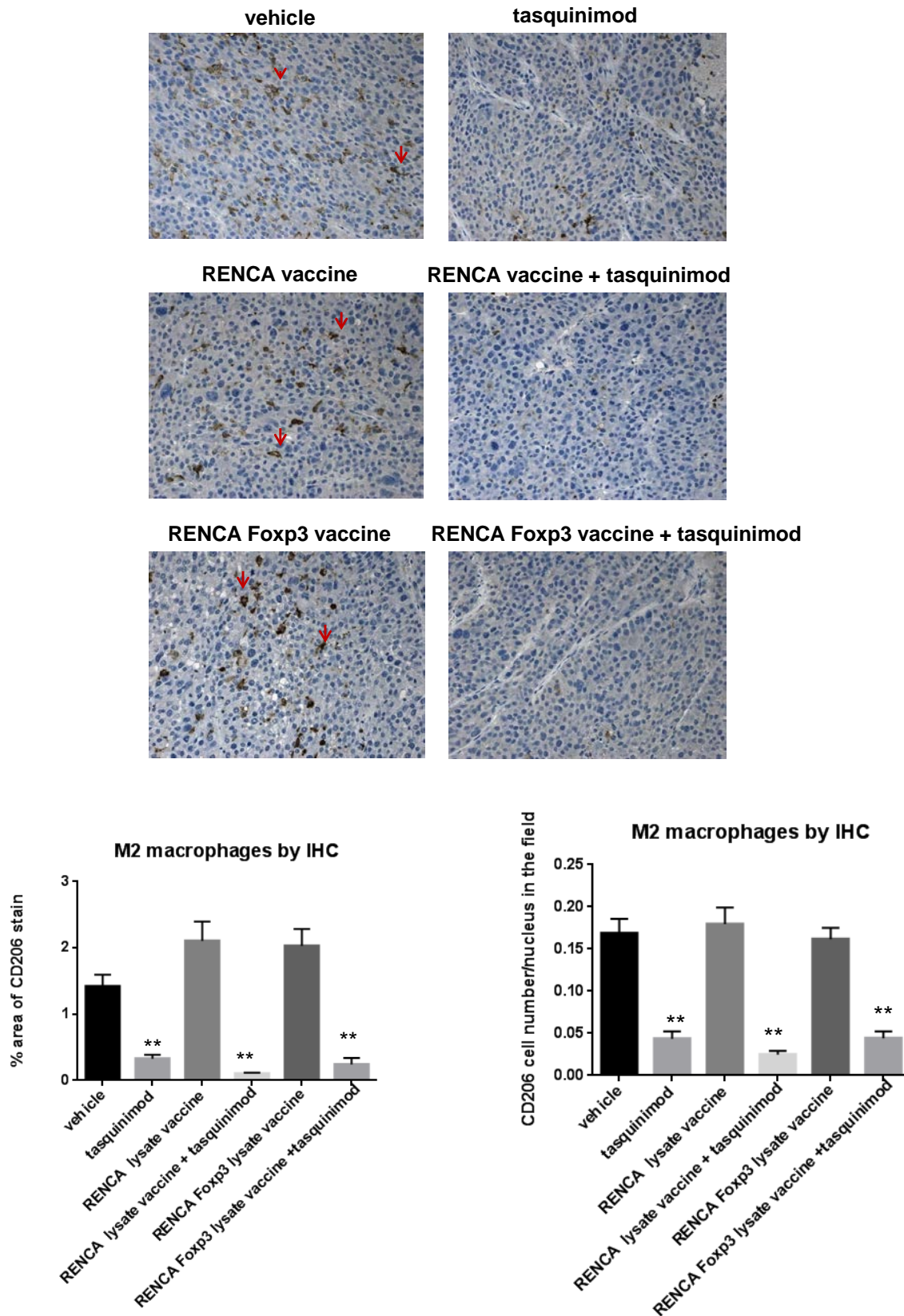
Figure 12. IHC experiment demonstrated reduction of tumor infiltrating M2 macrophages by tasquinimod. Tumors pieces were paraffin embedded and cut to 5uM sections, and subject to immunohistochemistry staining. A. representative CD206 staining from different treatment groups. Red arrows point to typical staining. B. quantification based on percentage of CD206 stain of total tumor field area. C. quantification as number of CD206 stained cells normalized to total number of nuclei in the field. ** $p < 0.01$

In addition, we have perform several other antigens, including activated caspase 3 (apoptosis marker), IL-10 (immunosuppressive cytokine), CD4 (effector T cell infiltrates), Foxp3 (Tregs), Gr1 (MDSCs). During test run, all the antigen staining were successful (see Figure 13). However, the staining of whole sets of the samples later were not working. We tried 3 times and used three different protocols, including different signal applification systems. These efforts were not successful. IHC was proposed as an alternative or supporting method to FACS analysis of tumor microenvironment. We did have success on FACS analysis, so we can work on IHC when we publish the study.

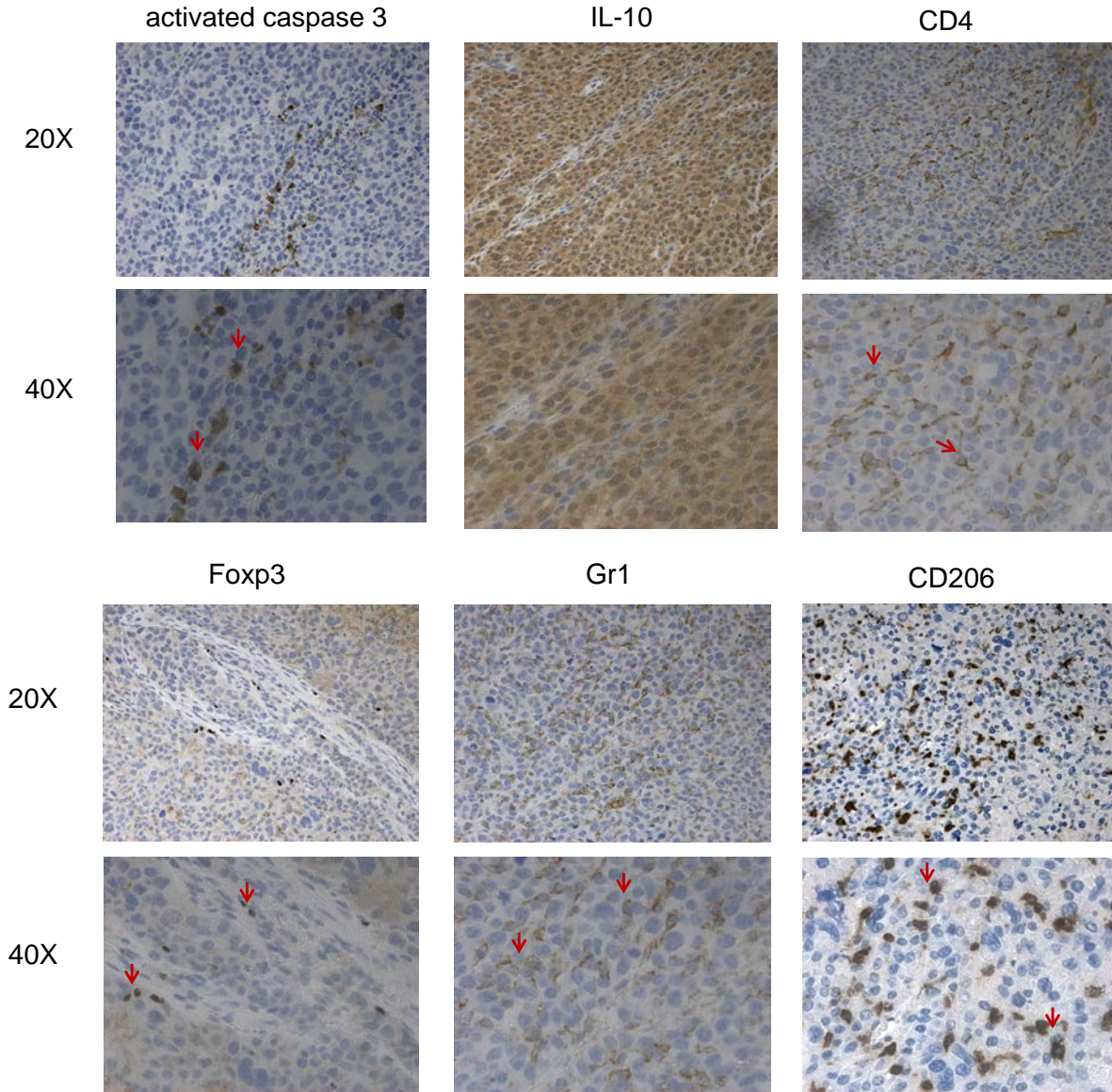**Figure 13.** IHC stainings of multiple antigens to analyze *in situ* tumor immune microenvironment . Tumors pieces were paraffin embedded and cut to 5uM sections, and subject to immunohistochemistry staining. Red arrows point to typical staining.

Task 3: Study the mechanisms by which tasquinimod suppresses MDSCs, and search additional molecular targets. (Month 17-24)

Results from this study and from our other reports (Appendices) suggests anti-inflammatory agent tasquinimod has potent activity to inhibit suppressive myeloid cells in the tumor microenvironment, modulate immune response and facilitating cancer immunotherapies. Specifically, tasquinimod reduces infiltration of MDSCs and M2 polarized macrophages in tumor, and impair their suppressive functions. The direct molecular target of tasquinimod is S100A9, an inflammatory protein. Receptors for S100A9 include TLR4 and RAGE, which are expressed on myeloid cells (monocytes, DC, MDSCs, macrophages) and endothelial cell, tumor cells. Both TLR4 and RAGE signing pathways are involved in myeloid cell accumulation, differentiation, and function. We planned to investigate regulation of suppressive myeloid cell through a high throughput approach, RNA sequencing, or whole transcriptome shotgun sequencing. Here we present the results from RNA Seq analysis of tumor infiltrating myeloid cells.

RENCA Luc tumor bearing mice were treated with vehicle or tasquinimod for 2.5 weeks. Tumors were excised and prepared into cell suspension. Infiltrating myeloid cells were isolated from suspension with anti-CD11b magnetic beads (Miltenyi Biotec). RNA were extracted from isolated CD11b cells and used for sequencing experiment. We have prepared six biological repeats for each treatment group. Here is the working flow for the experiment and analysis (Fig. 14).
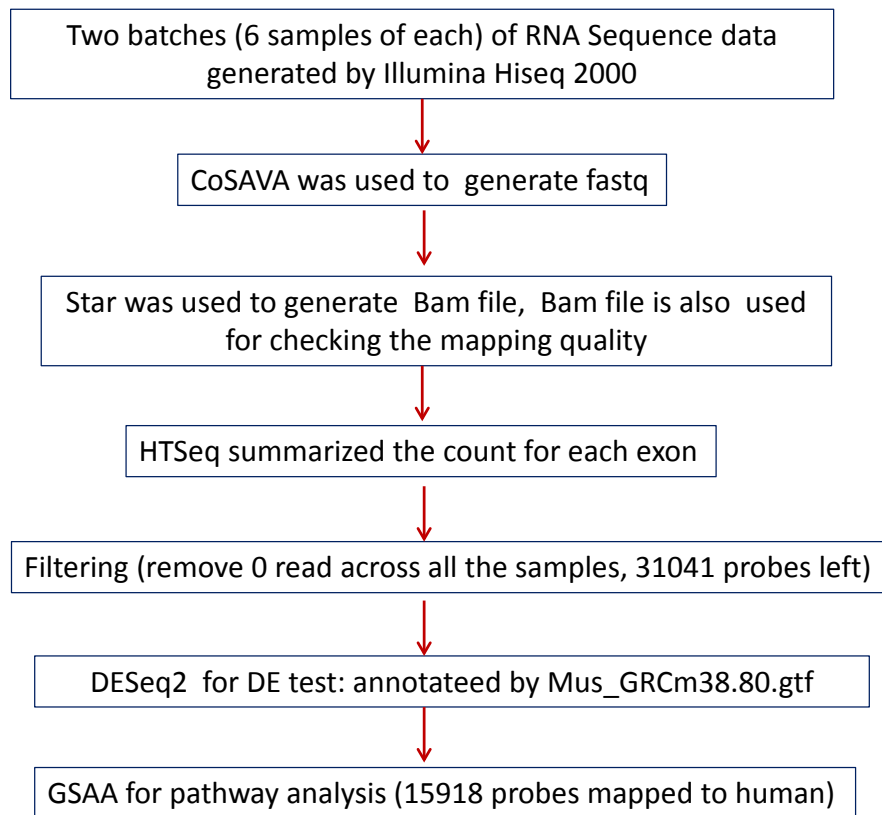

Figure 14. RNA sequencing work flow.

Probe-by-probe analysis revealed differential expressed genes from treated vs.vehicle group. Tasquinimod treatment led to 1723 up regulated with at least 2 fold change, and 1996 down regulated with at least 2 fold change. We checked differentially expressed genes in pathways in GSAA database, with **focus on immunological signature collection.**

GSAA pathway analysis show up-regulation of 137 gene sets are significantly associated with tasquinimod treated expression phenotype at nominal p value <0.01. With tasquinimod treated expression phenotype, up-regulation of 275 gene sets are significantly associated at nominal p value <0.05. On the other hand, 87 gene sets and 153 gene sets are significantly down-regulated at nominal p value <0.01 and <0.05, respectively.

In Figure 15 and Figure 16, we summarized top 20 significantly up-regulated or down-regulated gene sets, respectively.

	GS follow link to MSigDB	GS	SIZE	AS	NAS	NOM p-val	FDR q-val	FWER p-	RANK AT
1	GOLDRATH_EFF_VS_MEMORY_CD8_TCELL_UP	Details ...	190	-0.41771	-1.87305	0	0.003966552	0.018	3438
2	GSE17974_IL4_AND_ANTI_IL12_VS_UNTREATED_12H_ACT_CD4_TCELL_DN	Details ...	141	-0.43209	-1.88436	0	0.00470121	0.016	2430
3	GSE30962_PRIMARY_VS_SECONDARY_ACUTE_LCMV_INF_CD8_TCELL_UP	Details ...	189	-0.41399	-1.84729	0	0.005825564	0.032	4262
4	GSE20366_EX_VIVO_VS_DEC205_CONVERSION_NAIVE_CD4_TCELL_UP	Details ...	186	-0.42452	-1.89124	0	0.006183968	0.014	1981
5	GSE17721_0.5H_VS_24H_CPG_BMDM_DN	Details ...	190	-0.39336	-1.78015	0	0.007275989	0.096	1781
6	GSE29618_MONOCYTE_VS_MDC_DAY7_FLU_VACCINE_DN	Details ...	179	-0.39793	-1.77466	0	0.00732606	0.102	2046
7	GSE11864_CSF1_PAM3CYS_VS_CSF1_IFNG_PAM3CYS_IN_MAC_DN	Details ...	161	-0.40159	-1.76838	0	0.007437471	0.112	2547
8	GSE1432_CTRL_VS_IFNG_24H_MICROGLIA_DN	Details ...	163	-0.39938	-1.7868	0	0.007456577	0.09	3443
9	GSE2706_2H_VS_8H_LPS_STIM_DC_DN	Details ...	157	-0.40422	-1.78696	0	0.008202235	0.09	3079
10	GSE36476_CTRL_VS_TSST_ACT_40H_MEMORY_CD4_TCELL_YOUNG_DN	Details ...	189	-0.39165	-1.78939	0	0.008526932	0.084	4358
11	GSE2706_UNSTIM_VS_8H_R848_DC_DN	Details ...	169	-0.3905	-1.75083	0	0.008671427	0.153	2648
12	GSE24142_EARLY_THYMIC_PROGENITOR_VS_DN2_THYMOCYTE_DN	Details ...	190	-0.39634	-1.79512	0	0.008816197	0.077	3476
13	GSE15750_DAY6_VS_DAY10_TRAF6KO_EFF_CD8_TCELL_UP	Details ...	186	-0.42812	-1.92434	0	0.008824304	0.01	3881
14	GSE22886_NAIVE_CD8_TCELL_VS_MONOCYTE_UP	Details ...	174	-0.39411	-1.75258	0	0.009048041	0.15	3759
15	GSE22886_TCELL_VS_BCELL_NAIVE_DN	Details ...	164	-0.4075	-1.79903	0.00128866	0.009200472	0.071	2357
16	GSE14000_UNSTIM_VS_4H_LPS_DC_DN	Details ...	168	-0.39098	-1.73888	0	0.009367971	0.174	2775
17	GSE16755_CTRL_VS_IFNA_TREATED_MAC_DN	Details ...	174	-0.40284	-1.80259	0	0.009563476	0.063	3481
18	GSE1432_CTRL_VS_IFNG_6H_MICROGLIA_DN	Details ...	175	-0.39152	-1.75299	0	0.009592192	0.149	3197
19	GSE20715_0H_VS_6H_OZONE_TLR4_KO_LUNG_DN	Details ...	188	-0.38156	-1.73395	0	0.009849959	0.19	3246
20	GSE360_DC_VS_MAC_T_GONDII_UP	Details ...	163	-0.38475	-1.71945	0	0.012179547	0.237	1969

Figure 15 In infiltrating myel;oid cells, top 20 up-regulated gene sets by tasquinimod treatment.

	GS follow link to MSigDB	GS DETAILS	SIZE	AS	NAS	NOM p-val	FDR q-val	FWER p-val	RANK AT MAX
1	GSE10325_LUPUS_BCELL_VS_LUPUS_MYELOID_DN	Details ...	183	0.411789	2.105621	0	0	0	2183
2	GSE15767_MED_VS_SCS_MAC_LN_UP	Details ...	188	0.425808	2.187678	0	0	0	2270
3	GSE29618_BCELL_VS_MONOCYTE_DAY7_FLU_VACCINE_DN	Details ...	187	0.417993	2.130092	0	0	0	2734
4	GSE9988_ANTI_TREM1_VS_LPS_MONOCYTE_UP	Details ...	180	0.411588	2.092847	0	0	0	2580
5	GSE9988_ANTI_TREM1_VS_LOW_LPS_MONOCYTE_UP	Details ...	175	0.391799	1.980367	0	0	0	2580
6	GSE22886_NAIVE_CD8_TCELL_VS_MONOCYTE_DN	Details ...	186	0.373381	1.912476	0	1.67E-04	0.001	2192
7	GSE22886_NAIVE_TCELL_VS_MONOCYTE_DN	Details ...	184	0.375046	1.925551	0	1.91E-04	0.001	2542
8	GSE9988_LOW_LPS_VS_ANTI_TREM1_AND_LPS_MONOCYTE_DN	Details ...	167	0.385181	1.965062	0	2.23E-04	0.001	2570
9	GSE14769_UNSTIM_VS_120MIN_LPS_BMDM_UP	Details ...	171	0.369204	1.865581	0	4.01E-04	0.003	4603
10	GSE14769_40MIN_VS_360MIN_LPS_BMDM_UP	Details ...	182	0.3649	1.870893	0	4.46E-04	0.003	4651
11	GSE13485_DAY3_VS_DAY21_YF17D_VACCINE_PBMC_UP	Details ...	167	0.3624	1.833231	0	5.63E-04	0.005	3233
12	GSE16755_CTRL_VS_IFNA_TREATED_MAC_UP	Details ...	174	0.369988	1.835781	0	6.14E-04	0.005	3178
13	GSE22886_NAIVE_BCELL_VS_MONOCYTE_DN	Details ...	185	0.358262	1.804288	0	6.19E-04	0.006	3507
14	GSE36476_CTRL_VS_TSST_ACT_72H_MEMORY_CD4_TCELL_OLD_UP	Details ...	166	0.339803	1.7229	0	0.001613584	0.019	2374
15	GSE29618_BCELL_VS_MONOCYTE_DN	Details ...	189	0.336303	1.726295	0	0.001721156	0.019	3644
16	GSE14769_20MIN_VS_360MIN_LPS_BMDM_UP	Details ...	189	0.337907	1.729789	0	0.001747729	0.018	3525
17	GSE10325_BCELL_VS_MYELOID_DN	Details ...	175	0.335143	1.701751	0	0.002886793	0.038	2486
18	GSE29618_MONOCYTE_VS_MDC_DAY7_FLU_VACCINE_UP	Details ...	182	0.335335	1.704346	0	0.002976727	0.037	1839
19	GSE10856_CTRL_VS_TNFRSF6B_IN_MACROPHAGE_UP	Details ...	160	0.339489	1.690955	0	0.003604797	0.05	3385
20	GSE14769_UNSTIM_VS_80MIN_LPS_BMDM_UP	Details ...	182	0.333017	1.68835	0	0.003624385	0.053	4618

Figure 16 In infiltrating myeloid cells, top 20 down-regulated gene sets by tasquinimod treatment.

First of all, our analysis successfully captured gene sets involved in stimulation and differentiation of myeloid cell linage. Gene set 4, 8, 9, 10, 20 from down-regulated gene set list are the gene sets associated with LPS stimulated myeloid cells. For example, Gene set GSE9988_ANTI_TREM1_VS_LPS_MONOCYTE_UP is a set of genes up-regulated in comparison of monocytes treated with anti-TREM1 versus monocytes treated with 5000 ng/ml LPS (TLR4 agonist). Since tasquinimod target TLR4 ligand and block TLR signaling, it is reasonable that down-regulation of this set is associated with tasquinimod treated phenotype. The association plot and heat map show down-regulation of core enriched genes (Figure 17).

Many significantly change gene sets on the list is related to differentiation of monocytes and macrophages, such as gene set 1, 6, 7 from Figure 16. For example, gene set GSE22886_NAIVE_TCELL_VS_MONOCYTE_DN is a gene set that are down-regulated in comparison of naive CD4, CD8 T cells versus monocytes. Therefore, these genes are down-regulated in monocyte lineage, as compared to CD4, CD8 cells. So tasquinimode treatment down-regulate this gene set, promote monocyte lineage differentiation. **Figure 18** shows that treatment down regulated the core enriched genes from this gene set.
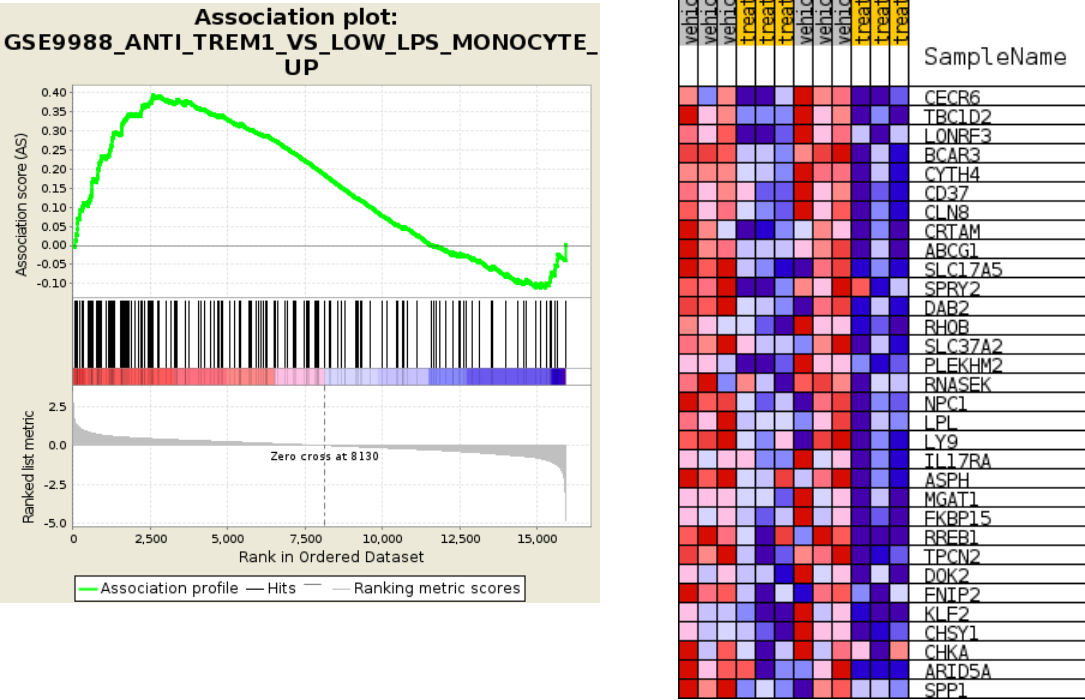
Figure 17. Gene set GSE9988_ANTI_TREM1_VS_LPS_MONOCYTE_UP is down-regulated with tasquinimod treatment.
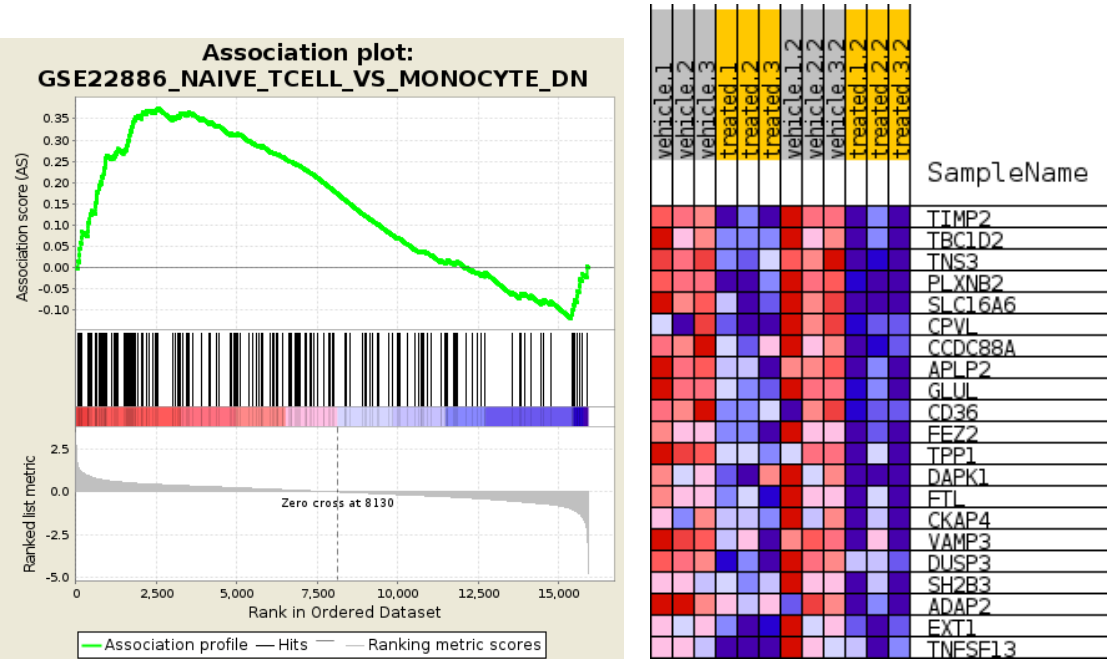

Figure 18. Gene set GSE22886_NAIVE_TCELL_VS_MONOCYTE_DN is down-regulated with tasquinimod treatment.

25

Interestingly, our analysis enriched gene sets that are related to effects of tasquinimod on myeloid cell function, such as TLR downstream signaling, antigen presenting cell function, Interferon responses, as well as TAM function. For example, from up-regulated gene set list, gene set GSE15750_DAY6_VS_DAY10_TRAF6KO_EFF_CD8_TCELL_UP is a set up-regulated in comparison of wild type CD8 effector T cells at day 6 versus those from mice deficient for TRAF6 at day 10. TRAF6 is a factor in TLR pathway, knockout this gene will mimic the block of TLR signal, which may be induced by tasquinimod treatment. Therefore, it is reasonable this set is up-regulated in TRAF6 deficient mice and also in tasquinimod treatment condition (Figure 19).
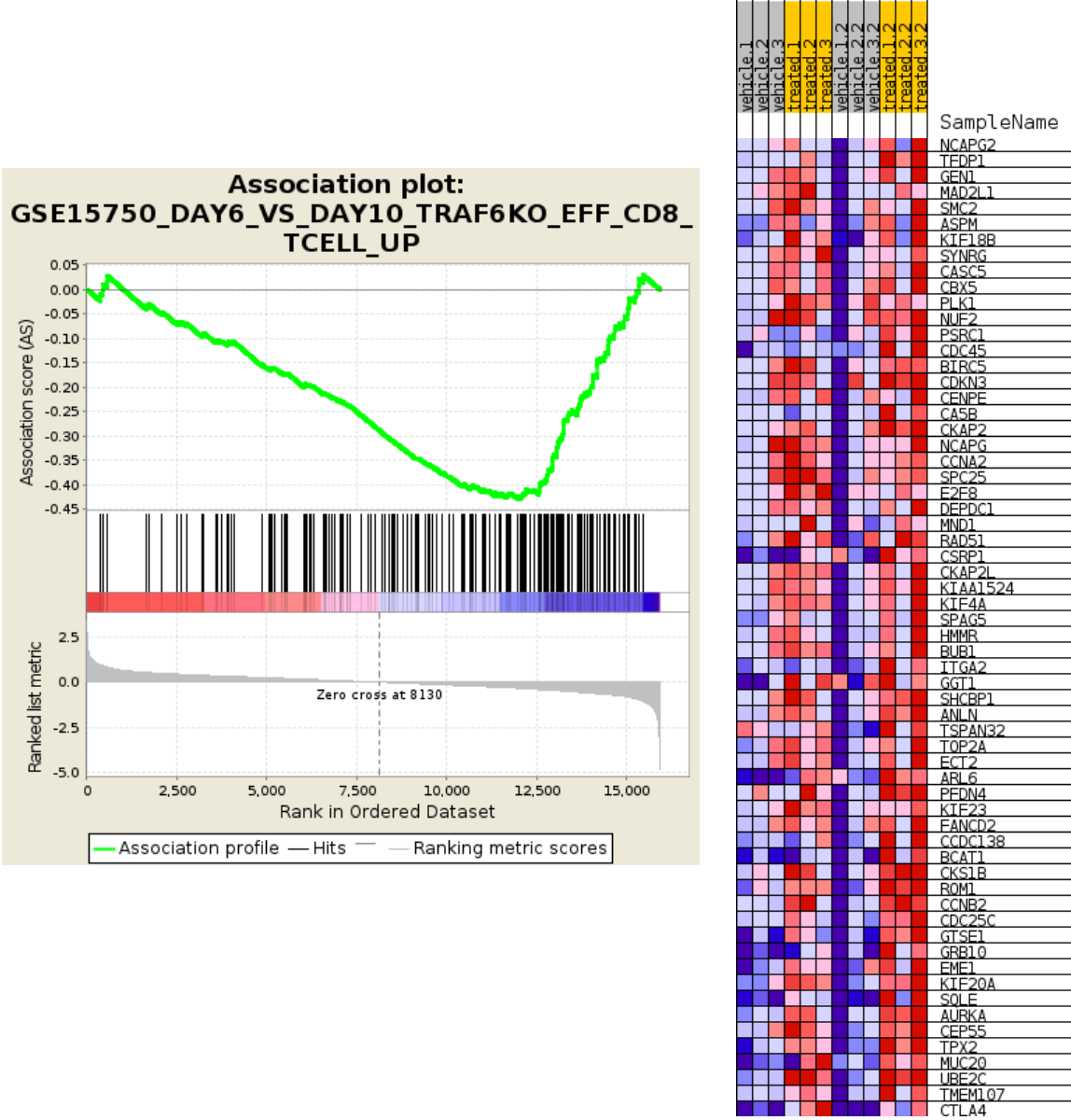

Figure 19. Gene set GSE15750_DAY6_VS_DAY10_TRAF6KO_EFF_CD8_TCELL_UP is up-regulated with tasquinimod treatment.

An enriched gene set, GSE10856_CTRL_VS_TNFRSF6B_IN_MACROPHAGE_UP (number 19 in Figure 16), is related to TAM differentiation. This is a set of gene up-regulated in comparison of macrophages treated with control (hIgG1) versus those treated with TNFRSF6B (DcR3). TNFRSF6B (DcR3) has been found to contribute to development of TAMs. The gene set up-regulated after DcR3 treatment was down-regulated in tasquinimod treated condition, which coincide with the fact that tasquinimod decreased suppressive TAMs.

Figure 20 display that the core enriched genes in this gene set are down-regulated in tasquinimod treated condition.
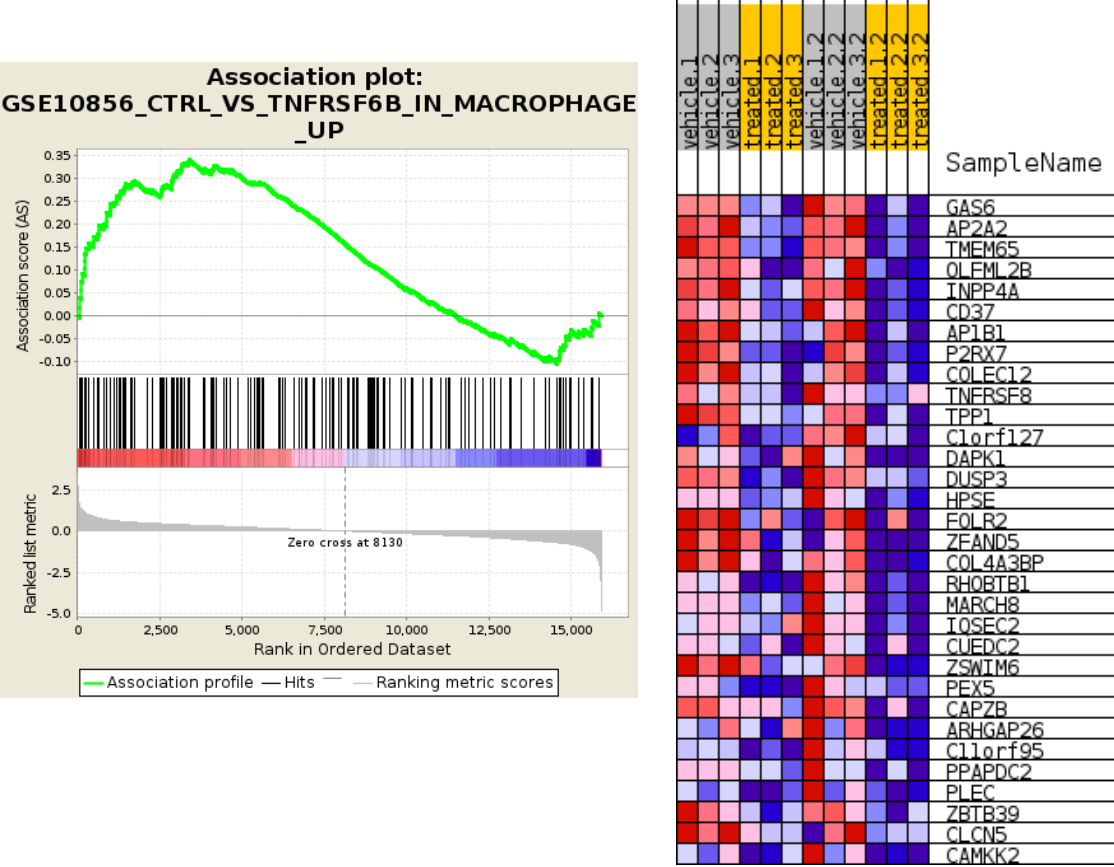

Figure 20. Gene set GSE10856_CTRL_VS_TNFRSF6B_IN_MACROPHAGE_UP is down-regulated with tasquinimod treatment.

Most excitingly, RNASeq experiment can reveal multiple unexpected, previously unknown clues, or mechanism of action of tasquinimod, such as regulation of interferon responses, regulation of memory status of effector cells, and answers to how tasquinimod regulate Tregs, which we previously didn't understand through cellular experiments. For example, gene set GOLDRATH_EFF_VS_MEMORY_CD8_TCELL_UP (number 1 set in Figure 15 is a set of gene up-regulated in comparison of effector CD8 T cells versus memory CD8 T cells. Core enriched genes in this gene set is up-regulated in tasquinimod condition (Figure 21), which suggest that tasquinimod may promote memory status of effector cells.

Another example is gene set GSE20366_EX_VIVO_VS_DEC205_CONVERSION_NAIVE_CD4_TCELL_UP (number 4 gene set in Figure 15). This gene set is up-regulated in comparison of TconvLP versus DEC-Pept CD25-. DEC-Pept CD25- can convert CD4+ CD25- cells to Tregs *in vivo*. Since tasquinimod up-regulated genes (core enriched ones) in this set (Figure 22) and show activity to promote Tregs, investigate core enriched genes in this set can potentially reveal the critical genes and mechanism underlying tasquinimod's Treg-promoting activity.
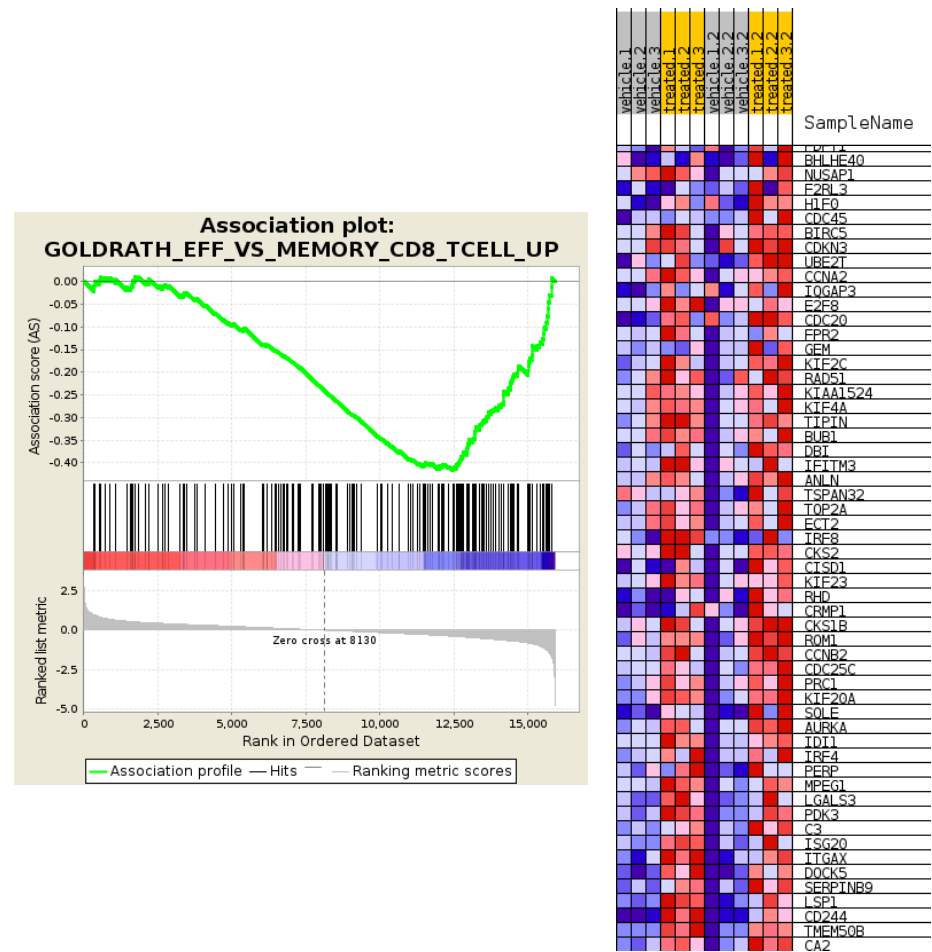
Figure 21. Gene set GOLDRATH_EFF_VS_MEMORY_CD8_TCELL_UP is up-regulated with tasquinimod treatment.

In summary, RNASeq experiment revealed multiple mechanisms for immunomodulatory activities of tasquinimod. The analysis enriched genes and signaling pathways worth further future investigation. Some of them are not previously identified for tasquinimod through ours and other's work.

Task 4: Data collection and statistical analysis. (Month 8-24)

Data collection and statistical analysis has been completed and incorporated in descrption of tasks above.

28
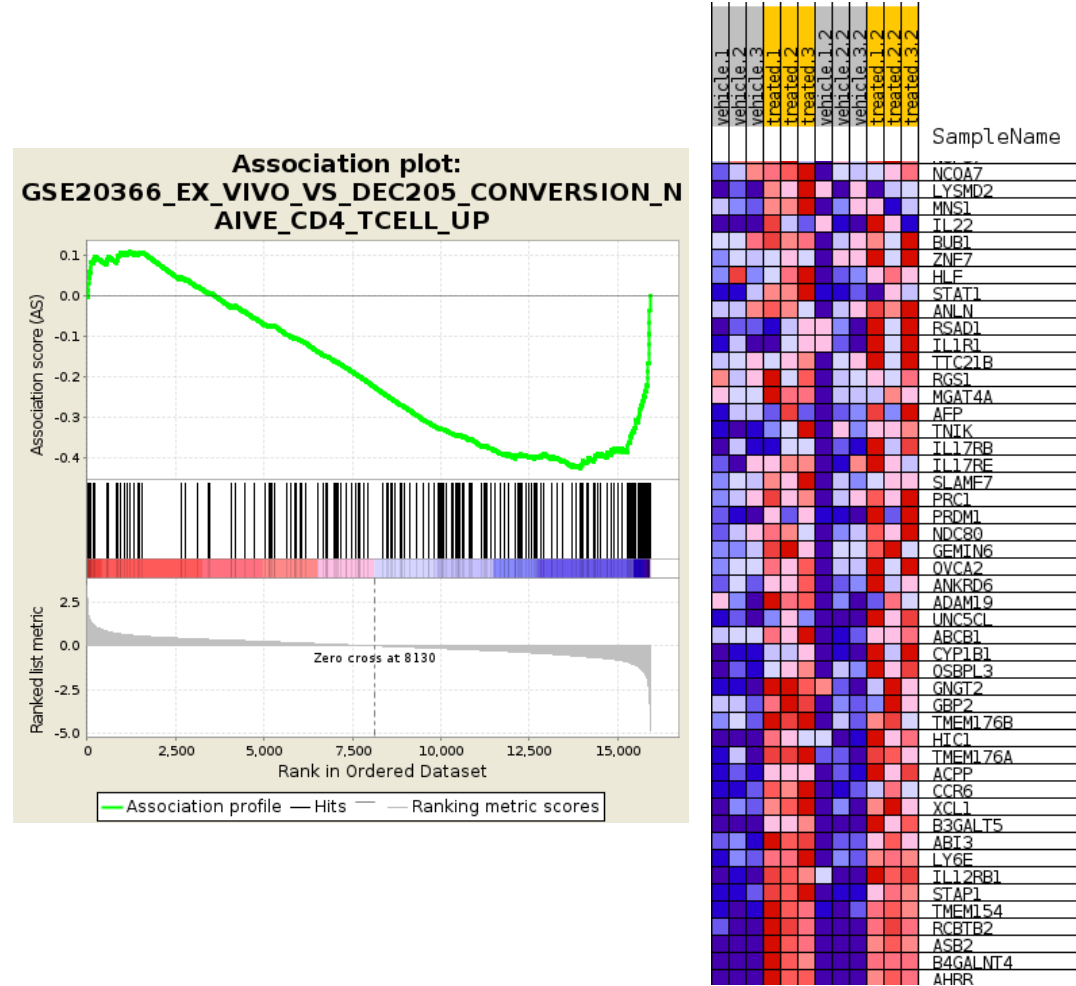
Figure 22. Gene set <u>GSE20366_EX_VIVO_VS_DEC205_CONVERSION_NAIVE_CD4_TCELL_UP</u> is up-regulated with tasquinimod treatment.

Key Research Accomplishment:

1. During second year of award period, our research team demonstrated tasquinimod, a S100A9 inhibitor and anti- inflammatory agent, potently modulated tumor immune microenvironment, and enhanced vaccine therapy by prolonged survival of tumor bearing host.

2. RNA sequence experiment with tumor infiltrating myeloid cells reveals novel mechanisms underlying tasquinimod actions. This is one of limited reported gene profiling with immune infiltrate, not with tumor cells. Critical pathway analysis provides foundation for future development of more specific approach to target immune suppressive populations.

Conclusions:

Our results showed the novel, tumor cell and Treg dual-targeting, RENCA Foxp3 tumor cell vaccine had significant anti-tumor activity against established tumor growth in an intervention setting of experiment. Novel anti-inflammatory agent, tasquinimod, had further benefit to prolong survival of tumor-bearing host. This accomplishment and finding from the research are exciting. Since the study focus on targeting established tumor, our approach can be readily translated into clinical setting, to benefit patient with establish disease and may have higher success rate in patient with advanced and metastatic disease. The strategy is also expected to be a candidate therapy for patients who have surgery to prevent recurrent and metastatic disease.

Importantly, we proved that a specific vaccine strategy can be used to target immunosuppressive Tregs in cancer therapy setting, which have not been reported previously by other groups. We demonstrated the potential potent immunomodulatory activity of tasquinimod, and suggesting novel actions of the agent such as modulation of Tregs and effector T cell memory status. Moreover, our study is one of the very limited reported studies to perform gene profiling of tumor infiltrating immune cell populations, which are most relevant components of tumor microenvironment. All these accomplishments, supported by this career development award, will have important impact in the immunotherapy and kidney cancer research field.

Publications, abstracts, and presentations:

A few publications/abstract resulted from the supported study.

1. Li Shen, Ashley Orillion, Remi Adelaiye, Eric Ciamporcero, Swathi Ramakrishnan, and Roberto Pili.

    Activity of a novel Foxp3-tumor cell vaccine in a murine model of renal cell carcinoma. Poster presentation. AACR annual meeting 2015.

There are two peer-reviewed journal publications during the award period. Although the experiments in the published papers are not directly supported by the award, there are overlap investigations on immunomodulatory activities of tasquinimod in both project supported by this award and published papers.

These papers are:

2. Shen L, Sundstedt A, Ciesielski M *et al*. Tasquinimod modulates suppressive myeloid cells and enhances cancer immunotherapies in murine models. *Cancer Immunol Res* 3(2), 136-148 (2015).

3. Shen L. and Pili R. Tasquinimod targets suppressive myeloid cells in the tumor microenvironment. *OncoImmunology.* 2015 **DOI:** 10.1080/2162402X.2015.1072672

Inventions, Patents, and Licenses: Nothing to report.

Reportable outcomes: RENCA Foxp3 cells were made to prepare vaccine.

Other Achievements: Nothing to report.

References: Nothing to report
.

Brief Description of Career Development:

PI of the study has completed proposed career/professional development activities during the award- supported period, as proposed in the award application.

First, PI kept regular meetings with mentor to discuss the project and progress, including regular weekly lab meeting and one on one meeting with mentor. Teleconferences were held when mentor was not local. Discussions were also held with other investigators/key personnel to promote progress of the supported project. PI closely worked with key facilities, such as mouse model core facility, flow cytometry and image core facility, and bioinformatics and biostatistics faculties.

Second, PI regularly participated and presented at seminars of GU program and Immunology program. Attended new technology development workshops, such as next generation sequencing, image stream, nanostring, etc…

PI also trained in workshops for professional development, such as one-on-one train for oral presentation, leadership workshop. PI was invited to give a talk at new faculty session of 2014 annual RPCI science retreat. Career development award also supported PI to attend 2015 AACR annual meeting to present results from supported project, and communicate with our researchers.

PI was recently appointed Assistant Professor of Oncology at RPCI upon completion of the award supported research.

Appendices:

See attached one poster and two peer-reviewed journal publications.

Activity of a novel Foxp3-tumor cell vaccine in a murine model of renal cell carcinoma

Li Shen[1], Ashley Orillion[1], Remi Adelaiye[1,2], Eric Ciamporcero[1], Swathi Ramakrishnan[1], and Roberto Pili[1,2]

[1]Genitourinary Program, Roswell Park Cancer Institute, Buffalo NY. [2]Department of Medicine, Indiana University, Indianapolis, IN

ABSTRACT

Introduction: Renal cell carcinoma (RCC) is the most common type of kidney cancer in adults and represents 80% of the cases. Treatment options for patients with advanced disease are limited. Targeted molecular therapies have shown survival benefit but most patients develop therapy resistance. Preclinical and clinical studies indicate that immunotherapies are effective and play a role in the treatment of advanced RCC. However, the response rate is ~ 20%, with a limited number of patients achieving durable remission. A major barrier to vaccine therapy is the presence of immunosuppressive cell populations including regulatory T cells (Tregs), myeloid-derived suppressor cells (MDSCs) and tumor-associated macrophages (TAMs).

Methods: We designed a tumor cell and Tregs dual-targeting vaccine by inducing Foxp3 expression in tumor cells, and tested this vaccine along with an unmodified vaccine in an orthotopic murine model of RCC, RENCA. Tumor cell lysates were administered via subcutaneous injection.

Results: Both RENCA cell vaccine and RENCA Foxp3 cell vaccine prevented tumor growth in 6 out 10 animals. Interestingly, in an intervention setting, the RENCA Foxp3 tumor cell vaccine was superior to the RENCA tumor cell vaccine with a significant anti-tumor activity (45% inhibition of tumor weights, p<0.01). Moreover, RENCA Foxp3 tumor cell vaccine reduced the number of tumor infiltrating Tregs (42% reduction, p<0.05) and Treg Foxp3 expression both in peripheral blood and tumor infiltrates. In summary, our results suggest that a strategy aimed to ablate Tregs and induce an antitumor response with a dual targeting vaccine strategy may be beneficial in established RCC. We also observed that suppressive myeloid cell (SMCs) populations dominate the established tumor microenvironment.

BACKGROUND

* Tregs are one of the major players in tumor immune tolerance. Studies have shown Tregs induction in cancer patients and Tregs expansion following immunotherapy. Clinical reports suggest that depletion of Tregs may enhance an antitumor immune response in cancer patients. (*Yokokawa, J et al Clin Cancer Res, 2008, 14 (4): 1032–40; Liyanage, UK et al, J Immunol, 2002, 169(5): 2756–61; Dannull, J et al, J Clin Invest, 2005, 115(12): 3623–33; Zhang, H et al, Nat Med, 2005, 11(11): 1238–43; Ahmadzadeh, M and Rosenberg, SA, Blood, 2006, 107(6): 2409–14.).

* We previously reported that a pharmacological approach, a class I HDAC inhibitor, entinostat, inhibited Foxp3 expression and suppressive function of Tregs, and enhanced cytokine and peptide vaccine therapy in murine models of renal cell carcinoma and prostate cancer, respectively (*Shen, L. et al, PLoS ONE, 2012, 7(1): e30815*)

* Autologous tumor cell vaccine have been in development for RCC. (*Kazuhiro, Y and Hirotsugu , U, International Journal of Urology, 2013, 20(8); Holtl , L et al, Clin Cancer Res, 2002, 8(11): 3369-76.*)
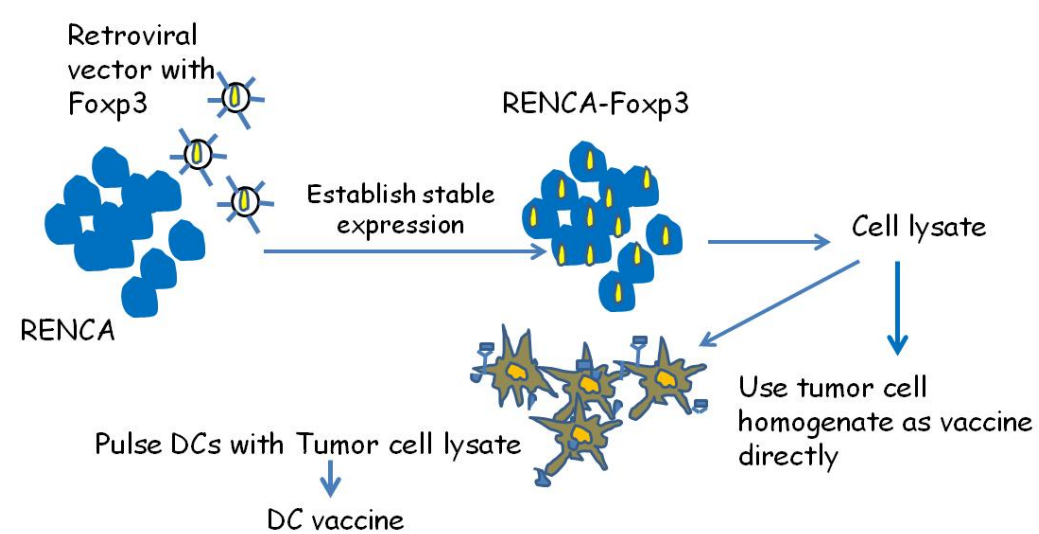
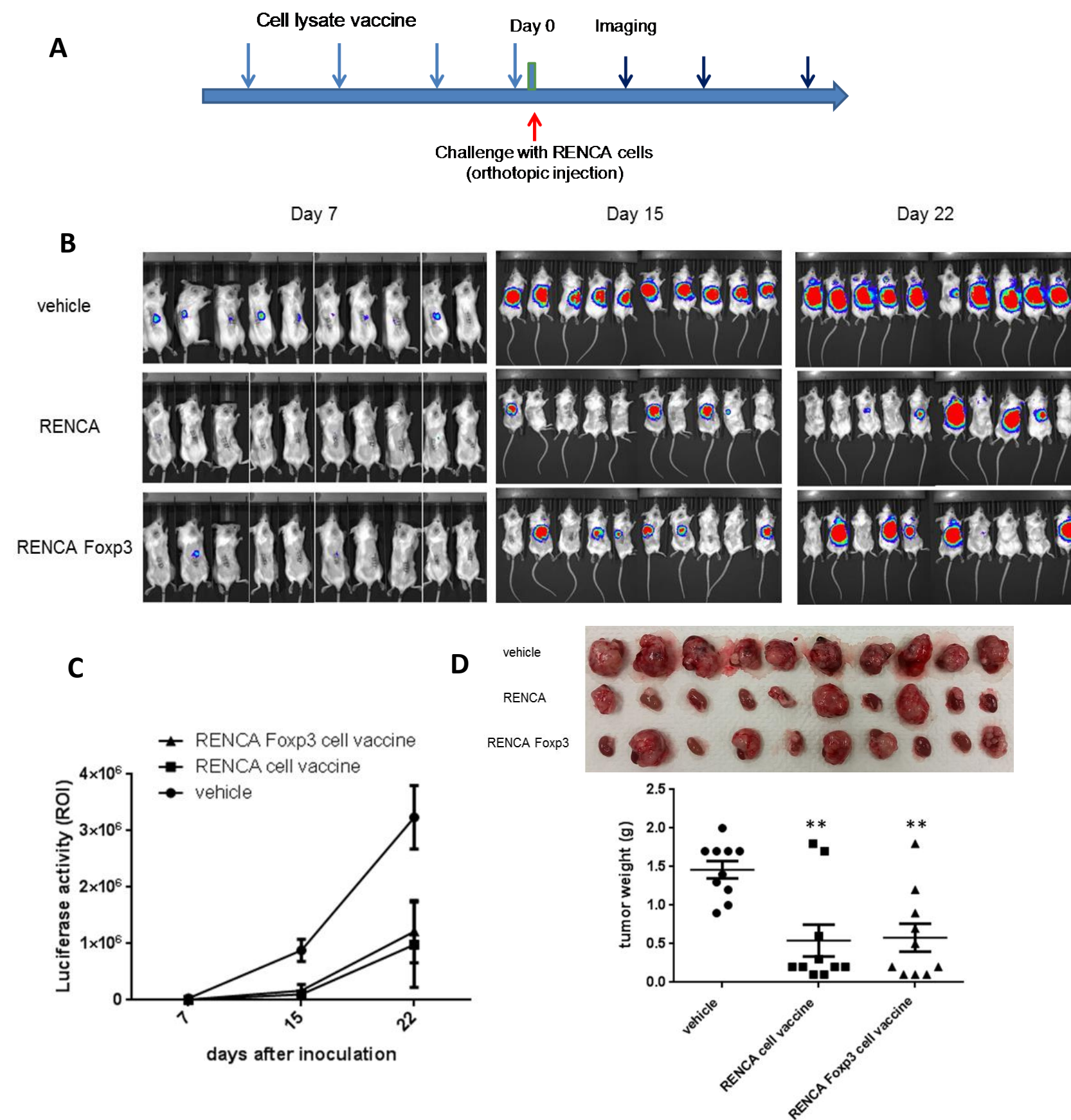## AKNOWLEDGEMENTS

RESULTS

Figure 2. Effects of tumor cell vaccines in a preventive schedule. Female Balb/C mice were randomly divided into three groups and received vehicle, RENCA, or RENCA Foxp3 tumor cell vaccine for three weeks, then inoculated with RENCA cells in the sub-capsular space of the right kidney. **A.** Preventive experiment schedule. **B**. Pictures show the image of three treatment groups taken at different time points. **C**. Quantification of imaging results, showing kinetics of orthotopic tumor growth. **D**. Top panel shows the picture of the tumors harvested from all groups at the end of treatment. Bottom panels show the end of experiment tumor weights. ** *p*< 0.01
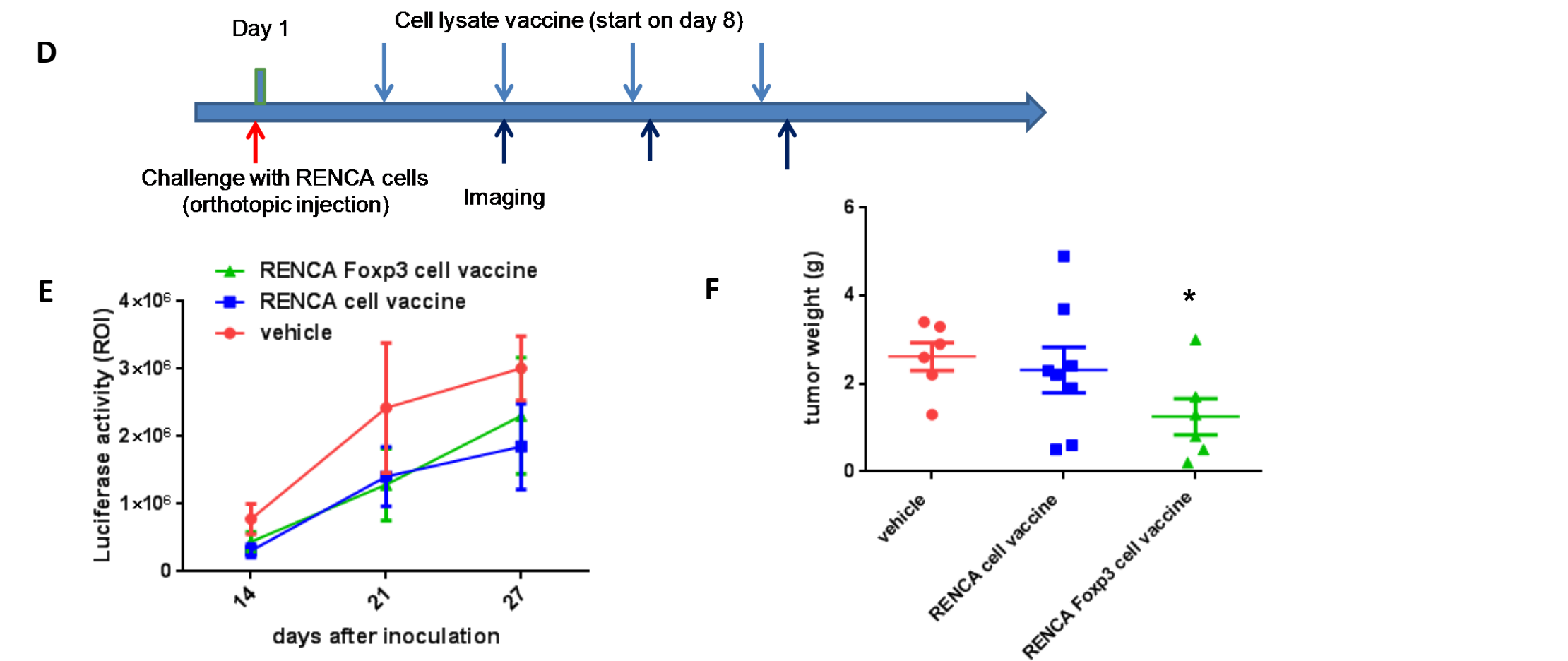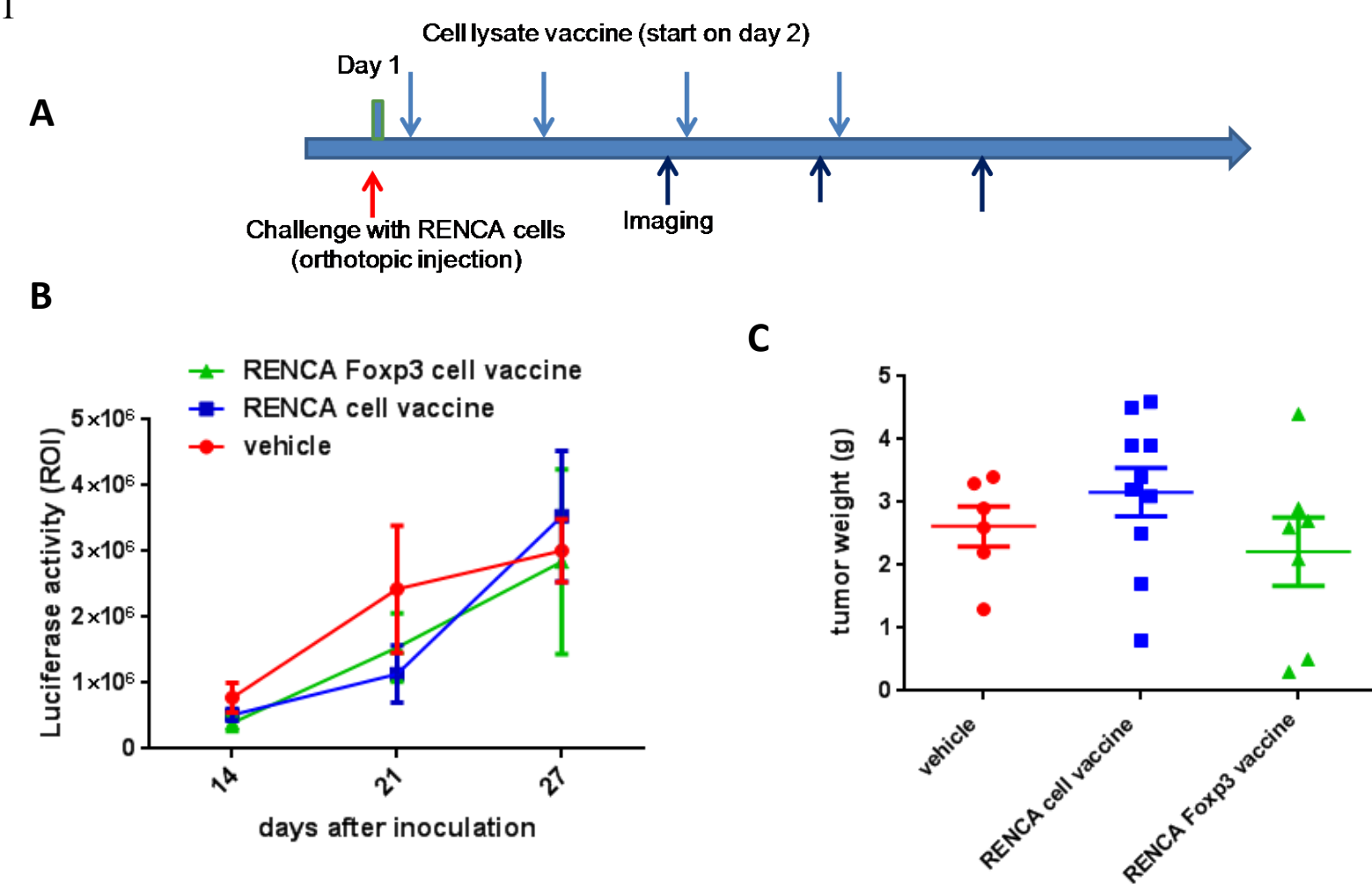

Figure 2. Effects of tumor cell vaccines with start of the treatment after inoculation (day 2 or 8). Female Balb/C mice were inoculated with RENCA cells in the sub-capsular space of the right kidney. Mice were randomized at day 2 or 8 to three groups and received vehicle, RENCA, or RENCA Foxp3 tumor cell vaccine. Experimental schedules are shown in **A** (day 2 start) and **D** (day 8 start). Xenogen imaging show orthotopic tumor growth, **B** and **E**. End point tumor weights are shown in **C** and **F**. *p<0.05.
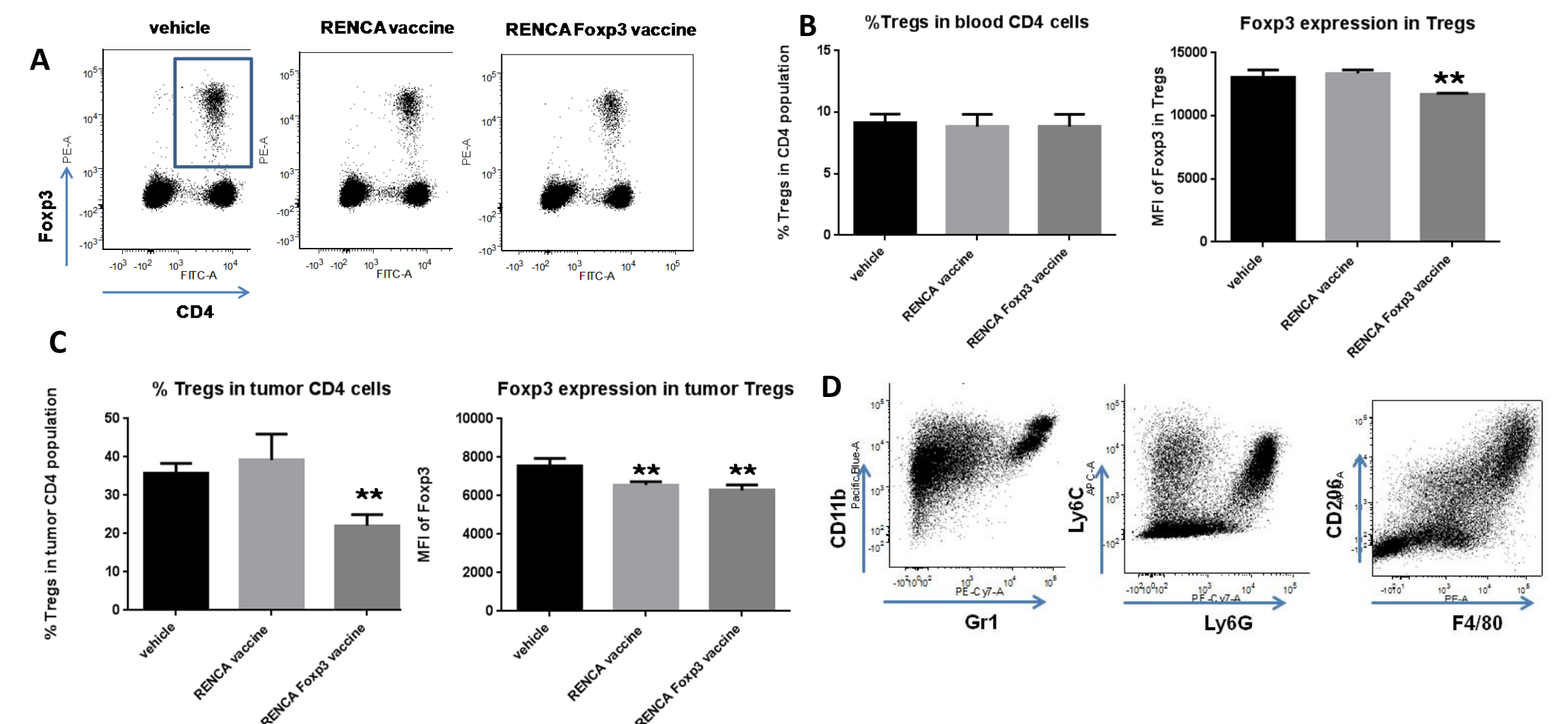

Figure 3. Effects of tumor cell vaccines on Tregs. RENCA-bearing mice received vehicle, RENCA, or RENCA Foxp3 tumor cell vaccine. Blood samples and tumor suspension samples were prepared, stained with cell surface and intercellular markers, subjected to flow cytometry analysis. **A.** Plots show Tregs in blood. **B**. RENCA Foxp3 vaccine decreased Foxp3 level in Tregs, without affecting Treg number in blood. **C**. RENCA Foxp3 vaccine reduced both number and Foxp3 expression of tumor infiltrating Tregs. **D**. MDSCs and TAMs accumulated in RENCA tumor microenvironment. **p<0.01.

CONCLUSIONS

- Both RENCA and RENCA Foxp3 tumor cell vaccines were effective in preventing tumor growth. However, only RENCA Foxp3 vaccine had significant anti-tumor effect against established tumors.
- RENCA Foxp3 vaccine decreased tumor infiltrating Tregs.
- MDSCs and TAMs accumulated in RENCA tumor, suggesting that targeting these immunosuppressive populations may further enhance the activity of the RENCA Foxp3 vaccine.
- Our study suggest that a Treg-targeting tumor vaccine may benefit patients with advanced RCC.

Tasquinimod Modulates Suppressive Myeloid Cells and Enhances Cancer Immunotherapies in Murine Models

Li Shen[1], Anette Sundstedt[2], Michael Ciesielski[3], Kiersten Marie Miles[1], Mona Celander[2], Remi Adelaiye[1], Ashley Orillion[1], Eric Ciamporcero[1], Swathi Ramakrishnan[1], Leigh Ellis[1], Robert Fenstermaker[3], Scott I. Abrams[4], Helena Eriksson[2], Tomas Leanderson[2,5], Anders Olsson[2], and Roberto Pili[1]

Abstract

A major barrier for cancer immunotherapy is the presence of suppressive cell populations in patients with cancer, such as myeloid-derived suppressor cells (MDSC) and tumor-associated macrophages (TAM), which contribute to the immunosuppressive microenvironment that promotes tumor growth and metastasis. Tasquinimod is a novel antitumor agent that is currently at an advanced stage of clinical development for treatment of castration-resistant prostate cancer. A target of tasquinimod is the inflammatory protein S100A9, which has been demonstrated to affect the accumulation and function of tumor-suppressive myeloid cells. Here, we report that tasquinimod provided a significant enhancement to the antitumor effects of two different immunotherapeutics in mouse models of cancer: a tumor vaccine (SurVaxM) for prostate cancer and a tumor-targeted superantigen (TTS) for melanoma. In the combination strategies, tasquinimod inhibited distinct MDSC populations and TAMs of the M2-polarized phenotype (CD206$^+$). CD11b$^+$ myeloid cells isolated from tumors of treated mice expressed lower levels of arginase-1 and higher levels of inducible nitric oxide synthase (iNOS), and were less immunosuppressive *ex vivo*, which translated into a significantly reduced tumor-promoting capacity *in vivo* when these cells were coinjected with tumor cells. Tumor-specific CD8$^+$ T cells were increased markedly in the circulation and in tumors. Furthermore, T-cell effector functions, including cell-mediated cytotoxicity and IFNγ production, were potentiated. Taken together, these data suggest that pharmacologic targeting of suppressive myeloid cells by tasquinimod induces therapeutic benefit and provide the rationale for clinical testing of tasquinimod in combination with cancer immunotherapies. *Cancer Immunol Res; 3(2); 136–48. ©2014 AACR.*

Introduction

Immunotherapies have gained momentum in cancer therapeutics following the recent approvals of drugs for the treatment of prostate cancer and melanoma. Sipuleucel-T dendritic cell (DC) vaccine is now available for treatment of patients with asymptomatic or minimally symptomatic, metastatic, and castration-resistant prostate cancer (1). Clinical observations have indicated that melanoma is an immunogenic tumor (2), and extended survival data have led to the approval of the immune checkpoint inhibitor ipilimumab for the treatment of metastatic melanoma (3). However, despite these clinical advances, immunotherapies for these diseases and solid tumors, in general, benefit only a subset of patients, as intrinsic or acquired tumor immune tolerance remains a major hurdle.

A significant barrier in vaccine therapy is the presence of immunosuppressive soluble and cellular components, including myeloid-derived suppressor cells (MDSC; ref. 4) and tumor-associated macrophages (TAM; ref. 5), which are induced by tumor- and stroma-secreted inflammatory mediators (6–8). MDSCs facilitate tumor progression by impairing T-cell and natural killer (NK)–cell activation (9) and by modulating angiogenesis. Preclinical data have suggested a role for MDSCs in suppressing T-cell responses and inducing tolerance against tumor-associated antigens (TAA; ref. 9). In addition, by secreting IL10 and TGFβ, MDSCs induce the accumulation of other immunosuppressive cell populations such as regulatory T cells (Treg; refs. 10–12). Similarly, the presence of TAMs in the tumor microenvironment (TME) may inhibit the immune response (13). Taken together, there is strong evidence indicating that targeting immunosuppressive MDSCs and TAMs and modifying the TME can improve the efficacy of immunotherapy.

Tasquinimod, a quinoline-3-carboxyamide analogue, is in clinical development for treatment of prostate cancer and other solid tumors. In a placebo-controlled, phase II randomized trial, tasquinimod doubled the median progression-free survival (PFS) period and prolonged survival of patients with metastatic,

AACR

castration-resistant prostate cancer (14, 15). A phase III clinical trial to test the effect of tasquinimod in the same patient population is ongoing (NCT01234311). Tasquinimod has been shown to inhibit prostate cancer growth and metastasis in animal models (16–18). Results from these studies have suggested that the antiangiogenic property of this molecule may be responsible for its antitumor activity, because tumor growth inhibition was associated with reduced microvasculature density, increased expression, and secretion of the angiogenesis inhibitor thrombospondin-1 (TSP-1), and downregulation of VEGF and hypoxia-inducible factor-1α (HIF1α; refs. 19, 20). More recent data have suggested that tasquinimod may affect HIF by interfering with histone deacetylase 4 (HDAC 4; ref. 21). However, in an orthotopic, metastatic prostate cancer model, tasquinimod reduced the rate of metastasis without affecting microvessel density in the primary tumor (18). Therefore, mechanisms other than impairing angiogenesis may play an important role in the antitumor and antimetastatic activities of tasquinimod.

S100A9, a Ca^{2+}-binding inflammatory protein, has been identified as a potential target of tasquinimod. S100A9 interacts with proinflammatory receptors Toll-like receptor 4 (TLR4) and receptor of advanced glycation end products (RAGE), and this interaction is inhibited by the specific binding of tasquinimod to S100A9 (22, 23). These receptors are expressed on the surface of multiple myeloid-cell populations, including MDSCs, macrophages, DCs, and endothelial cells. Functionally, S100A9 regulates the accumulation of MDSCs and inhibits DC differentiation (24, 25), which may lead to suppression of immune responses and tumor progression. Therefore, by targeting S100A9, tasquinimod has immunomodulatory activity and the potential to regulate multiple myeloid populations.

In this study, we tested the effect of tasquinimod on immunosuppressive myeloid-cell populations and investigated its immunomodulatory activity. We conducted preclinical studies of tasquinimod in combination with two different immunotherapeutic approaches in mouse models of prostate cancer and melanoma. Our results suggest that treatment with tasquinimod affects the TME by modulating suppressive myeloid-cell populations, leading to augmented immune responses and enhanced antitumor effects of immunotherapies.

Materials and Methods

Tumor cells

The development of castration-resistant Myc-CaP cell line has been reported previously (26). Castration-resistant Myc-CaP cell line was cultured in DMEM (Mediatech, Inc.) with 10% FBS. The 5T4-tranfected murine B16-F10 melanoma cell line (B16-h5T4; ref. 27) was kindly provided by Peter Stern (Paterson Institute for Cancer Research, Manchester, UK) and was cultured in R10 medium [RPMI-1640 with Ultra glutamine (BioWhittaker/Lonza); supplemented with 10% FBS (Fisher Scientific), 1 mmol/L sodium pyruvate, 10 mmol/L HEPES, 0.1 mg/mL gentamicin sulfate, and 50 μmol/L β-mercaptoethanol]. The castration-resistant Myc-CaP and B16-h5T4 cell lines were tested to be *Mycoplasma* free; no other authentication assay was performed.

In vivo tumor growth

The animal protocols were approved by the Institutional Animal Care and Use Committee at Roswell Park Cancer Institute (Buffalo,

NY; protocol 1137 M), or by the Bioethics Committee in Lund, Sweden (M60-10), as indicated, and were in accordance with the NIH Guide for the Care and Use of Laboratory Animals. Castration-resistant Myc-CaP cells (1×10^6) were inoculated subcutaneously (s.c.) in the right flank of castrated male FVB mice. Animals were distributed randomly into four treatment groups (7–9 animals/group): vehicle, vaccine (SurVaxM), tasquinimod (10 mg/kg/d in drinking water), or the combination. Mice were given 100 μg of SurVaxM peptide and 100 ng of GM-CSF by s.c. injection, once per week. The tumor size was measured by a caliper twice a week. At the end of the 3- to 4-week experiment, tumors and spleens were collected and analyzed. B16-h5T4 cells were cultured as described above, counted, resuspended, and maintained in ice-cold Matrigel (BD Biosciences) at a concentration of 0.3×10^5 cells/mL. Tumor cells were implanted s.c. into the hind flank of C57Bl/6 mice on day 0 in a volume of 0.1 mL Matrigel. Mice were treated with tasquinimod (30 mg/kg/d in drinking water) either from day 0 or 1 after tumor inoculation and throughout the experiments. For tumor-targeted superantigen (TTS) treatment, mice were given daily injections of 5T4Fab-SEA (25 μg/kg) on days 3 to 6, or on days 9 to 11 for analysis of TTS-reactive T cells in the tumors. Experiments were terminated between days 16 and 21. Tumor sizes were measured twice a week and tumor volumes were calculated as volume $= L \times W^2 \times 0.4$, where L is the length (mm) and W (mm) is the width of the tumor ($L > W$; ref. 28). Animal experiments and correlative studies in the castration-resistant Myc-CaP and the B16-h5T4 models were conducted at Roswell Park Cancer Institute and Active Biotech AB, respectively.

Splenocytes and tumor suspension preparation

For isolation of splenocytes, spleens were harvested, mashed on, and passed through a 70-μm strainer. These cell suspensions were centrifuged at $300 \times g$ for 10 minutes at $4°C$. Cell pellets were treated with ACK lysing buffer (Biosource). Splenocytes were then resuspended and cultured in complete media [RPMI supplemented with 10% FBS, 1 mmol/L sodium pyruvate, 100 mmol/L nonessential amino acid, 2 mmol/L L-glutamine, Pen (100 U/mL)–Strep (100 mg/mL), and 55 μmol/L β-mecaptoethanol]. Single-cell suspensions were prepared from tumors with mouse tumor dissociation kit (Miltenyi Biotec). Briefly, tumors were cut into small pieces and incubated in an enzyme-cocktail solution for 40 minutes at $37°C$ with agitation, followed by meshing the tumors in a 70-μm cell strainer. Alternatively, the tumors were cut into small pieces and incubated in 0.5 mg/mL collagenase IV (Worthington Biochemical Corporation) and 0.1% DNase (Sigma-Aldrich) for 45 minutes at $37°C$, followed by meshing the tumors in a 70-μm cell strainer.

Cell staining and flow cytometry

Splenocytes, tumor single-cell suspensions, or peripheral blood cells were washed with flow buffer (PBS with 1% of FBS and 2 mmol/L of EDTA), then incubated with an Fc-blocking antibody (anti-mouse CD16/CD32 mAb 2.4G2; BD Biosciences), and stained with fluorescence-conjugated antibodies against surface markers. Cells were then fixed in Fix/Perm buffer (eBioscience) and stained with antibodies against intracellular proteins. The following fluorochrome-labeled antibodies were used: Gr1 (clone RB6-8C5), CD11b (clone M1/70), Ly6G (clone 1A8), Ly6C (clone AL-21), F4/80 (clone BM8), CD206 (clone C068C2), Arg 1 (polyclonal antibody; R&D Systems; Cat: IC5868A), iNOS

(clone CXNFT), CD4 (clone RM4-5), CD8a (clone 53-6.7), TCR-Vβ3 (clone KJ25), and TCR-Vβ8 (clone F23.1) were purchased from BD Biosciences, eBioscience, BioLegend, and R&D Systems. Cells stained with specific antibodies, as well as isotype-control–stained cells, were assayed on a FACSCalibur, a FACSCantoII, or a LSR II flow cytometer (BD Biosciences). Data analysis was performed using the FCS Express (De Novo Software) or FACS Diva software (BD Biosciences).

IFNγ induction assay
Splenocytes (1×10^6) were cultured with stimulation of PMA (Sigma; 20 ng/mL) and ionomycin (Sigma; 1 μg/mL) for 5 hours. Brefeldin A (Sigma) was added to the cultures to block protein secretion. Cells were harvested and stained for surface markers, then fixed and stained for intracellular IFNγ (eBioscience), and analyzed by flow cytometry.

Granzyme B induction assay
Splenocytes (1×10^6) were cultured with stimulation of CD3 (eBioscience; 1 μg/mL) and CD28 (0.5 μg/mL) for 72 hours. Brefeldin A (Sigma) was added to the cultures during the last 5 hours of culture to block protein secretion. Cells were harvested and stained for surface markers, then fixed and stained for intracellular Granzyme B (eBioscience) and analyzed by flow cytometry.

T-cell suppression assays
T cells (1×10^5; isolated with a Pan T cell isolation kit; Miltenyi Biotec) were cultured in plates coated with CD3 (eBioscience; 1 μg/mL) and CD28 (0.5 μg/mL) for 72 hours. Different numbers of magnetic beads–purified CD11b$^+$ cells from tumors were added to the culture at the beginning. ^{3}H-thymidine (1 μCi) was added to the culture for the last 12 hours. Cells were then harvested and the incorporated ^{3}H-thymidine was detected with scintillation counting. Alternatively, CD11b$^+$ cells were added to CFSE-(Vybrant CFDA SE Cell Tracer Kit; Molecular Probes)–labeled T cells (isolated from naïve spleens using a Pan T cell isolation kit; Miltenyi Biotec) activated by anti–CD3/anti–CD28-coated beads (Dynabeads; Dynal) and incubated for 72 hours. The frequencies of divided CD4$^+$ and CD8$^+$ T cells were determined by FACS analysis.

Splenocyte- and CD8 T cell–mediated cytotoxicity assay
Cytotoxicity assay was performed by using LIVE/DEAD cell-mediated cytotoxicity kit (Invitrogen). Castration-resistant Myc-CaP cells were labeled with Dio and cultured in complete medium. Splenocytes or isolated CD8$^+$ T cells were added to the culture in different ratios to tumor cells. After 5-hour incubation, all cells in culture were harvested and propidium iodide (PI) staining was performed to detect dead cells. Cell cytotoxicity was analyzed by calculating percentage of dead cells with Dio label compared with the whole-cell population with Dio label. Cell events were acquired using LSRII and FACSDiva. Data were analyzed with FCS Express (De Novo Software).

Antigen-specific tetramer binding assay
Blood samples (100 μL) and splenocytes (1×10^6 cells) were incubated for 30 minutes with 10 μL of iTAg MHC Class I Murine H2-K^b Tetramer-SA-PE bound by MFFCFKEL peptide with specificity for SurVaxM (Beckman Coulter) or iTAg MHC Class I Murine H2-K^b Tetramer-SA-PE bound by SIINFEKL ovalbumin

peptide to represent negative control (Beckman Coulter). Samples were also labeled with 10 μL of anti–CD8-FITC (clone 53.6.7; BioLegend). Following incubation, 1 mL of iTAg MHC Tetramer Lyse Reagent (Beckman Coulter) supplemented with 25 μL of iTAg MHC Tetramer Fix Reagent (Beckman Coulter) was added to the samples, which were then incubated for 10 minutes at room temperature, subsequently washed with PBS, and resuspended in 400 μL of FluoroFix Buffer (BioLegend).

Immunofluorescence staining of tumor sections
Snap-frozen tumors were sliced into 8-μm frozen sections and fixed in cold acetone for 10 minutes, before fluorescence labeling. Primary antibody, rat anti-mouse CD31 (BD, Mec 13.3; 1:1,000) and secondary antibody, goat anti-rat Alexa Fluor-555 (Invitrogen; AF555; 1:500) in PBS (5% and 2% mouse serum, respectively) were used, and slides were washed in PBS and mounted with fluorescence mounting medium (Dako; S3023). The sections were analyzed in a Leica DMRX-E microscope. Representative photos were taken and the density of CD31-positive cells (fluorescence) was measured with Leica QWin image analysis system.

Immunohistochemistry staining
Tissue specimens were fixed for 24-hour, paraffin-embedded and 4-μm sections were prepared. Sections were deparaffinized and rehydrated through graded alcohol washes. Antigen unmasking was achieved by boiling slides in sodium citrate buffer (pH, 6.0). Sections were further incubated in hydrogen peroxide to reduce endogenous activity. Then tissue sections were blocked with 2.5% horse serum (Vector Laboratories) and incubated overnight in primary antibodies against CD31 (1:100; Dianova). Following anti-CD31 incubation, tissue sections were incubated in horseradish peroxidase-conjugated anti-rat antibody according to the manufacturer's protocol (Vector Laboratories) followed by enzymatic development in diaminobenzidine (DAB) and counterstained in hematoxylin. Sections were dehydrated and mounted with cytoseal 60 (Thermo Scientific). Corresponding isotype negative controls were used for evaluation of specific staining. Stained sections were analyzed under bright field using the Zeiss Axio microscope. The number of positive cells was determined in a blinded fashion by analyzing four random 20× fields per tissue and quantified using ImageJ software.

Quantitative real-time PCR
mRNA was extracted from CD11b$^+$ cells that were isolated as anti-CD11b$^+$ magnetic bead fractions from single-cell suspensions of B16-h5T4 tumors. mRNA extraction was performed using the RNeasy Mini Kit (Qiagen) and RNA concentration and purity was determined through measurement of A260/A280 ratios with a NanoDrop ND-1000 spectrophotometer. cDNA was prepared using the iScript Kit (Bio-Rad) and qPCR was performed using a CFX384 real-time PCR detection system (Bio-Rad) with a three-step PCR protocol (95°C for 10 minutes, followed by 45 cycles of 95°C for 10 seconds, and 58°C for 30 seconds) using SYBR Green (SsoFast EvaGreen; Bio-Rad) as fluorophore and expression levels were calculated (CFX Manager software; Bio-Rad) as normalized ΔC_t expression values between the target gene and the two "housekeeping" genes β-actin and Ywhaz. Data were presented as fold-induction ($2^{\Delta\Delta Ct}$) levels of treated tumors compared with control tumors ($\Delta\Delta C_t$). The primers used

for target genes were: β-actin_fw 5′-ATG CTC CCC GGG CTG TAT-3′, β-actin_rev 5′-CAT AGG AGT CCT TCT GAC CCA TTC-3′; Ywhaz_fw 5′-AAC AGC TTT CGA TGA AGC CAT-3′ Ywhaz_rev 5′-TGG GTA TCC GAT GTC CAC AAT-3′; CD206_fw 5′-GCA AAT GGA GCC GTC TGT GC-3′, CD206_rev 5′-CTC GTG GAT CTC CGT GAC AC-3′; Arg-1_fw 5′-GTG AAG AAC CCA CGG TCT GT-3′, Arg-1_rev 5′-CTG GTT GTC AGG GGA GTG TT-3′; iNOS_fw 5′-TGG TGG TGA CAA GCA CAT TT-3′, iNOS_rev 5′-AAG GCC AAA CAC AGC ATA CC-3′; Cxcl9_fw 5′-TCA ACA AAA GAG CTG CCA AA-3′, Cxcl9_rev 5′-GCA GAG GCC AGA AGA GAG AA-3′; CxCl10_fw 5′-TCTGAGTCCTCGCTCAAGTG-3′, CxCl10_rev 5′-CCTTGGGAAGATGGTGGTTA-3′; Cxcl11_fw 5′-TCC TTT CCC CAA ATA TCA CG-3′, Cxcl11_rev 5′-CAG CCA TCC CTA CCA TTC AT-3′; Ccr2_fw 5′-ACT TTT CCG AAG GAC CGT CT-3′, Ccr2_rev 5′-GTA ACA GCA TCC GCC AGT TT-3′; Ccl2_fw 5′-CAGGTCCCTGTCATGCTTCT-3′, Ccl2_rev 5′-GTCAGCACAGAC CTCTCTCT-3′; S100A9_fw 5′-CAG CAT AAC CAC CAT CAT CG-3′, S100A9_rev 5′-GCC AAC TGT GCT TCC ACC AT-3′; S100A8_fw 5′-GCT CCG TCT TCA AGA CAT CGT-3′, S100A8_rev 5′-GGC TGT CTT TGT GAG ATG CC-3′; and IL12b_fw 5′-GAAAGACCCTGACCATCACT-3′, IL12b_rev 5′-CCTTCTCTGCAGACAGAGAC-3′.

Nitric oxide synthase activity assay

The assay was performed with an ultra-sensitive assay for nitric oxide synthase (NOS) from Oxford Biomedical Research (Cat: NB78). Briefly, lysates from isolated CD11b cells were first incubated with substrates and cofactors. Then, the mixtures were incubated with nitrate reductase to transform nitrate to nitrite, and mixed with coloring reagent to quantify total end-product concentration. These reactions were performed in a 96-well plate and absorbance was read at 540 nm.

Statistical analysis

The difference in tumor weight between treatment groups was statistically evaluated by the nonparametric Mann–Whitney U test. Differences between experimental groups were tested by either the Student t test or for variances by ANOVA. $P < 0.05$ was considered statistically significant.

Results

Tasquinimod enhances immunotherapy in castration-resistant prostate cancer and melanoma models

Results from previous studies in experimental tumor models indicated that immunomodulatory effects of tasquinimod may contribute to its antitumor activity (23). To investigate the potential immunomodulatory activities of tasquinimod, we tested this agent in combination with a survivin peptide vaccine (SurVaxM) in a survivin-expressing castration-resistant Myc-CaP prostate cancer model and with a TTS in a B16 melanoma model.

Survivin is an intracellular TAA expressed in several solid tumors, including prostate cancer (29). SurVaxM is a modified survivin peptide vaccine SVN53-67/M57-KLH (30) that we have tested previously in multiple tumor models (31). FVB mice were inoculated with castration-resistant Myc-CaP cells s.c. Tumor-bearing mice were divided into four groups and treated with vehicle, SurVaxM (1 dose/wk), tasquinimod (10 mg/kg/d in drinking water), or the combination of SurVaxM and tasquinimod. In the castration-resistant Myc-CaP model,

SurVaxM and tasquinimod single treatments displayed modest antitumor effect but did not induce significant change in tumor growth (Fig. 1A, left). However, the combination of SurVaxM and tasquinimod significantly inhibited tumor growth (58% reduction; combination vs. vehicle; $P = 0.0002$). The combination treatment also significantly inhibited tumor growth compared with that of single treatment groups (tasquinimod vs. combination, $P = 0.009$; survivin vs. combination, $P = 0.017$). Similarly, both SurVaxM and tasquinimod single treatments induced modest, but not statistically significant, reductions of tumor weight at the endpoint of the study, whereas the combination induced more than additive effect, a 65% reduction from vehicle level (Fig. 1A, right; vehicle vs. combination; $P = 0.0002$).

In parallel, we tested tasquinimod in combination with a different immunotherapy approach, TTS in a transplantable B16 melanoma model. TTS immunotherapy activates and directs T lymphocytes to attack tumor cells by means of fusion proteins between bacterial superantigens, such as staphylococcal enterotoxin A (SEA) and Fab-fragments of tumor-reactive monoclonal antibodies (mAb; ref. 32). Superantigens activate a high number of CD4$^+$ and CD8$^+$ T cells expressing particular T-cell receptor (TCR)-Vβ chains (33). In this study, B16-h5T4–expressing tumors were treated with tasquinimod (30 mg/kg/d in drinking water), the TTS fusion protein 5T4Fab-SEA at a suboptimal therapeutic dose (25 μg/kg), or the combination. Tasquinimod treatment began the day after tumor-cell inoculation, and 5T4Fab-SEA was administered on days 3 to 6. Although both TTS and tasquinimod single-agent treatments elicited substantial antitumor effects, the combination regimen led to a significant reduction in tumor size at the endpoint (>75% reduction; vehicle vs. combination; $P < 0.0001$; Fig. 1B). Thus, the combination of tasquinimod with two different immunotherapeutic strategies resulted in a significant enhancement of antitumor effects.

Enhanced immunotherapy is associated with induction of effector T cells and increased antitumor immune responses

To determine whether the observed inhibition of tumor growth induced by the combination strategy was associated with improved immune responses, we examined CD8$^+$ T cells harvested at the end of the experiment. First, using a survivin vaccine-specific peptide-MHC class I tetramer binding assay, we showed that the survivin vaccine, as a single treatment or in combination with tasquinimod, induced antigen-specific CD8$^+$ T cells (Supplementary Fig. S1). We also tested the cellular expression of IFNγ and Granzyme B, which are critical for CD8$^+$ effector T-cell functions. Splenocytes were isolated from differentially treated mice, stimulated, and then stained for cell-surface markers and intracellular proteins. IFNγ expression was increased slightly in CD8$^+$ T cells from combination-treated animals as compared with vehicle group (Fig. 2A), while no significant changes were observed in CD8$^+$ T cells from single agent–treated animals. Similarly, when compared with vehicle- and single agent–treated groups, Granzyme B expression in CD8$^+$ T cells from combination-treated animals was significantly higher (Fig. 2B).

To determine whether the changes in specific CD8$^+$ T cells were associated with an improvement in cytotoxic T lymphocyte (CTL) activity, we tested ex $vivo$ the ability of splenocytes and purified
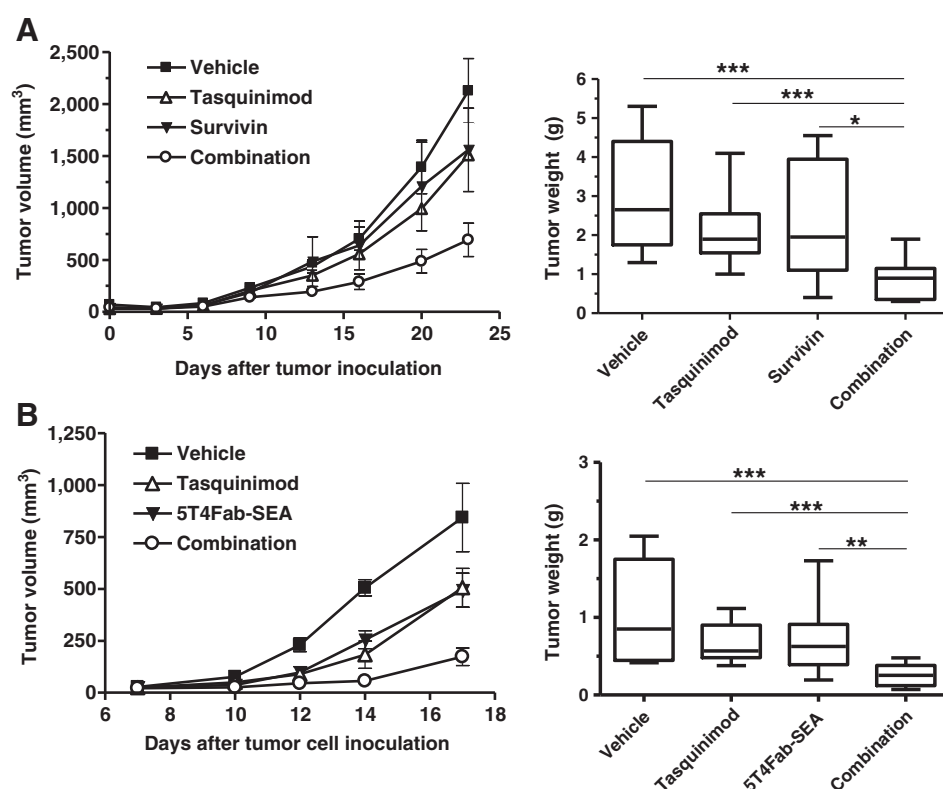
Figure 1.
Tasquinimod improves immunotherapy in castration-resistant Myc-CaP prostate cancer and B16 melanoma models. A, mice were inoculated s.c. with castration-resistant Myc-CaP cells. When the tumors reached an average size of 25 mm^2, mice were treated with vehicle, survivin, tasquinimod, or the combination of survivin and tasquinimod. Left, tumor growth curves by serial caliper measurements. Right, tumor weights at the endpoint. B, mice were inoculated s.c. with B16-h5T4 cells and treatment with tasquinimod was initiated the day after inoculation and continued throughout the experiment. The TTS protein 5T4Fab-SEA (25 µg/kg) was given as daily i.v. injections on days 3 to 6. Left, tumor growth curves by serial caliper measurements. Right, end-of-treatment tumor weights. The experiments were repeated at least twice. Results from one representative experiment are shown (*, $P < 0.05$; **, $P < 0.01$; ***, $P < 0.001$, Mann–Whitney U test; error bars indicate SEM).

$CD8^+$ T cells to kill castration-resistant Myc-CaP tumor cells. Consistent with enhanced antitumor activity observed following combination treatment, splenocytes from these mice displayed significantly improved tumor-cell killing capacity as compared with those from other treatment groups (Fig. 2C, left). Interestingly, when purified $CD8^+$ T cells were used ex vivo in the same assay, tumor-cell killing capacity was equal in all treatment groups (Fig. 2C, right). These results thus suggest that the combination therapy does not enhance CTL activity per se but rather inhibits T cell–suppressing factor(s) in the cultured splenocytes.

In the B16-h5T4 melanoma model, analysis of tumor-infiltrating cells showed that the combination treatment significantly increased accumulation of $CD4^+$ and $CD8^+$ T cells measured at the endpoint as compared with those of control and single-agent treatments (Fig. 2D). To address the influence of tasquinimod on the activation of TTS-reactive T cells, B16-h5T4 tumors were allowed to grow until day 9 before giving three daily injections of 5T4Fab-SEA. Tumor-infiltrating cells were analyzed at different days (day 12–16) to follow the kinetics of specific T-cell expansion. Tasquinimod significantly enhanced and prolonged tumor infiltration of TTS-reactive TCR-Vβ3$^+$CD8$^+$ T cells induced by 5T4Fab-SEA (Fig. 2E). The TTS-nonreactive TCR-Vβ8$^+$CD8$^+$ T cells were only marginally affected by the treatment (Fig. 2F). In contrast, the TCR-Vβ3$^+$CD4$^+$ T-cell population was less enhanced by the combination (Fig. 2G).

Tasquinimod has been reported to display antiangiogenic activity in prostate cancer models (19, 34). To determine whether the antiangiogenic effect of tasquinimod was involved in enhancing the antitumor effects of immunotherapy, we assessed the microvasculature density (CD31 expression) in

the harvested tumor tissue by either immunofluorescence or immunohistochemistry analysis in the two therapeutic strategies, respectively. The results showed that tasquinimod treatment reduced microvasculature density in B16 tumors (Fig. 3A), but it did not change tumor vasculature in the castration-resistant Myc-CaP model (Fig. 3B). In summary, these results suggest that the immunomodulatory effects of tasquinimod may be dissociated from its antiangiogenic activity, and in the B16-h5T4 tumor model, the tasquinimod-induced inhibition of tumor blood vessel formation may account at least in part for its antitumor effect in this model.

Infiltration of suppressive myeloid-cell populations is reduced by tasquinimod treatment in immunotherapy

S100A9 is an inflammatory protein that affects the accumulation of immunosuppressive myeloid cells, including MDSCs (24, 25). Tasquinimod binds to S100A9, inhibiting its downstream signaling, and thus has the potential to affect myeloid cells. To investigate the mechanism of immune-promoting activity of tasquinimod in combination with immunotherapy, we analyzed the peripheral and tumor-infiltrating myeloid-cell populations.

In the castration-resistant Myc-CaP tumor model, blood samples were taken from differentially treated mice after 2 weeks of treatments and subjected to immunofluorescence staining and FACS analysis. We observed three different $CD11b^+$ cell populations in the blood distinct by their expression levels of the Gr1 marker: $Gr1^{negative}$, $Gr1^{low}$, and $Gr1^{high}$ (Supplementary Fig. S2A). Tasquinimod did not affect the number of either $Gr1^{low}$ $CD11b^+$ cells or $Gr1^{high}CD11b^+$ MDSCs in the blood, but decreased the $Gr1^-CD11b^+$ population (Supplementary
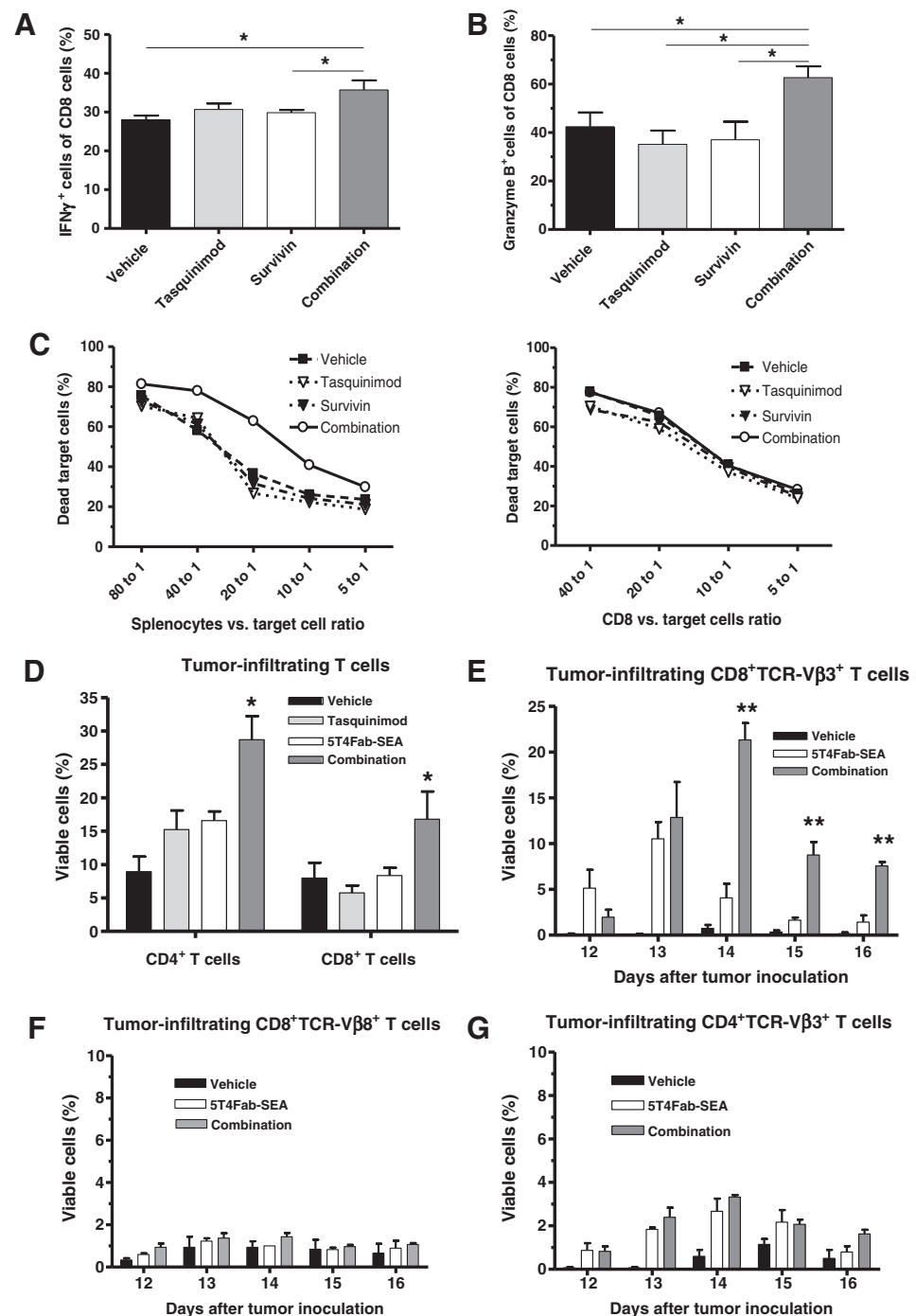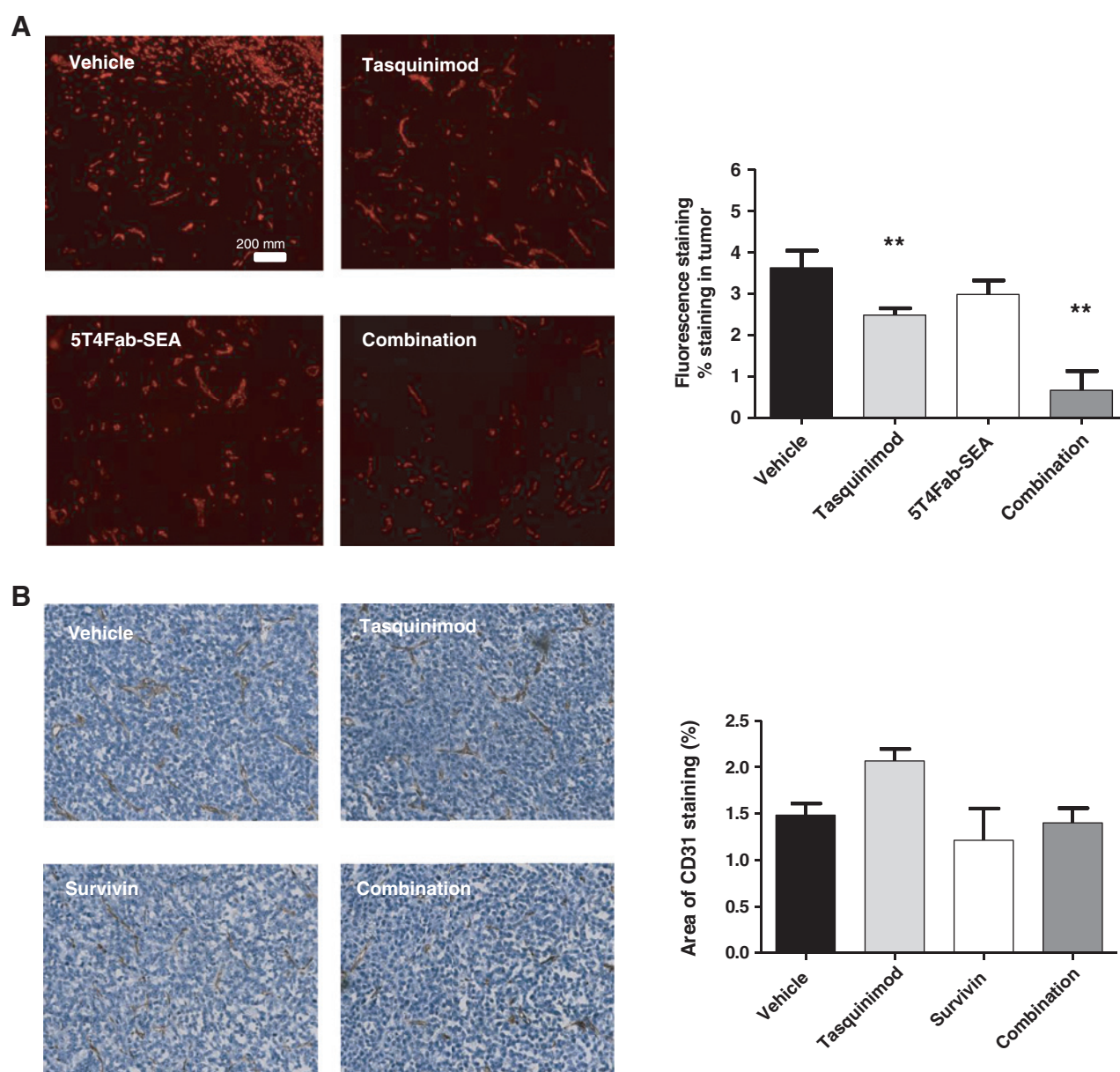
Figure 2.
Tasquinimod in combination with vaccine or TTS improves T-cell immune responses. Splenocytes isolated from castration-resistant Myc-CaP tumor-bearing mice were stimulated with PMA and ionomycin for 5 hours in the presence of BFA for IFNγ production (A), or on CD3- and CD28-coated plates for 72 hours for Granzyme B production (BFA was added during the last 5 hours; B). C, splenocytes (left) or purified CD8$^+$ T cells (right) from castration-resistant Myc-CaP tumor-bearing mice were cocultured with DIO-labeled tumor cells in different ratios for 5 hours. PI was added at the end of incubation to detect tumor cell death. D, FACS analysis of tumor-infiltrating T cells performed at the endpoint of the experiment depicted in Fig. 1B. E–G, FACS analysis of infiltrating T cells in B16-h5T4 tumors at different time points. 5T4Fab-SEA was administered on days 9 to 11 ($*$, $P < 0.05$; $**$, $P < 0.01$; $***$, $P < 0.001$, t test; error bars indicate SEM).

Fig. S2A). Similarly, the number of MDSCs in the spleen did not change following treatments (Supplementary Fig. S2C). In addition, tumors were harvested from differentially treated mice and processed into suspension. Interestingly, tasquinimod significantly reduced the number of tumor-infiltrating MDSCs when given as a single agent or in combination with the vaccine (Fig. 4A). Further analysis of MDSC subpopulations present in the blood and tumors revealed a striking dominance of the granulocytic CD11b$^+$Ly6C^{low}Ly6G$^+$ population (Supplementary Fig. S2B and S2D).

A similar analysis of CD11b$^+$ cells and MDSC subpopulations was performed in the B16-h5T4 model (C57Bl/6 strain). The frequency of tumor-infiltrating CD11b$^+$ cells was not altered following tasquinimod treatment (Supplementary Fig. S3A), whereas a significant reduction of the number of CD11b$^+$ cells was observed in the spleen (Supplementary Fig. S3B). In contrast to the castration-resistant Myc-CaP model, the majority of MDSCs in untreated B16-h5T4 tumors were of the CD11b$^+$Ly6C^{high}Ly6G$^-$ monocytic subtype (Fig. 4B, left). Moreover, a significant reduction of the CD11b$^+$Ly6C^{high}Ly6G$^-$ monocytic

Figure 3.
Tasquinimod effects on tumor vasculature (CD31) in B16-h5T4 and castration-resistant Myc-CaP tumors. A, immunofluorescence staining of CD31$^+$ vasculature in B16-h5T4 tumors. B, immunohistochemistry staining of CD31$^+$ vasculature in castration-resistant Myc-CaP tumors. The experiments were repeated at least twice. Results from one representative experiment are shown (**, $P < 0.01$, t test; error bars indicate SEM).

subpopulation was observed while the proportion of CD11b$^+$Ly6C^{low}Ly6G$^+$ granulocytic MDSCs increased in tumors upon tasquinimod treatment (Fig. 4B). A comparable picture was also seen in the spleen (Supplementary Fig. S3C). Interestingly, the tumor-infiltrating CD11b$^+$Ly6C^{high}Ly6G$^-$ MDSCs expressed high levels of the angiopoietin receptor Tie2 (data not shown), which plays a key role in tumor angiogenesis (35). Thus, the decrease in microvasculature density by tasquinimod in the B16 model could be the consequence of reducing proangiogenic monocytic cells within the tumors.

TAMs are important components of the immunosuppressive TME. Immature monocytes and monocytic MDSCs migrate to

the tumor in response to inflammatory mediators released from the TME. When infiltrating the tumor tissue, these cells adapt to the environment and differentiate into TAMs by losing Gr1 marker expression and gaining an even more immunosuppressive M2 macrophage phenotype (36–38). Therefore, we assessed the effect of tasquinimod on TAMs. Results from the castration-resistant Myc-CaP model showed that tasquinimod treatment led to a reduction of infiltrating CD206$^+$ M2 TAMs (Fig. 4C). Similarly, analysis of macrophages in B16-h5T4 tumors also revealed a strong reduction of this subpopulation in tasquinimod-treated mice (Fig. 4D).
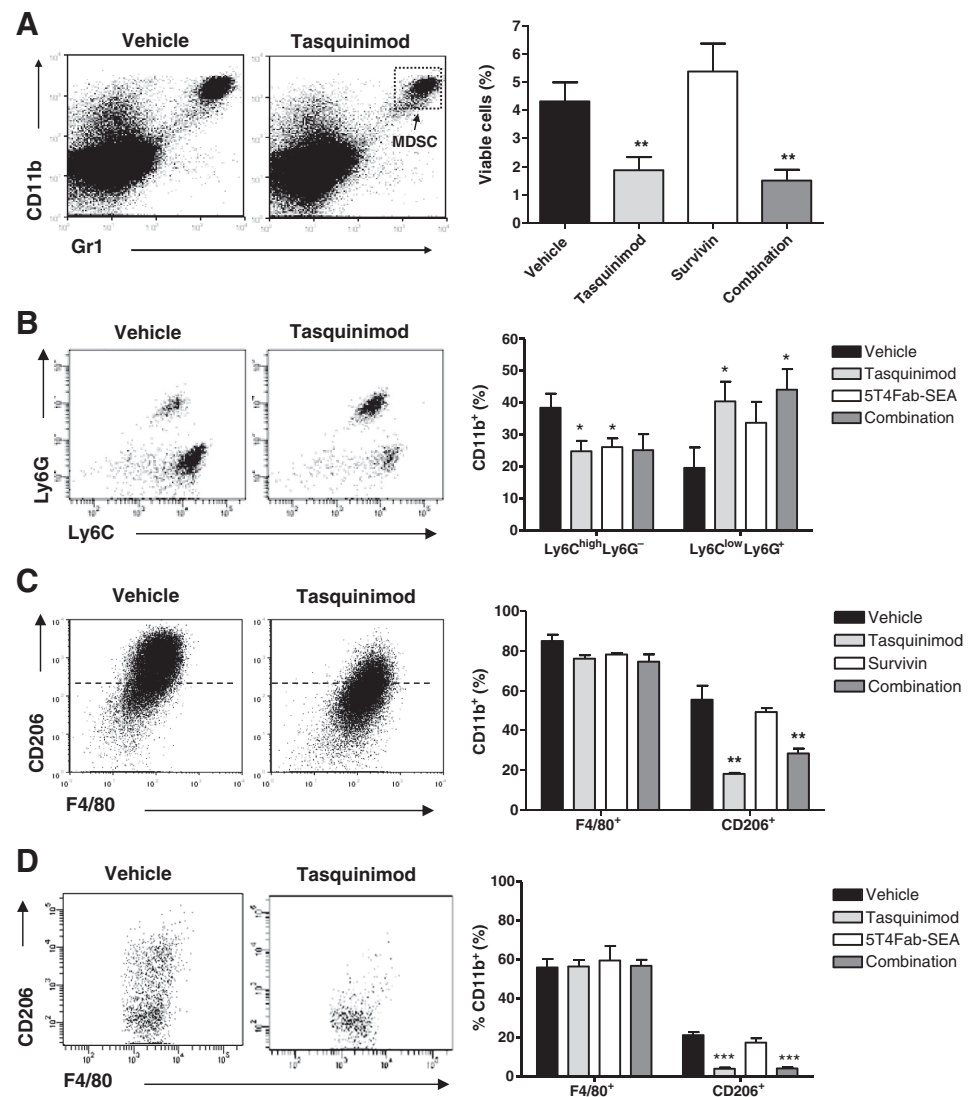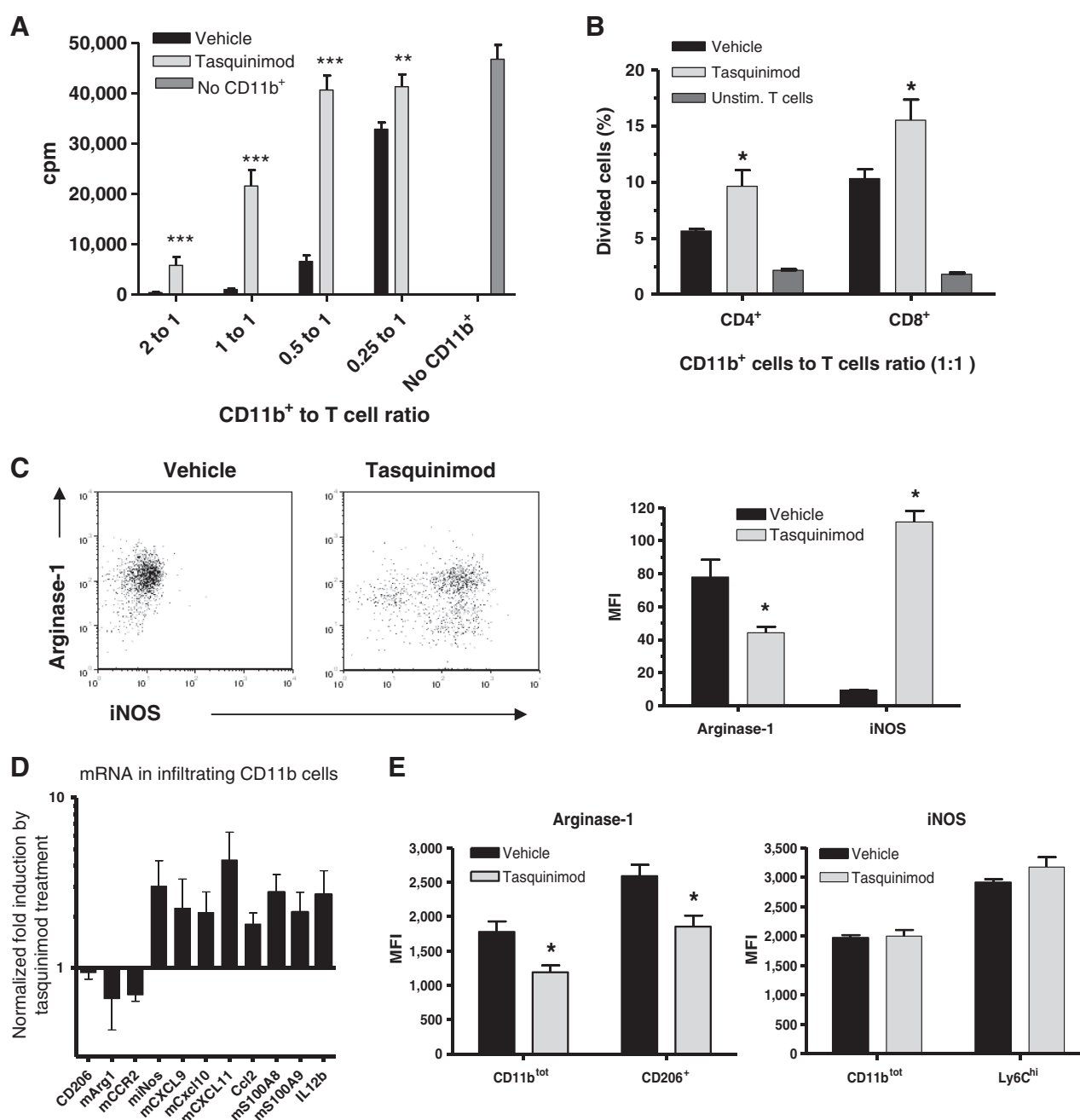
Figure 4.
Tasquinimod modulates MDSC and TAM populations in the castration-resistant Myc-CaP and B16-h5T4 tumor models. A, FACS analysis of tumor-cell suspensions from the castration-resistant Myc-CaP model for $CD11b^+Gr1^+$ MDSCs after tasquinimod treatment. B, FACS analysis of tumor-cell suspensions from the B16-h5T4 model for granulocytic $Ly6G^+Ly6C^{low}$ and monocytic $Ly6G^-Ly6C^{high}$ $GR1^+$ MDSCs. FACS analysis of tumor-cell suspensions for $F4/80^+$ macrophages and for CD206 expression from castration-resistant Myc-CaP tumors (C) and B16-5T4 tumors (D). FACS plots and quantifications are depicted throughout (*, $P < 0.05$; **, $P < 0.01$; ***, $P < 0.001$, t test; error bars indicate SEM).

In addition to MDSCs and TAMs, we also investigated whether tasquinimod treatment affects immune-promoting activities of other myeloid and lymphoid cells. Tasquinimod did not impair T-cell expansion upon activation either in T cells isolated from differentially treated mice (Supplementary Fig. S4A) or when tasquinimod was added in culture (Supplementary Fig. S4B). Tregs represent an immunosuppressive lymphocyte population whose accumulation can be regulated by MDSCs. In both castration-resistant Myc-CaP (Supplementary Fig. S4C, left) and B16-h5T4 (Supplementary Fig. S4C, right) models, tasquinimod increased the accumulation of Tregs. DC differentiation has been shown to be regulated by the S100A9 protein (24). Although tasquinimod slightly reduced the number of DCs in the spleen (Supplementary Fig. S5A), drug treatment did not impair the capacity of DCs to stimulate T cells (Supplementary Fig. S5B). These data suggest that immunosuppressive myeloid cells, such as MDSCs and TAMs, but not other myeloid or lymphoid populations, are the potential cellular targets of tasquinimod and they may be responsible for the immune-promoting activity of tasquinimod in combination with immunotherapies.

Tasquinimod inhibits immunosuppressive functions of tumor-associated myeloid cells and modulates relevant gene expression

So far, we have shown that tasquinimod significantly reduced the numbers of distinct MDSCs and altered the TAM populations in two different tumor models, suggesting that tasquinimod may affect the accumulation/trafficking of immunosuppressive myeloid cells into the tumors. To investigate the mechanisms by which tasquinimod regulates these cells, we measured the immunosuppressive capacity of intratumoral $CD11b^+$ myeloid cells on T-cell activation. $CD11b^+$ cells were purified from tumor tissue and cultured with purified, stimulated T cells. As expected, $CD11b^+$ cells from tumors inhibited T-cell proliferation (Fig. 5A). However, $CD11b^+$ cells isolated from tasquinimod-treated castration-resistant Myc-CaP tumors showed significantly less suppression on T-cell proliferation compared with that of the controls (Fig. 5A). Similarly, $CD11b^+$ cells purified from tasquinimod-treated B16-h5T4 tumors were also less suppressive (Fig. 5B). In this experiment, a CFSE-based method was used to detect $CD4^+$ and $CD8^+$ T-cell proliferation. Inhibition of T-cell division by $CD11b^+$ cells was significantly lower following

Figure 5.
Tasquinimod treatment reduces the suppressive capacity of tumor-infiltrating CD11b^{+} cells in the castration-resistant Myc-CaP and B16-h5T4 tumor models. A, CD11b^{+} cells were enriched from castration-resistant Myc-CaP tumors, and added at different ratios to stimulated T-cell cultures. ^{3}H-thymidine was added to the cultures during the last 12 hours of 3 days of culturing. B, CD11b^{+} cells were purified from B16-h5T4 tumors and cocultured with purified CFSE-labeled T cells for 3 days. The frequencies of divided cells among CD4^{+} and CD8^{+} T cells were measured by FACS. C, intracellular staining of Arg1 and iNOS in infiltrating CD11b^{+} cells from castration-resistant Myc-CaP tumors. D, qRT-PCR analyses of selected genes expressed in purified CD11b^{+} cells from B16-h5T4 tumors. E, intracellular staining of Arg1 and iNOS in infiltrating CD11b^{+} cells isolated from B16h5T4 tumors (*, $P < 0.05$; **, $P < 0.01$; ***, $P < 0.001$, t test; error bars indicate SEM).

tasquinimod treatment. Taken together, these results suggest that tasquinimod modulates not only the infiltration but also the suppressive capacity of tumor-infiltrating myeloid-cell populations.

As shown in Fig. 4C, the majority of the tumor-infiltrating myeloid cells in the castration-resistant Myc-CaP model are macrophages, and tasquinimod treatment reduced CD206^{+} immunosuppressive M2 macrophages (Fig. 4C and D). This observation led us to investigate the expression of two mechanistically relevant genes, arginase-1 (Arg1) and inducible NOS (iNOS) in the tumor-infiltrating myeloid cells (Fig. 5C–E). Previous studies have shown that Arg1 expression is critical to the

suppressive function of MDSCs and TAMs. It has been reported that Arg1 gene expression can be regulated by the TLR4 pathway (39), which is a target receptor for S100A9. The iNOS marker can be used to differentiate cytotoxic M1 macrophages from immunosuppressive M2 macrophages. Intracellular staining and flow cytometry analysis of castration-resistant Myc-CaP tumors showed that tasquinimod reduced Arg1 expression in myeloid cells and induced significant iNOS expression, which indicates an increase in immune-promoting M1 macrophages (Fig. 5C). In the B16-5T4 model, mRNA analysis also indicated that tasquinimod shifted an M2 macrophage (immunosuppressive) gene expression signature into an M1 macrophage signature (Fig. 5D). FACS analysis confirmed the reduction of Arg1 expression and the induction of iNOS in tumor-infiltrating Ly6C^{high} monocytic cells, although not as dramatically as those in the castration-resistant Myc-Cap model (Fig. 5E).

We also tested the enzymatic activities of NOS and Arg1 in infiltrating myeloid cells. Tasquinimod treatment in vivo led to a significant increase of NOS activity, as compared with vehicle treatment (Supplementary Fig. S6). The arginase activity assay did not reveal a significant change between these two conditions (data not shown).

Tasquinimod treatment reduces the ability of suppressive myeloid cells to support tumor growth

In the therapeutic studies, tasquinimod treatment enhanced immune responses and vaccine effects (Figs. 1 and 2 and Supplementary Fig S1). We hypothesized that suppressive myeloid cells, including MDSCs and TAMs and not the other populations, are potential targets of tasquinimod immunomodulatory activity (Figs. 4 and 5 and Supplementary Figs. S4 and S5). To test this hypothesis, castration-resistant Myc-CaP cells were inoculated into FVB mice as described. When tumor growth was established, mice were randomized into two groups receiving either vehicle or tasquinimod treatment for 4 weeks. CD11b$^+$ myeloid cells, isolated from tumors that were harvested from different treatment groups, were mixed with fresh

castration-resistant Myc-CaP cells and inoculated into recipient FVB mice receiving SurVaxM vaccine therapy. As shown in Fig. 6, inoculations containing tasquinimod-treated tumor-derived myeloid cells induced significantly slower tumor growth, as compared with those containing vehicle-treated tumor-derived myeloid cells. These data indicate that tasquinimod directly impairs the tumor-promoting activity of immunosuppressive myeloid cells.

Discussion

The aim of immunotherapy is to induce durable and effective immune responses. MDSCs and TAMs contribute to immune tolerance in the TME and consequently affect the efficacy of immunotherapies. Our study provides evidence supporting the development of tasquinimod as a novel approach to target the immunosuppressive TME and facilitate immunotherapy. The data were generated in parallel in two different laboratories, providing evidence for reproducibility of our observations.

We tested two different immunotherapeutic strategies in combination with tasquinimod in two murine tumor models, and observed a similar immune-promoting effect by tasquinimod coupled to modulation of tumor-infiltrating MDSCs and TAMs. These myeloid populations express receptors for S100A9 and are likely cellular targets for tasquinimod. Furthermore, we demonstrated that the adoptively transferred tasquinimod-treated myeloid cells were sufficient to delay tumor growth in vaccinated animals, as compared with tumor inoculates with vehicle-treated myeloid cells (Fig. 6). There were differences in the subpopulations of tumor-induced myeloid cells in the two models, possibly due to the different tumor origins. Granulocytic MDSCs are prevalent in the castration-resistant Myc-CaP model on FVB background, whereas monocytic MDSCs comprise the major population in B16-h5T4 mouse melanoma on C57Bl/6 background. Upon tasquinimod treatment, the Ly6C^{high}Ly6G$^-$ monocytic MDSCs were reduced in the
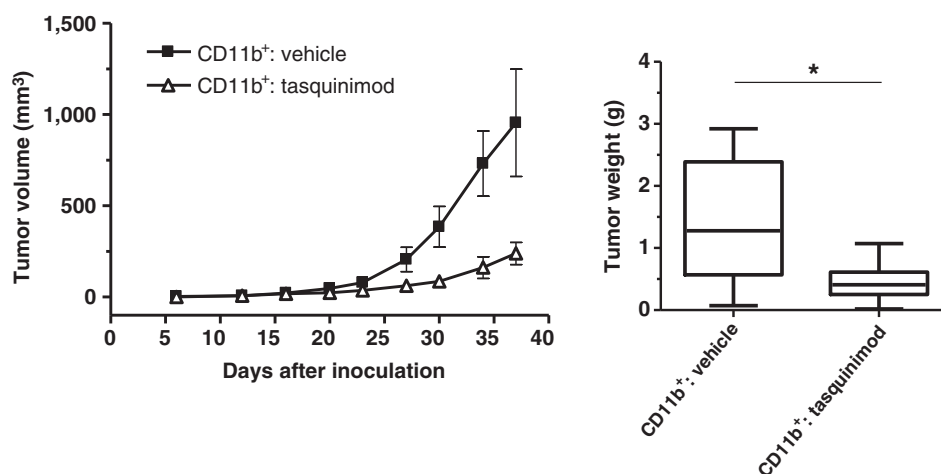

Figure 6.
Tasquinimod treatment reduces the ability of suppressive myeloid cells to support tumor growth. CD11b$^+$ cells were isolated from tumors collected from either vehicle or tasquinimod-treated donor mice, mixed with fresh castration-resistant Myc-CaP cells (mixture contained 1.5×10^6 castration-resistant Myc-CaP cells and 0.75×10^6 CD11b cells), and inoculated s.c. into recipient mice receiving SurVaxM vaccine. Recipient mice received two doses of the vaccine before inoculation and two additional doses were administered after tumor-cell inoculation. Left, tumor growth curves by serial caliper measurements. Right, end of treatment tumor weights (*, $P < 0.05$, Mann–Whitney U test; error bars indicate SEM).

B16-h5T4 tumors (Fig. 4B), and the total number of $Gr1^+$ $CD11b^+$ MDSCs was reduced in castration-resistant Myc-CaP tumors (Fig 4A). At peripheral sites, tasquinimod treatment led to depletion of $Gr1^-CD11b^+$ monocytes in castration-resistant Myc-CaP tumor-bearing mice (Supplementary Fig. S2A), and a significant reduction of the $CD11b^+$ $Ly6C^{high}Ly6G^-$ and $CD11b^+Ly6C^{low}Ly6G^-$ monocytic populations in the B16-h5T4 tumor-bearing animals (Supplementary Fig. S3 and data not shown). These observations suggest that immature monocytes are potential targets for tasquinimod. Because monocytic MDSCs or immature monocytes can be precursors of TAMs (38), the reduction of monocytes at peripheral sites could lead to an altered profile of TAMs observed in both models (Fig. 4C and D).

As shown in Fig. 2C, splenocytes from mice treated with the combined regimen of vaccine and tasquinimod presented increased tumor-cell killing *ex vivo*, compared with that of vehicle and single treatment groups. However, the purified $CD8^+$ effector T cells from mice treated with the combined regimen did not show a significant difference in cytotoxicity against tumor cells. This result suggests that the combined treatment does not affect effector T-cell functions directly but instead it relieves the immunosuppression present in the cultures, such as the inhibition by immunosuppressive MDSCs. We observed no inhibition of T-cell proliferation *ex vivo* or when tasquinimod was added to culture at high concentrations (Supplementary Fig. S4). The effect of combination treatment on specific T-cell activation in tumors was addressed in the B16-h5T4 model. Tracking of superantigen-reactive T cells by TCR-Vβ expression demonstrated increased and prolonged presence of TTS-activated $CD8^+$ T cells in tumors following tasquinimod cotreatment, further supporting the induction of a less immunosuppressive environment. A similar increase in tumor-infiltrating CTLs in B16 tumors was reported recently following TTS therapy in combination with anti–CTLA-4 checkpoint blockade (40).

Previous reports have shown that MDSC-targeting strategies affect systemic or peripheral MDSC accumulation (25, 41). For example, mAbGB3.1, an antibody against the carboxylated N-glycan on RAGE, reduced MDSC accumulation in blood, spleen, and lymph nodes in 4T1 tumor-bearing animals, but not in the metastatic site. However, this antibody treatment did not affect the suppressive function of MDSCs (25). In our castration-resistant Myc-CaP model, tasquinimod did not change the number of $Gr1^+CD11b^+$ MDSCs at peripheral sites (Supplementary Fig. S2), which would suggest that tasquinimod does not affect the generation or expansion of MDSCs. However, tasquinimod reduced tumor-infiltrating MDSCs (Fig. 4A). This observation suggests that tasquinimod may inhibit MDSC trafficking/accumulation in the tumor, leading to modulation of the TME and relief of immune tolerance. In support of this finding, S100A9 signaling has been reported to regulate both expansion and migration of MDSCs (24, 25). It has also been shown that intracellular S100A9 expression in myeloid progenitor cells induces MDSC expansion (24, 42). However, extracellular (secreted) S100A9 protein binds to carboxylated N-glycan receptors (RAGE) that are expressed on the surface of MDSCs and promotes MDSC migration to the site of tumors (25, 43). Taken together, our results provide evidence supporting a mechanism of action by tasquinimod in blocking extracellular S100A9 and receptor

signaling that may be critical to MDSC tumor infiltration via cell surface receptors such as TLR4 (23) and RAGE (22).

The notion of a cross-talk between different regulatory myeloid cells is well established (44). Aside from the reduction and modulation of tumor-associated MDSCs, tasquinimod treatment resulted in decreased numbers of $CD206^+$ M2-polarized TAMs and reduced the suppressive function of CD11b-expressing myeloid infiltrates (Figs. 4 and 5). Macrophages are categorized as either the classically activated, cytotoxic M1 macrophages, or the alternatively activated, suppressive M2 macrophages. The M2-polarized TAMs are enriched in hypoxic tumor areas with a superior proangiogenic activity *in vivo*, a limited capacity to present antigen, and the ability to suppress adaptive immune responses such as T-cell activation (38, 45). In the castration-resistant Myc-CaP and B16-5T4 models, $F4/80^+$ macrophages represent the major population of tumor infiltrates and a large component of these infiltrating macrophages are $CD206^+$, M2-like type, which is significantly reduced upon tasquinimod treatment (Fig. 4C and D). The function of macrophages depends on the expression of Arg1 and iNOS. Although classically activated M1-polarized macrophages express both Arg1 and iNOS, suppressive TAMs only express Arg1, which is critical for the immunosuppressive function. As shown in Fig. 5, tasquinimod treatment reduced Arg1 expression in $CD11b^+$ cells in both models (Fig. 5C–E), which could explain the reduced suppressive function of these cells (Fig. 5A and B). An important regulator of Arg1 gene expression is TLR4 signaling (39), which is a receptor for a tasquinimod-target protein, S100A9. Potentially, the S100A9–TLR4–Arg1 pathway may be involved in tasquinimod-induced changes of suppressive myeloid cells. Interestingly, in the castration-resistant Myc-CaP model, tasquinimod induced iNOS expression in $CD11b^+$ cells (Fig. 5C). An assay testing NOS enzyme also showed that tasquinimod-treated CD11b cells had higher NOS activity (Supplementary Fig. S6). iNOS is mainly expressed in macrophages and monocytic MDSCs, whereas granulocytic MDSCs have low iNOS. Therefore, the increase of iNOS in CD11b cells is likely due to an increase of M1 macrophages in the tumor, rather than an induction of monocytic MDSCs because the vast majority of MDSCs in the tumors of this model are of the granulocytic type (Supplementary Fig. S2D).

Tasquinimod has pleiotropic effects that contribute to its antitumor activity, including antiangiogenesis, immunomodulation, and inhibition of metastasis. As demonstrated in this study, modulation of suppressive myeloid cells may represent a critical biologic mechanism of action of tasquinimod and the common target giving rise to the diverse effects. Immunosuppressive myeloid cells (MDSCs and TAMs) secrete multiple factors, including VEGF and MMP9, which promote angiogenesis (46). In a hypoxic microenvironment, myeloid cells can also recruit endothelial cells and their precursors (47). MDSCs have also been reported to promote tumor-cell dissemination (48) and cancer stemness (49). In addition, MDSCs and TAMs have the potential to prime distal sites to promote the seeding of metastatic tumor cells (50–52). Moreover, MDSCs have been found to promote cancer cell survival upon chemotherapy by producing certain chemokines (53). These findings suggest that suppressive myeloid populations represent key mediators of multiple critical aspects of cancer immune tolerance, metastasis, and drug resistance. The inhibitory effects of tasquinimod on tumor-infiltrating

immunosuppressive myeloid cells, and, in particular, on the M2-polarized TAMs, have been observed in preclinical syngeneic tumor models. These biologic properties of tasquinimod support the further development of this agent for clinical combination strategies with immunotherapies such as vaccines and immune checkpoint inhibitors. On the basis of our preliminary data, a clinical trial of tasquinimod in combination with sipuleucel-T in patients with metastatic castration-resistant prostate cancer is planned to open in 2014.

In conclusion, tasquinimod is a small-molecule inhibitor with a potentially unique mechanism of action that targets the TME. Future preclinical and clinical testing of this agent will define its application in a wide range of therapeutic strategies including immunotherapies, antiangiogenic agents, and antimetastatic drugs.

Disclosure of Potential Conflicts of Interest

A. Sundstedt, M. Celander, H. Eriksson, T. Leanderson, and A. Olsson have ownership interest (including patents) in Active Biotech. R. Pili reports receiving a commercial research grant from ActiveBiotech AB and is a consultant/advisory board member for Ipsen. M. Ciesielski has ownership interest (including patents) in MimiVax, LLC. R. Fenstermaker is the founder of MimiVax LLC. No potential conflicts of interest were disclosed by the other authors.

Authors' Contributions

Conception and design: L. Shen, A. Sundstedt, M. Ciesielski, M. Celander, H. Eriksson, T. Leanderson, A. Olsson, R. Pili
Development of methodology: L. Shen, A. Sundstedt, M. Ciesielski, M. Celander, A. Olsson, R. Pili

Acquisition of data (provided animals, acquired and managed patients, provided facilities, etc.): L. Shen, A. Sundstedt, M. Ciesielski, K.M. Miles, M. Celander, R. Adelaiye, A. Orillion, E. Ciamporcero, L. Ellis, A. Olsson, R. Pili
Analysis and interpretation of data (e.g., statistical analysis, biostatistics, computational analysis): L. Shen, A. Sundstedt, M. Ciesielski, M. Celander, R. Adelaiye, E. Ciamporcero, R. Fenstermaker, S.I. Abrams, T. Leanderson, A. Olsson, R. Pili
Writing, review, and/or revision of the manuscript: L. Shen, A. Sundstedt, R. Fenstermaker, S.I. Abrams, H. Eriksson, T. Leanderson, A. Olsson, R. Pili
Administrative, technical, or material support (i.e., reporting or organizing data, constructing databases): L. Shen, R. Adelaiye, S. Ramakrishnan, A. Olsson, R. Pili
Study supervision: T. Leanderson, A. Olsson, R. Pili

Acknowledgments

Grant Support

References

1. Small EJ, Schellhammer PF, Higano CS, Redfern CH, Nemunaitis JJ, Valone FH, et al. Placebo-controlled phase III trial of immunologic therapy with sipuleucel-T (APC8015) in patients with metastatic, asymptomatic hormone refractory prostate cancer. J Clin Oncol 2006;24:3089–94.

2. Smith JL Jr, Stehlin JS Jr. Spontaneous regression of primary malignant melanomas with regional metastases. Cancer 1965;18:1399–415.

3. Culver ME, Gatesman ML, Mancl EE, Lowe DK. Ipilimumab: a novel treatment for metastatic melanoma. Ann Pharmacother 2011;45:510–9.

4. Gabrilovich DI, Nagaraj S. Myeloid-derived suppressor cells as regulators of the immune system. Nat Rev Immunol 2009;9:162–74.

5. Oosterling SJ, van der Bij GJ, Meijer GA, Tuk CW, van Garderen E, van Rooijen N, et al. Macrophages direct tumour histology and clinical outcome in a colon cancer model. J Pathol 2005;207:147–55.

6. Pan PY, Wang GX, Yin B, Ozao J, Ku T, Divino CM, Chen SH. Reversion of immune tolerance in advanced malignancy: modulation of myeloid-derived suppressor cell development by blockade of stem-cell factor function. Blood 2008;111:219–28.

7. Sinha P, Clements VK, Fulton AM, Ostrand-Rosenberg S. Prostaglandin E2 promotes tumor progression by inducing myeloid-derived suppressor cells. Cancer Res 2007;67:4507–13.

8. Song X, Krelin Y, Dvorkin T, Bjorkdahl O, Segal S, Dinarello CA, et al. CD11b$^+$/Gr-1$^+$ immature myeloid cells mediate suppression of T cells in mice bearing tumors of IL-1beta–secreting cells. J Immunol 2005;175:8200–8.

9. Solito S, Bronte V, Mandruzzato S. Antigen specificity of immune suppression by myeloid-derived suppressor cells. J Leukoc Biol 2011;90:31–6.

10. Huang B, Pan PY, Li Q, Sato AI, Levy DE, Bromberg J, et al. Gr-1$^+$CD115$^+$ immature myeloid suppressor cells mediate the development of tumor-induced T regulatory cells and T-cell anergy in tumor-bearing host. Cancer Res 2006;66:1123–31.

11. Serafini P, Mgebroff S, Noonan K, Borrello I. Myeloid-derived suppressor cells promote cross-tolerance in B-cell lymphoma by expanding regulatory T cells. Cancer Res 2008;68:5439–49.

12. Yang Z, Zhang B, Li D, Lv M, Huang C, Shen GX, Huang B. Mast cells mobilize myeloid-derived suppressor cells and Treg cells in tumor micro-environment via IL-17 pathway in murine hepatocarcinoma model. PLoS ONE 2010;5:e8922.

13. Mills CD, Kincaid K, Alt JM, Heilman MJ, Hill AM. M-1/M-2 macrophages and the Th1/Th2 paradigm. J Immunol 2000;164:6166–73.

14. Pili R, Häggman M, Stadler WM, Gingrich JR, Assikis VJ, Björk A, et al. Phase II randomized, double-blind, placebo-controlled study of tasquinimod in men with minimally symptomatic metastatic castrate-resistant prostate cancer. J Clin Oncol 2011;29:4022–8.

15. Armstrong AJ, Häggman M, Stadler WM, Gingrich JR, Assikis V, Polikoff J, et al. Long-term survival and biomarker correlates of tasquinimod efficacy in a multicenter randomized study of men with minimally symptomatic metastatic castration-resistant prostate cancer. Clin Cancer Res 2013;19:6891–901.

16. Dalrymple SL, Becker RE, Isaacs JT. The quinoline-3-carboxamide anti-angiogenic agent, tasquinimod, enhances the anti-prostate cancer efficacy of androgen ablation and taxotere without effecting serum PSA directly in human xenografts. Prostate 2007;67:790–7.

17. Dalrymple SL, Becker RE, Zhou H, DeWeese TL, Isaacs JT. Tasquinimod prevents the angiogenic rebound induced by fractionated radiation resulting in an enhanced therapeutic response of prostate cancer xenografts. Prostate 2012;72:638–48.

18. Jennbacken K, Welén K, Olsson A, Axelsson B, Törngren M, Damber JE, et al. Inhibition of metastasis in a castration resistant prostate cancer model by the quinoline-3-carboxamide tasquinimod (ABR-215050). Prostate 2012;72:913–24.

19. Isaacs JT, Pili R, Qian DZ, Dalrymple SL, Garrison JB, Kyprianou N, et al. Identification of ABR-215050 as lead second generation quinoline-3-carboxamide anti-angiogenic agent for the treatment of prostate cancer. Prostate 2006;66:1768–78.

20. Olsson A, Björk A, Vallon-Christersson J, Isaacs JT, Leanderson T. Tasquinimod (ABR-215050), a quinoline-3-carboxamide anti-angiogenic agent, modulates the expression of thrombospondin-1 in human prostate tumors. Mol Cancer 2010;9:107.

21. Isaacs JT, Antony L, Dalrymple SL, Brennen WN, Gerber S, Hammers H, et al. Tasquinimod is an allosteric modulator of HDAC4 survival signaling

within the compromised cancer microenvironment. Cancer Res 2013;73: 1386–99.

22. Bjork P, Björk A, Vogl T, Stenström M, Liberg D, Olsson A, et al. Identification of human S100A9 as a novel target for treatment of autoimmune disease via binding to quinoline-3-carboxamides. PLoS Biol 2009;7:e97.

23. Kallberg E, Vogl T, Liberg D, Olsson A, Björk P, Wikström P, et al. S100A9 interaction with TLR4 promotes tumor growth. PLoS ONE 2012;7:e34207.

24. Cheng P, Corzo CA, Luetteke N, Yu B, Nagaraj S, Bui MM, et al. Inhibition of dendritic cell differentiation and accumulation of myeloid-derived suppressor cells in cancer is regulated by S100A9 protein. J Exp Med 2008; 205:2235–49.

25. Sinha P, Okoro C, Foell D, Freeze HH, Ostrand-Rosenberg S, Srikrishna G. Proinflammatory S100 proteins regulate the accumulation of myeloid-derived suppressor cells. J Immunol 2008;181:4666–75.

26. Ellis L, Lehet K, Ramakrishnan S, Adelaiye R, Pili R. Development of a castrate resistant transplant tumor model of prostate cancer. Prostate 2011;72:587–91.

27. Mulryan K, Ryan MG, Myers KA, Shaw D, Wang W, Kingsman SM, et al. Attenuated recombinant vaccinia virus expressing oncofetal antigen (tumor-associated antigen) 5T4 induces active therapy of established tumors. Mol Cancer Ther 2002;1:1129–37.

28. Attia MA, Weiss DW. Immunology of spontaneous mammary carcinomas in mice. V. Acquired tumor resistance and enhancement in strain A mice infected with mammary tumor virus. Cancer Res 1966;26: 1787–800.

29. Kishi H, Igawa M, Kikuno N, Yoshino T, Urakami S, Shiina H. Expression of the survivin gene in prostate cancer: correlation with clinicopathological characteristics, proliferative activity and apoptosis. J Urol 2004;171: 1855–60.

30. Ciesielski MJ, Ahluwalia MS, Munich SA, Orton M, Barone T, Chanan-Khan A, et al. Antitumor cytotoxic T-cell response induced by a survivin peptide mimic. Cancer Immunol Immunother 2010;59:1211–21.

31. Shen L, Ciesielski M, Ramakrishnan S, Miles KM, Ellis L, Sotomayor P, et al. Class I histone deacetylase inhibitor entinostat suppresses regulatory T cells and enhances immunotherapies in renal and prostate cancer models. PLoS ONE 2012;7:e30815.

32. Dohlsten M, Abrahmsén L, Björk P, Lando PA, Hedlund G, Forsberg G, et al. Monoclonal antibody-superantigen fusion proteins: tumor-specific agents for T-cell-based tumor therapy. Proc Natl Acad Sci U S A 1994;91:8945–9.

33. Kappler J, Kotzin B, Herron L, Gelfand EW, Bigler RD, Boylston A, et al. V beta-specific stimulation of human T cells by staphylococcal toxins. Science 1989;244:811–3.

34. Raymond E, Dalgleish A, Damber JE, Smith M, Pili R. Mechanisms of action of tasquinimod on the tumour microenvironment. Cancer Chemother Pharmacol 2014;73:1–8.

35. De Palma M, Venneri MA, Galli R, SergiSergi L, Politi LS, Sampaolesi M, et al. Tie2 identifies a hematopoietic lineage of proangiogenic monocytes required for tumor vessel formation and a mesenchymal population of pericyte progenitors. Cancer Cell 2005;8:211–26.

36. Sica A, Bronte V. Altered macrophage differentiation and immune dysfunction in tumor development. J Clin Invest 2007;117:1155–66.

37. Peranzoni E, Zilio S, Marigo I, Dolcetti L, Zanovello P, Mandruzzato S, et al. Myeloid-derived suppressor cell heterogeneity and subset definition. Curr Opin Immunol 2010;22:238–44.

38. Movahedi K, Guilliams M, Van den Bossche J, Van den Bergh R, Gysemans C, Beschin A, et al. Identification of discrete tumor-induced myeloid-derived suppressor cell subpopulations with distinct T cell-suppressive activity. Blood 2008;111:4233–44.

39. El Kasmi KC, Qualls JE, Pesce JT, Smith AM, Thompson RW, Henao-Tamayo M, et al. Toll-like receptor-induced arginase 1 in macrophages thwarts effective immunity against intracellular pathogens. Nat Immunol 2008;9:1399–406.

40. Sundstedt A, Celander M, Eriksson H, Törngren M, Hedlund G. Mono-therapeutically nonactive CTLA-4 blockade results in greatly enhanced antitumor effects when combined with tumor-targeted superantigens in a B16 melanoma model. J Immunother 2012;35:344–53.

41. Rigamonti N, Capuano G, Ricupito A, Jachetti E, Grioni M, Generoso L, et al. Modulators of arginine metabolism do not impact on peripheral T-cell tolerance and disease progression in a model of spontaneous prostate cancer. Clin Cancer Res 2011;17:1012–23.

42. Chen X, Eksioglu EA, Zhou J, Zhang L, Djeu J, Fortenbery N, et al. Induction of myelodysplasia by myeloid-derived suppressor cells. J Clin Invest 2013;123:4595–611.

43. Ichikawa M, Williams R, Wang L, Vogl T, Srikrishna G. S100A8/A9 activate key genes and pathways in colon tumor progression. Mol Cancer Res 2011;9:133–48.

44. Ostrand-Rosenberg S, Sinha P, Beury DW, Clements VK. Cross-talk between myeloid-derived suppressor cells (MDSC), macrophages, and dendritic cells enhances tumor-induced immune suppression. Semin Cancer Biol 2012;22:275–81.

45. De Palma M, Lewis CE. Macrophage regulation of tumor responses to anticancer therapies. Cancer Cell 2013;23:277–86.

46. Murdoch C, Muthana M, Coffelt SB, Lewis CE. The role of myeloid cells in the promotion of tumour angiogenesis. Nat Rev Cancer 2008;8:618–31.

47. Li B, Vincent A, Cates J, Brantley-Sieders DM, Polk DB, Young PP. Low levels of tumor necrosis factor alpha increase tumor growth by inducing an endothelial phenotype of monocytes recruited to the tumor site. Cancer Res 2009;69:338–48.

48. Toh B, Wang X, Keeble J, Sim WJ, Khoo K, Wong WC, et al. Mesenchymal transition and dissemination of cancer cells is driven by myeloid-derived suppressor cells infiltrating the primary tumor. PLoS Biol 2011;9: e1001162.

49. Cui TX, Kryczek I, Zhao L, Zhao E, Kuick R, Roh MH, et al. Myeloid-derived suppressor cells enhance stemness of cancer cells by inducing micro-RNA101 and suppressing the corepressor CtBP2. Immunity 2013;39: 611–21.

50. Hiratsuka S, Watanabe A, Aburatani H, Maru Y. Tumour-mediated upregulation of chemoattractants and recruitment of myeloid cells predetermines lung metastasis. Nat Cell Biol 2006;8:1369–75.

51. Sawant A, Deshane J, Jules J, Lee CM, Harris BA, Feng X, et al. Myeloid-derived suppressor cells function as novel osteoclast progenitors enhancing bone loss in breast cancer. Cancer Res 2013;73:672–82.

52. Kaplan RN, Riba RD, Zacharoulis S, Bramley AH, Vincent L, Costa C, et al. VEGFR1-positive haematopoietic bone marrow progenitors initiate the pre-metastatic niche. Nature 2005;438:820–7.

53. Acharyya S, Oskarsson T, Vanharanta S, Malladi S, Kim J, Morris PG, et al. A CXCL1 paracrine network links cancer chemoresistance and metastasis. Cell 2012;150:165–78.

Tasquinimod targets suppressive myeloid cells in the tumor microenvironment

Li Shen & Roberto Pili
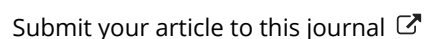
Full Terms & Conditions of access and use can be found at
http://www.tandfonline.com/action/journalInformation?journalCode=koni20

Tasquinimod modulates tumor microenvironment

Tasquinimod targets suppressive myeloid cells in the tumor microenvironment

Li Shen[1,*], Roberto Pili[1,2,**]

[1]Genitourinary Program, Roswell Park Cancer Institute, Buffalo NY

[2]Department of Medicine, Indiana University-Simon Cancer Center, Indianapolis IN

[*]**Corresponding authors**: Li Shen Ph.D., Roswell Park Cancer Institute, Li.Shen@RoswellPark.org

[**]**Corresponding authors**: Roberto Pili MD, Indiana University-Simon Cancer Center, rpili@iupui.edu

Key Words

tasquinimod, suppressive myeloid cells (SMCs), immunotherapy, S100A9, myeloid-derived suppressor cells (MDSCs), tumor associated macrophages (TAMs).

Abstract

Infiltrating myeloid derived suppressor cells and tumor associated macrophages are important components of the immunosuppressive tumor microenvironment. We recently reported that tasquinimod, which binds to S100A9, impairs both infiltration and function of these cells. Here we discuss the underlying mechanisms responsible for targeting multiple suppressive populations and the modulation of the tumor microenvironment.

1

Suppressive myeloid cells (SMCs), including myeloid-derived suppressor cells (MDSCs) and tumor associated macrophages (TAMs), are associated with tumor progression and metastasis[1]. MDSCs expand and accumulate in many cancers [1], whereas TAMs are differentiated from immature monocytes or MDSCs when these precursors infiltrate and adapt to the tumor environment[2]. Both MDSCs and TAMs are critical components of the immunosuppressive tumor microenvironment that can directly inhibit activation and function of T and NK cells[3]. Therefore, modulating and/or depleting these cells in the tumor environment is expected to help counteracting SMC-associated immunosuppression, tumor progression, and metastasis.

Previous reports have shown different approaches to deplete MDSCs or to affect their expansion[4]. While reduction of peripheral MDSCs has been observed, few of these efforts have been able to reduce infiltration of MDSCs in the tumor sites or impair their suppressive function[4]. Tasquinimod is an orally active synthetic quinoline-3-carboxamide derivate that has shown effect in a phase II clinical trial in patients with castration resistance prostate cancer (CRPC)[5]. We have recently reported that tasquinimod reduced tumor infiltrating MDSCs and M2 polarized macrophages and impaired the suppressive function of these infiltrating myeloid cells in two different experimental cancer models, namely the CR Myc-CaP prostate cancer model and the B16-5T4 melanoma model[6]. Combining tasquinimod with two different immunotherapy strategies in these models clearly showed an enhanced effect on tumor growth in both models. Interestingly, tasquinimod did not affect accumulation of MDSCs in the peripheral sites in CR Myc-CaP model, but slightly reduced MDSCs in spleen in the B16-5T4 model, suggesting that modulation of SMCs in tumors is sufficient to facilitate immunotherapies

The composition and suppressive function of tumor-infiltrating myeloid cells are usually different from those of peripheral suppressive myeloid cells. In the CR Myc-CaP prostate

2

cancer model, Gr1$^+$CD11b$^+$ MDSCs accumulate in peripheral blood with tumor growth. Gr1^{low}CD11b$^+$ and Gr1$^-$CD11b$^+$ immature monocytes are also present in peripheral blood[6], In CR Myc-CaP tumors, Gr1$^+$CD11b$^+$ MDSCs are one of the major populations, and Ly6G$^+$Ly6C$^-$ granulocytic MDSCs are the major subpopulation. However, the majority of tumor infiltrating Gr1$^-$CD11b$^+$ cells are F4/80$^+$ macrophages (up to 80% of CD11b$^+$ cells), and most of these are M2 polarized TAMs[6], We have compared the suppressive function of peripheral and tumor infiltrating myeloid cells. The CD11b$^+$ cells isolated from Myc-CaP tumors efficiently inhibited T cell proliferation upon CD3 and CD28 stimulation[6], whereas the CD11b$^+$ cells from spleen did not have inhibitory effect on T cell proliferation upon the same stimulation (data not shown). These observations are consistent with the report from another showing that tumor and peripheral site MDSCs have different functions[7]. Importantly, we observed that tasquinimod treatment not only reduced CD206$^+$Arginase-1^{high} M2 macrophages, but also induced iNOS^{high} macrophages with M1 polarized phenotype. This indicates that tasquinimod may switch the differentiation of tumor infiltrating macrophages from M2 polarized immunosuppressive phenotype to M1 phenotype. As compared to infiltrating MDSCs, M2 polarized TAM may represent an even more important component of tumor-promoting, immunosuppressive environment. To confirm our hypothesis, we isolated infiltrating myeloid cells from vehicle or tasquinimod treated tumors from donor mice, and mixed them with fresh tumor cells to make inoculates in recipient mice. We observed that transferred SMCs from tasquinimod-treated tumor were less supportive of tumor growth. [6] The analysis of the composition of tumor immune microenvironment specific to different models or diseases of interest may be critical to develop effective strategies to modulate the environment and facilitate the development of anti-tumor therapies.

Our study provides clues to the underlying mechanism for myeloid cell modulation by tasquinimod (Figure 1). S100A9 is a potential target of tasquinimod that may

be involved in immuno-modulatory activity[8], and S100A9 has been shown to regulate accumulation of MDSCs[4, 9]. Tasquinimod binds to S100A9[10], and blocks the interaction of this ligand with its receptors, including receptor for advanced glycation end product (RAGE) and Toll-like receptor (TLR)-4 and EMMPRIN. In an additional, metastatic model, we observed that tasquinimod was able to dramatically reduce M2 macrophages in renal cell tumors and at the metastatic site (lung; unpublished data). This observation suggests that tasquinimod may act through inhibiting the trafficking of MDSCs, via inhibition of S100A9, into the tumor in our tested models. However, a previous report showed that antibody against RAGE, mAbGB3.1, inhibited the accumulation of MDSCs in peripheral sites, but not in the metastatic tumor site (the primary tumors were resected)[4]. The discrepancy between these results may originate from the fact that tasquinimod binds and inhibits the ligand, S100A9, whereas mAbGB3.1 blocks one of receptors for the ligand, RAGE. Therefore, the other receptor for S100A9, TLR4 and/or EMMPRIN, may mediate the SMC-targeting activity of tasquinimod. At the same time, other tumor or stroma-secreted inflammatory factors may still induce peripheral MDSC expansion when S100A9 protein ligand is blocked. We have also demonstrated that expression of suppressive function-related genes, Arginase-1 (reduction) and iNOS (induction) was regulated by tasquinimod treatment. It has been reported that TLR-4 pathway is an important regulator of Arginase-1 expression. This finding would suggest that tasquinimod may affect function and polarization of SMCs by inhibiting S100A9ô TLR4ô Arginase axis. Though tasquinimod did not change accumulation of Gr1$^+$CD11b$^+$ MDSCs in blood, it depleted Gr1$^-$CD11b$^+$ monocytes from peripheral blood. Therefore, tasquinimod may also reduce the CD206$^+$ M2 TAMs through depletion of these Gr1$^-$CD11b$^+$ precursor cells from blood.

In summary, tasquinimod is an agent that has the potential of overcoming the suppressive tumor environment. Targeting the suppressive tumor microenvironment

4

continues to be an active field of exploration to address management of metastatic cancers as

part of immuno-oncology at large.

References cited

1. Gabrilovich DI, Nagaraj S. Myeloid-derived suppressor cells as regulators of the immune system. Nat Rev Immunol 2009; 9:162-74.

2. Sica A, Bronte V. Altered macrophage differentiation and immune dysfunction in tumor development. J Clin Invest 2007; 117:1155-66.

3. Solito S, Bronte V, Mandruzzato S. Antigen specificity of immune suppression by myeloid-derived suppressor cells. J Leukoc Biol 2011.

4. Sinha P, Okoro C, Foell D, Freeze HH, Ostrand-Rosenberg S, Srikrishna G. Proinflammatory S100 proteins regulate the accumulation of myeloid-derived suppressor cells. J Immunol 2008; 181:4666-75.

5. Pili R, Haggman M, Stadler WM, Gingrich JR, Assikis VJ, Bjork A, Nordle O, Forsberg G, Carducci MA, Armstrong AJ. Phase II randomized, double-blind, placebo-controlled study of tasquinimod in men with minimally symptomatic metastatic castrate-resistant prostate cancer. J Clin Oncol 2011; 29:4022-8.

6. Shen L, Sundstedt A, Ciesielski M, Miles KM, Celander M, Adelaiye R, Orillion A, Ciamporcero E, Ramakrishnan S, Ellis L, et al. Tasquinimod modulates suppressive myeloid cells and enhances cancer immunotherapies in murine models. Cancer Immunol Res 2015; 3:136-48.

7. Corzo CA, Condamine T, Lu L, Cotter MJ, Youn JI, Cheng P, Cho HI, Celis E, Quiceno DG, Padhya T, et al. HIF-1alpha regulates function and differentiation of myeloid-derived suppressor cells in the tumor microenvironment. J Exp Med 2010; 207:2439-53.

8. Bjork P, Bjork A, Vogl T, Stenstrom M, Liberg D, Olsson A, Roth J, Ivars F, Leanderson T. Identification of human S100A9 as a novel target for treatment of autoimmune disease via binding to quinoline-3-carboxamides. PLoS Biol 2009; 7:e97.

6

9. Cheng P, Corzo CA, Luetteke N, Yu B, Nagaraj S, Bui MM, Ortiz M, Nacken W, Sorg C, Vogl T, et al. Inhibition of dendritic cell differentiation and accumulation of myeloid-derived suppressor cells in cancer is regulated by S100A9 protein. J Exp Med 2008; 205:2235-49.

10. Kallberg E, Vogl T, Liberg D, Olsson A, Bjork P, Wikstrom P, Bergh A, Roth J, Ivars F, Leanderson T. S100A9 interaction with TLR4 promotes tumor growth. PLoS One 2012; 7:e34207.
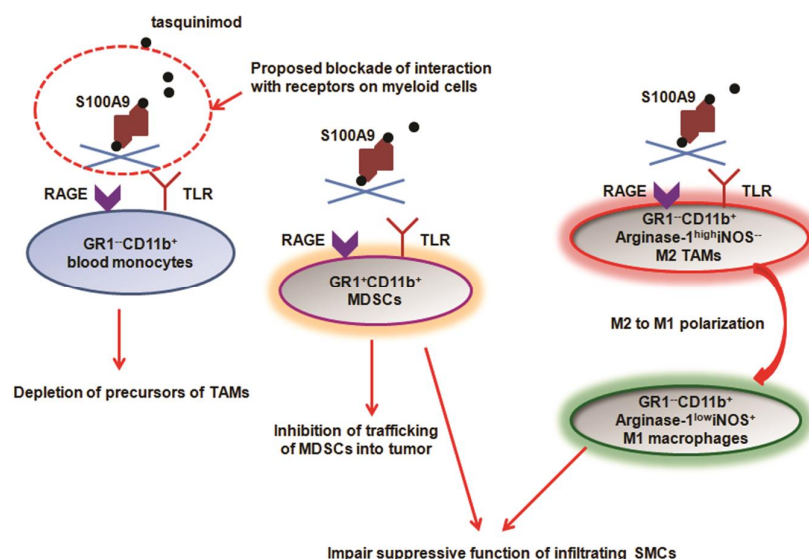
7

Figure 1 Proposed potential mechanisms underlying modulation of tumor microenvironment by tasquinimod. Tasquinimod binds to S100A9 homodimers in a 1:1 fashion[10] and blocks its interaction with receptors expressed on multiple myeloid cell populations. The blockade may lead to depletion of Gr1$^-$CD11b$^+$ blood monocytes, which are one of the precursors of TAMs. In addition, the trafficking of Gr1$^+$CD11b$^+$ MDSCs to tumor sites is inhibited. Tasquinimod also induce M2 to M1 polarization of macrophages in the tumors, associated with down-regulation of Arginase-1 and induction of iNOS expression in these cells. Thus, tasquinimod may impair the suppressive function of infiltrating SMCs through blockade of S100A9-TLR4-Arginase-1 signaling.

8